UNIVERSIDADE DE SÃO PAULO
INSTITUTO DE FÍSICA DE SÃO CARLOS

JESSICA DIPOLD

Two-photon absorption studies in organic compounds and polymers

São Carlos
2019

JESSICA DIPOLD

Two-photon absorption studies in organic compounds and polymers

Dissertation or Thesis presented to the Graduate Program in Physics at the Instituto de Física de São Carlos, Universidade de São Paulo to obtain the degree of Doctor of Science.

Concentration area: Applied Physics

Advisor: Prof. Dr. Cleber Renato Mendonça

Corrected version

(Original version available on the Program Unit)

São Carlos

2019

I AUTHORIZE THE REPRODUCTION AND DISSEMINATION OF TOTAL OR PARTIAL COPIES OF THIS DOCUMENT, BY CONVENCIONAL OR ELECTRONIC MEDIA FOR STUDY OR RESEARCH PURPOSE, SINCE IT IS REFERENCED.

Dipold, Jessica
Two-photon absorption studies in organic compounds and polymers / Jessica Dipold; advisor Cleber Renato Mendonça - revised version -- São Carlos 2019.
116 p.

Thesis (Doctorate - Graduate Program in Física Aplicada) -- Instituto de Física de São Carlos, Universidade de São Paulo - Brasil , 2019.

1. Z-Scan. 2. Nonlinear optics. 3. Organic compounds. 4. Two-photon absorption. I. Mendonça, Cleber Renato, advisor. II. Title.

To my parents, who supported me and gave me strength to keep going.

ACKNOWLEDGEMENTS

I would like to thank first and foremost to my mother and father, who supported me and all my decisions during the phD period as they did since I was born. Without their care and words, I might never have gotten this far with a healthy mental state.

I'd also like to thank my boyfriend, who was with me every day and helped me during all situations during the phD, good and bad ones, and never left my side. Your support and friendly shoulder were very important, and I am sure I would not have gotten this far without your help.

Thank you also to my new friends from the University of Central Florida, who showed me other means of research and friendly work that gave me more strength to finish the phD with a stronger heart.

To my supervisor, Dr. Cleber Renato Mendonça, thank you for all the orientation and patience, and for showing me how to guide a large group without losing focus of any of your student works. I admire both your social and research skills, both which I watched and learned and will propagate during my researcher life. I'd also like to thank the Photonic's group for the support, from the students to the technicians, who helped with discussions and technical support for the four years of research.

Lastly but not least, I'd like to thank CAPES for the financial support, and IFSC for the structure and for these ten years of studies, as well as for the financial support for conferences.

“For even the very wise cannot see all ends.”

J.R.R. Tolkien – The Fellowship of the Ring

ABSTRACT

DIPOLD, J. **Two-photon absorption studies in organic compounds and polymers**. 2019. 116 p. Thesis (Doctor in Science) – Instituto de Física de São Carlos, Universidade de São Paulo, São Carlos, 2019.

High two-photon absorption (2PA) cross-section materials have been frequently studied during the latest years due to the wide variety of technological applications, such as two-photon absorption microscopy (2PM) and microfabrication. The characterization of new materials with high nonlinearities is, therefore, indispensable to develop new applications and improve previously existing ones. Here, three different groups of novel organic compounds had their nonlinearities characterized through two-photon absorption measurements: fluorenone based compounds, which are usually used in two-photon absorption microscopy; BF2-naphthyridine (BODIPY) complexes, which have a wide range of applications, from solar cells to photodynamic therapy; and binaphthalene-based polymers, with structures built to generate large nonlinearities through inherent chirality. All compounds had their two-photon absorption spectra studied through absorptive Z-Scan, with density functional theory (DFT) calculations made to interpret the results for the first two groups of compounds, and polarization controlled measurements made for the polymers. The highest 2PA cross-section presented by the fluorenone-based compounds was of 224 GM at 710 nm, large and within the wavelength range for 2PM applications; for the BODIPYs, the largest observed cross-section was of 268 GM at 990 nm, of the same order of magnitude of more complex compounds; and 680 GM at 1100 nm for the polymer, showing a high cross-section as expected from its structure. The desired applications for the studied molecules were shown valid, and their characterization gave a better understanding of how to increase their nonlinearities depending on the compound manufacture.

Keywords: Z-Scan. Nonlinear optics. Organic compounds. Two-photon absorption.

RESUMO

DIPOLD, J. **Estudos de absorção de dois fótons em moléculas orgânicas e polímeros**. 2019. 116 p. Tese (Doutorado em Ciências) – Instituto de Física de São Carlos, Universidade de São Paulo, São Carlos, 2019.

Materiais com grande seção de choque de absorção de dois fótons (2PA) tem sido estudados com frequência nos últimos anos graças a ampla variedade de aplicações tecnológicas, tais como microscopia por absorção de dois fótons (2PM) e microfabricação. A caracterização de materiais com altas não-linearidades é, portanto, indispensável para o desenvolvimento de novas aplicações e para o aprimoramento das técnicas já existentes. Aqui, três diferentes grupos de novos compostos orgânicos tiveram suas não-linearidades caracterizadas através de medidas de 2PA: compostos baseados em fluorenona, geralmente utilizados em 2PM; compostos baseados em BF_2-naftiridina (BODIPY), que possuem grande variedade de aplicações, desde células solares até terapia fotodinâmica; e polímeros baseados em binaftaleno, com estruturas sintetizadas para gerar altas não-linearidades através de sua quiralidade inerente. Para caracterizar o espectro de 2PA de todos os compostos a técnica de Z-Scan absortiva foi utilizada, com cálculos de funcional densidade (DFT) realizados para corroborar os resultados obtidos para os dois primeiros grupos de compostos, e medidas com controle de polarização foram realizados para o estudo dos polímeros. A maior seção de choque obtida para as fluorenonas foi de 224 GM em 710 nm, alta e dentro do comprimento de onda necessário para as aplicações de 2PM; para os BODIPYs, a maior seção de choque observada foi de 268 GM em 990 nm, da mesma ordem de magnitude que compostos mais complexos que os estudados; e 680 GM em 1100 nm para o polímero, mostrando um valor alto como esperado por sua estrutura. Com isso, demonstramos que as moléculas estudadas possuem as aplicações desejadas, e sua caracterização permitiu uma melhor compreensão de como aumentar suas não-linearidades dependendo da engenharia dos compostos.

Palavras-chave: Z-Scan. Ótica não-linear. Compostos orgânicos. Absorção de dois fótons.

LIST OF FIGURES

LIST OF TABLES

CONTENT

1 Introduction

1.1 Nonlinear light-matter interaction

One of the most significant events in physics during the 20th century was the development of the quantum theory of light-matter interaction. In such theory light is treated as *photons*, while matter consists of either molecules or atoms. When they interact, there is an energy exchange between them that can be described either by photons absorption or emission processes. At first, only one-photon interactions were studied since they could be easily seen in regular laboratory conditions and in daily life.[1] In a general form, the one-photon absorption process can be described as the energy of a single photon being absorbed by a molecule (or atom) that makes a transition from a lower to a higher energy level. For an emission process, the molecule emits a photon upon transitioning from a higher energy level to a lower one. Since energy must be conserved, the energy difference between the levels involved in these processes has to be the same of the incident or emitted photon.

This interaction of matter with light can be, in general, described by the induced polarization ($\vec{P}$) in the optical media when an electric field $\vec{E}$ is applied. For one-photon processes, the applied electric field is much smaller than the interatomic electric field (which has ~ 5.14×10^{11} m/V), and its polarization is given by[2]

$$\vec{P}(t) = \varepsilon_0 \chi^{(1)} \cdot \vec{E} \tag{1.1}$$

Such polarization describes the linear optics regime, in which it is possible to obtain the first order susceptibility $\chi^{(1)}$ of the material, which is directly related to its refractive index and linear absorption.[3]

Another possible situation occurs when the electric field applied to the material is of the order of the interatomic field. Under this condition, the charges are perturbed in a non-harmonic way, which leads to nonlinear effects that are felt by the electric field itself. In this case the induced polarization of the media is no longer

linear with the electric field, and the response of the material becomes dependent of the electric field as well. This polarization can be described approximately as[2]

$$\vec{P}(t) = \varepsilon_0(\chi^{(1)} \cdot \vec{E} + \chi^{(2)} : \vec{E}^2 + \chi^{(3)} \vdots \vec{E}^3 + \cdots) \quad (1.1)$$

in which the first term is related to the linear polarization while the others give rise to the nonlinear effects in the material. From Eq. (1.1), the terms $\chi^{(2)}$ and $\chi^{(3)}$ are the nonlinear optics susceptibility of second and third order, respectively. These non-linear terms act as new electric field generators for the material. $\chi^{(2)}$ is a third order tensor and its magnitude describe second order processes, such as second harmonic generation (SHG) and frequency sum generation. This term generates two electric fields contributions, one independent of frequency, which shows that when a material with second-order non-linearity is irradiated by light a constant polarization should appear, known as optical rectification; and one dependent of 2ω, which is responsible for the second harmonic generation. $\chi^{(3)}$ is a fourth order tensor, and describes third order processes, which may give, for instance, responses with frequencies at ω and 3ω. In the first case, the electric field describes a nonlinear contribution for the polarization of the same frequency as the incident electric field, which gives a nonlinear contribution for the refractive index. A temporary change in the refractive index happens, and this effect is called as Kerr effect. The term with 3ω is responsible for the third harmonic generation. $\chi^{(3)}$ is also related to nonlinear absorption, more specifically to the two-photon absorption process, by making the absorption coefficient become dependent on the light intensity.

1.2 Nonlinear phenomena

In 1931, after the quantum light-interaction theory was further developed, the multi photonic absorption was finally proposed. Marie Göppert-Mayer,[4] during her phD studies under the supervision of the German physicist Max Born, showed theoretically the existence of a new absorptive phenomenon, where two-photons caused a transition between two excited states instead of a single one. To prove this, she proposed the existence of a virtual intermediate state, based on the quantum theory of light-matter interaction. In this process, two or more photons that do not

present necessarily the same frequency are absorbed by a material in the same quantum event. The real state accessed by these photons has the energy corresponding to the sum of the energy of the incident photons. However, since the probability of this effect occurring is small and there is neeed of a high intensity light source to observe it, it could not be experimentally observed until the laser development in 1960 by Maiman. In 1961, Kaiser and Garret[5] reported the first observation of a two-photon absorption (2PA) transition, confirming Göppert-Mayer prediction.

The multi-photon absorption efficiency depends on the wavelength and on the material itself, being similar to the one-photon absorption. However, for the two-photon absorption, the transition rate increases with the square of the photon number per unity of area and time. This nonlinear dependency with the light intensity is responsible for several properties that allows different applications for 2PA. One of these properties is the spatial confinement, which is a tridimensional inherent property that comes from the nonlinear dependency with the intensity that allows, for example, that a process only occurs in the focal volume of a strongly focalized light source within a sample. This has given rise to several applications, described in the next subsections.

1.2.1 Microfabrication through two-photon polymerization

The 2PA process, thanks to its spatial confinement, allows the possibility of activating physical or chemical processes with high spatial resolution. With that, the two-photon polymerization technique became extensively studied due to the possibility of fabricating microstructures with resolution smaller than the light diffraction limit.[6-7] The technique consists of a high intensity laser beam focalized in a photosensitive resin, which only solidifies at the center of the focal spot of the beam. There, the resin is solidified by the interaction with light, which can be moved across the *xyz* axes, making complex shapes with high resolution.[8] Examples of structures made through two-photon polymerization can be seen on Figure 1.1. The structures produced can have resolution below the light diffraction limit, due to the nonlinear effects and the polymerization limit.[9]

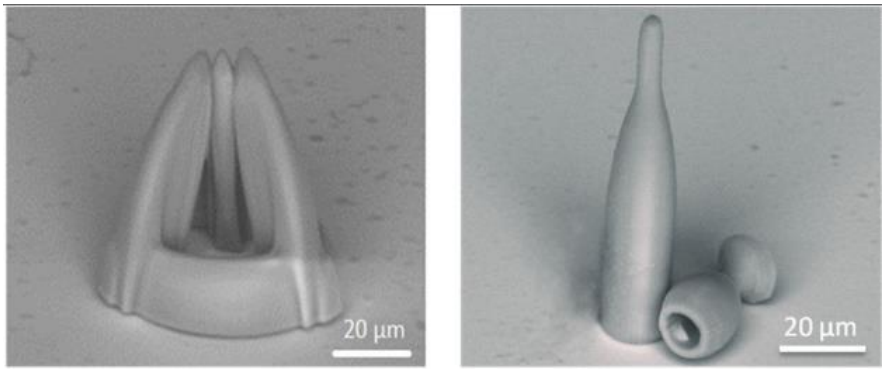

Figure 1.1 - Scanning electron image of structures made through two-photon polymerization. Source: Adapted from KONIG.[10]

1.2.2 Two-photon absorption microscopy

Standard one-photon microscopy uses UV light (around 350 nm) to excite fluorophores within materials to collect their fluorescence. The obtained images are only of superficial depth, and due to the UV wavelength used, functioning living cells can be degraded, pointing out for the development of a new kind of microscopy to improve these conditions.[11]

Two-photon microscopy was proposed by Webb et al. in 1990,[12] and is based on generating smaller wavelengths from longer ones to produce high quality three dimensional images. Since it uses near infra-red (IR) radiation, the depth the light can reach increases and there is no clear damage caused by it, even in living cells. This technique consists of adding a fluorescent dye to the sample, which is then excited by a laser pulse in the IR region by a focused beam. This focusing gives a high intensity to the light source, allowing the fluorophore to absorb two-photons instead of one to reach its excited state, emitting light in the visible region. This light is collected and processed, and produces a smaller noise-to-signal ratio than the one-photon microscopy.[13-14] This technique helps to increase the resolution of the images thanks to its spatial localization property, which gives more detailed images. Also, due to the emission wavelength being very different from the absorbed one, it is easier to filter the wavelength that does not belong to the fluorescence signal. Advances on two-photon microscopy are only made with the development of high two-photon absorption cross-section fluorophores,[15-16] necessary to increase the fluorescence of the cells and, as consequence, its resolution. Figure 1.2 shows a multidimensional two-photon microscopy image of living cells, produced with a 100

mW laser focused on a 0.5 μm spot within the sample, with 100 fs pulses every 10 ns.

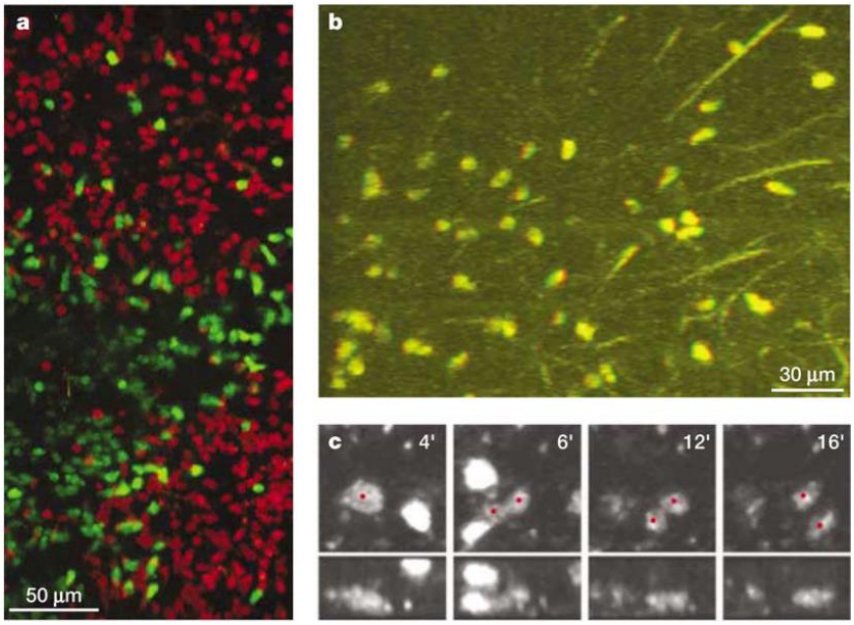

Figure 1.2 - Multidimensional two-photon microscopy images of (a) an intact lymph node, with B cells (red) and T cells (green); (b) T cells moving in a meshwork of reticular fibers; and (c) an *in vivo* proliferation event inside the lymph node.
Source: Adapted from CAHALAN et al. [17]

1.2.3 Photodynamic therapy (PDT)

Photodynamic therapy is a treatment first used to kill carcinogenic cells using light and a photosensitizer. In it, carcinogenic cells are doped with a photosensitizer, which is then irradiated by a light source at an appropriate wavelength, causing cytotoxicity via the generation of reactive molecular species thus killing the sick cells.[18] This process was at first done with one-photon absorption. Since most used photosensitizers have absorption bands between 300-500 nm, it has depth limitations that affects the treatment effectivity due to the fact that it is a region that the human tissue presents high absorptivity.[19] Also, photo damage may occur to surrounding cells due to the lack of localization of the one-photon process. Since the two-photon absorption excitation uses near infra-red wavelengths, its penetration depth is increased 10-100 folds in respect to the UV wavelengths, and the spatial confinement allows a more precise cell excitation, causing less photo damage to

healthy surrounding cells.[20] To increase the PDT capabilities, studies of high two-photon absorption cross-section sensitizers must be made,[21-23] allowing a stronger 2PA to eliminate the carcinogenic cells more effectively.

1.2.4 Optical Limiting

An optical limiter is a device in which the optical transmission decreases when the input signal increases, as illustrated by the plot shown in Figure 1.3. They can be used as protectors for the eyes, optical devices or as optical sensors. There are two main kinds of optical limiting devices: the energy-spreading type, which is based on the spatial changes of the laser beam going through a nonlinear medium; and the energy-absorbing type, based on intensity-dependent nonlinear attenuation of the laser energy in a nonlinear medium.[1] The second type mentioned is the one more dependent on nonlinear characteristics, such as the material nonlinear absorption or transmission.

To produce a good optical limiter, some requirements should be met. There should be no linear absorption in the working range, making the material completely transparent in that wavelength; the nonlinear transmission should be strongly dependent of the input light intensity, making sure that the medium is highly absorptive for intense signals; very fast temporal response of the nonlinear transmission following changes in the input intensity; and the spatial quality of the beam should not change after passing through the material.[1]

The optical limit process can be done either by linear processes, using the reverse saturable absorption (RSA),[24-25] or by nonlinear absorption.[26] At first, RSA was more used since it is based on the one-photon absorption process. However, it presented disadvantages since it degrades the beam quality and avoids low intensity input signals being detected. This does not happen for multi-photon absorption, which has the advantage of reducing fluctuations of the transmittance, as well as being able to smooth temporal or spatial profiles of intense laser beams. Semiconductors,[27] organic materials[28-30] and organic materials mixed with nanoparticles[31] are studied to improve optical limiting applications.

1.2.5 Three dimensional optical storage

The need of data storage has been increasing in the past few years, with the development of CDs and DVDs to carry on data. These devices use laser beams to read and write information. At first, one-photon materials were used in applications, being easily manufactured and with low power needed as the absorption is high. However, the information density of a material has a limitation depending on the resolution of the focusing system, which is directly related to the minimum size of the focal spot. For one-photon absorption materials, the beam easily penetrates the whole material, making it possible to only create a single layer of information (2D information) in the material, which limits the amount of data that can be stored within the disks.[1] If multi-photonic reactive materials are used instead, higher laser intensity will be necessary to write in the material. The fundamental procedure in this kind of application is focusing the beam with a high numerical aperture microscope objective in the material. Since two-photon absorption is a process dependent of the square of intensity, it will be confined within the focal volume of the beam, making the writing strongly localized. This allows several layers of information being written in the same material, increasing the capacity of data storing in 10 to 100 times in relation to linear absorptive materials.[32]

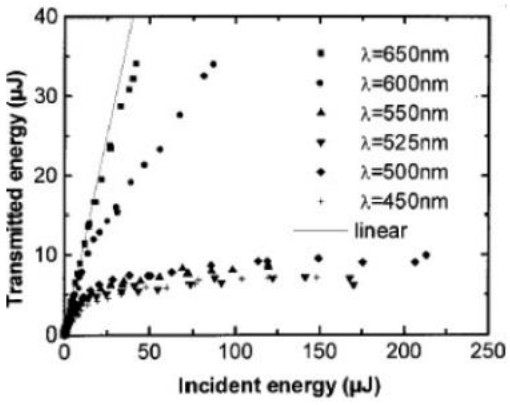

Figure 1.3 - Optical limit behavior using two-photon absorption properties of an organic compound (biofluorene).
Source: Adapted from MOREL et al. [33]

There is a strong need for chromophores with high two-photon absorption to increase the data storage capability. The four major mechanisms used for this storage are the photochromic reaction,[32;34-35] photobleaching reaction,[36-37]

photorefractive reaction[38] and photopolymerization reaction.[39] In Figure 1.4, an experimental result of a photobleaching mechanism used for 3D data storage is exhibited, exemplifying how the information can be recorded in several layers with multiphotonic processes.

Figure 1.4 - Nine frames of an animation stored in different depths of a polymer block doped with a two-photon absorption dye.
Source: Adapted from DAGANI.[40]

Besides these applications, the two-photon absorption is also important in spectroscopic studies since it allows transitions that are forbidden by one photon, increasing the electronic transition knowledge of the materials.[41]

Since all the mentioned applications use two-photon absorption as their main process, the development and characterization of materials with high nonlinearities becomes necessary to amplify and improve the 2PA process. Among the most promising materials are the organic ones, which have proved themselves as an important class of optical materials.[42] These have many possibilities of applications thanks to their simple manufacture and large variety of structures that allows an increase of their nonlinear capabilities. Some examples of what can be done is the increase in molecules conjugation length, adding strong donors or acceptors along the compound structure or adding chiral components to it.

Studying these new compounds made for nonlinear applications is important to indicate which kind of application they can be used for, as well as quantifying their two-photon absorption cross-sections and the wavelength range they can be used

for. This is what is done through nonlinear spectroscopy, which is the scope of this dissertation.

1.3 Organic Molecules

Π-conjugated organic molecules have emerged as important candidates for nonlinear optical applications thanks to their chemical stability, molecular manipulation possibilities and for having electronic clouds that are highly changed by optical fields. This kind of molecules presents delocalized π-electrons, which are related to high nonlinear properties, allowing applications in all the areas mentioned previously in this chapter. The development of novel applications is only possible with the manufacture of new organic compounds which are designed to increase the nonlinear properties of previously known ones. In order to design new compounds it is important to relate structure with properties for a large number of molecules, both organic and inorganic. Some of the techniques used for the synthesis of compounds with high nonlinearities are related to high conjugation lengths, push-pull structures, high planarity and bond lengths.

1.3.1 Conjugation in organic molecules

Carbon atoms present **s** and **p** atomic orbitals , and their bonding is possible due to the formation of two kinds of molecular orbitals, σ and π. The σ orbital is formed by the spatial superposition of two **s** orbitals, while the π orbital is formed by the interaction between two parallel orbitals. These bondings are allowed because of the carbon hybridization, which comes from the linear combination of the atomic orbitals **2s** and **2p**. The hybrid orbitals generated by this combination are $\mathbf{sp^3}$, which only allows σ bonding; $\mathbf{sp^2}$ and **sp**, forming both σ and π bonds. The π bonding is weaker than σ bonding, and allows transitions between the ligand (π) and antiligand (π*) states with electromagnetic radiation in the visible and near UV regions of the spectrum.[42] In Figure 1.5, a representative image is shown for an ethylene molecule with a σ and a π bond between the carbons.

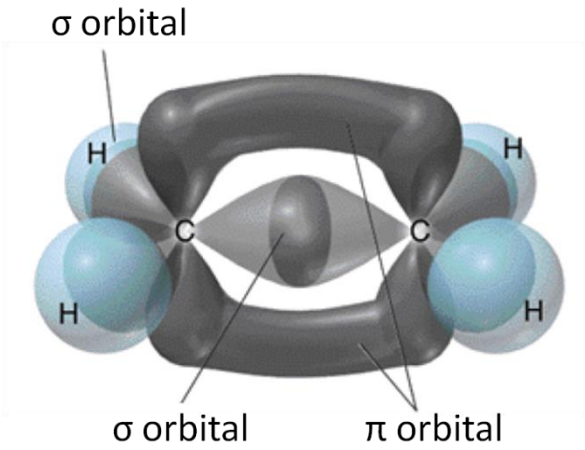

Figure 1.5 – Schematic representation of the π transversal bonding and the σ internuclear bonding.
Source: Adapted from PRASAD et al. [42]

When a structure presents a continuous alternation between simple, double, and even triple bonds between adjacent atoms, it is called a conjugated structure, as shown in Figure 1.6. These structures allow π electrons to move across the whole length of the molecule. This delocalization makes the electron distribution highly changeable in the presence of optical fields, which makes polarizability easier even outside of the resonance with the excitation field.

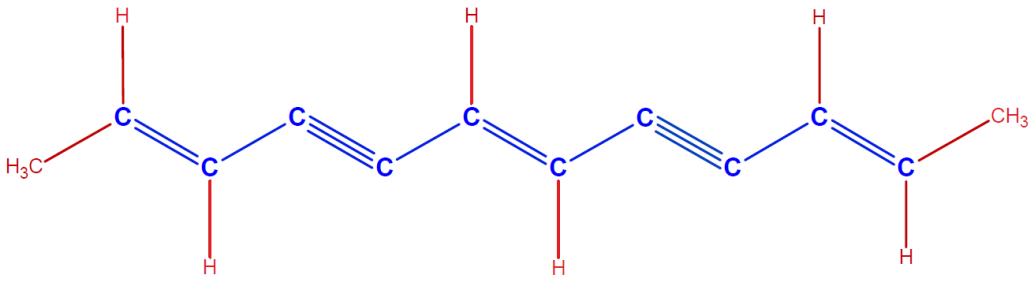

Figure 1.6 – Illustrative example of a conjugated molecule. There is an altercation between simple, double and triple bonds.
Source: VIVAS.[43]

Also, the electronic delocalization affects the electrostatic potential of the molecules. In a molecule with only carbons bonded by single bonds the charge is located near the carbon atoms, while for compounds with double and triple bonds, that is, in a conjugated molecule, the charges become more delocalized over the whole structure.

When the conjugated structures are excited by light, there is an intramolecular charge transfer that generates an induced electron dipole, $\vec{p}$, which is

proportional to the electronic delocalization. In other words, the movement of these electrons generates polarizabilities proportional to the conjugation length of the molecule.

1.3.2 Electron donor and acceptor groups

There is a strong correlation between intramolecular charge transfer and nonlinear absorptivity when seen from the point of view of electronic and photophysical processes.[1] In this sense, both the permanent dipole moment from the ground state as well as the dipole moment of the transitions from the ground state to excited states, are considered important factors for the multiphotonic processes.

To synthesize a compound with high nonlinearity, adding electron donor and acceptor groups to the π-conjugated material is essential. Since the intramolecular charge transfer process leads to polarizability, the addition of elements with electrons and others that need electrons is necessary. The conjugation length between these added elements is also important, since it leads to a large separation of charges. Figure 1.1 shows a representative diagram of a structure containing an electron donor (D) group and an electron acceptor (A) group, usually called a push-pull structure.[44-45] In this diagram, a photon irradiates the molecule and leads to an intramolecular charge transfer, which induces a dipole moment in the D-π-A direction. This increases the molecular polarizability of the compound, and, therefore, increases the multiphoton absorption cross-section.

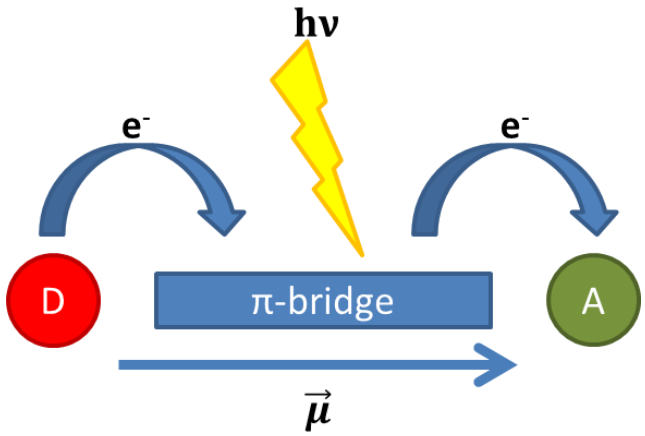

Figure 1.7 – Representative diagram of a push-pull structure irradiated by a photon.
Source: By the author.

Push-pull structures can be divided in two types depending on the direction of the intramolecular charge transfer. It is called a type I structure if the charge moves from the side groups to the center of the molecule, or type II if it moves from the center to the extremities instead.

Therefore, there are three main components for synthesizing compounds with high multiphoton absorption cross-sections: a strong electron donor group (D); a polarized π-conjugated structure; and a strong electron acceptor group (A).

1.3.3 Molecular planarity degree

The co-planarity is also a relevant factor for the efficiency of the intramolecular charge transfer. For example, the addition of an electron donor or acceptor at the extremity of a π-conjugated compound might worsen the nonlinear effect instead of increasing it. There might be an influence in the two-photon absorption cross-section of a compound depending on the number of *para* or *meta* (shown in Figure 1.8) bonds in the π-conjugated structure, as studied by Lee et al.[46] in a Donor-π-Acceptor type of structure. They studied four kinds of compounds with differences only in the position of the ligand in the π-conjugated structure. Depending on the combination between para and meta bonds introduced in the π-conjugated structure, a huge difference was noticed in the 2PA cross-section. For a compound with a *para* bond, the cross-section was ten times smaller than for the compound with two *meta* bonds. This is caused by a break in the conjugation generated by the introduction of donor and acceptor groups in a non-planar configuration, which diminishes the electronic mobility. Although the configurations were calculated, external effects such as temperature and the solvent polarity can also change the electronic delocalization, changing the dipole transition and the 2PA cross-section as a consequence.

De Boni et al. showed an interesting study on how the temperature might affect the 2PA cross-section of azoaromatic compounds. They showed that the increase of temperature on a compound with the DR19 chromophore changes the angle between the azo and the aromatic ring, which makes the 2PA cross-section get smaller. They observed a rate of loss of 2 GM/ºC, and used quantum chemistry

calculations to verify that the cause was the change in the angle between the components of the molecule.

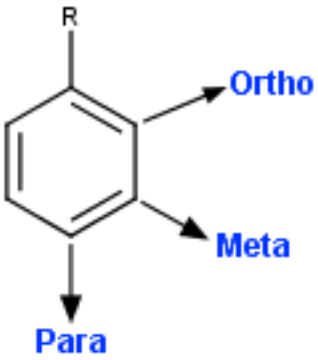

Figure 1.8 – Para, meta and ortho positions on an organic molecule. R is any group connected to the benzene.

Source: By the author.

1.4 Dissertation proposal

During the period of the PhD, we studied the two-photon absorption cross-section spectra of different organic compounds with particular characteristics. These spectra were analyzed quantitative and qualitatively to properly understand the nature of the nonlinearity for each set of samples, thus establishing relationships between the molecular structure and nonlinear optical properties. Here, we studied three different types of compounds.

The first kind of compound studied is based on a fluorenone. Fluorenones are molecules that usually present regular two-photon absorption cross-sections and low cytotoxicity, being commonly studied for two-photon microscopy applications. We investigated seven new compounds with a fluorenone core and different ligands attached to its extremities, comparing their measured two-photon absorption cross-section maxima with ones calculated by DFT (Density Functional Theory). Since their main application also requires high fluorescence, we also present a quantum yield study of the compounds.

Borondipyrromethene (BODIPY) derivatives have been drawing interest because of their wide range of applications, such as light-harvesting systems and laser dyes. The second kind of compound studied in this dissertation is a set of five

different BODIPY-like compounds with short conjugation length, with either a single or two electron donor or acceptor attached to its extremities. Their 2PA spectra were compared to ones calculated by DFT, which also allowed understanding the molecular polarizability within each studied compound and its relationship with the optical properties.

Lastly, four different chiral polymers based on binaphthalene were studied. Because of their chirality, such compounds might display different nonlinear behavior depending on the light polarization, which can be related to contributions from electric dipole moment, electric quadrupole moment and magnetic dipole.[47-48] Therefore, studies with polarization control were performed in these polymers.

In summary, the dissertation is organized as follows. In Chapter 2, the two-photon absorption process is described theoretically using a semi-classical light/matter interaction treatment. In Chapter 3, the materials studied along the dissertation are described, as well as the experimental procedures. Chapter 4 shows the results obtained for the fluorenone-base compounds, with the 2PA cross-section spectra for each molecule, as well as their quantum yields, which are compared with theoretical results carried out by DFT. The BODIPY-like compounds results are shown in Chapter 5, which presents the 2PA spectra obtained through the Z-Scan measurements, as well as the ones calculated through DFT. In Chapter 6 we present the chiral polymers study, specifically their 2PA with linear polarization and the circular-linear dichroism measurements. Finally, Chapter 7 summarizes the results obtained in the dissertation with the final considerations of this work.

2 MULTI-PHOTON ABSORPTION FUNDAMENTS

The multi-photon absorption concept was proposed for the first time by Marie Göppert-Mayer[4] in 1931. Since the effect only happens with high light intensities, it could only be experimentally verified years later, in 1961, after the development of the laser.

Generally speaking, the two-photon absorption process depends on the incident light intensity, and has its absorption coefficient described as[2]

$$\alpha(I) = \alpha_0 + \beta I \tag{2.1}$$

where α_0 is the linear absorption coefficient, *I* is the incident light intensity and β is the two-photon absorption coefficient. The β coefficient is important since it is related to the two-photon absorption cross-section through

$$\sigma_{2PA} = \frac{\hbar\omega\beta}{2N} \tag{2.2}$$

with N being the number of molecules/cm^3 of the sample and ω the angular frequency of the incident wave.

The two-photon absorption cross-section can also be calculated from other characteristics of the studied compound, such as its dipole moment, considering the number of the states that are accessible through the two-photon absorption. These calculations will be detailed in section 2.1. Further on, depending of the molecular structure of the studied compound, the cross-section might be dependent on the light polarization, which demands the addition of certain conditions that take this change in consideration. This shall be studied in section 2.2.

2.1 Two-photon absorption

The two-photon absorption occurs when a sample excited by an electromagnetic wave absorbs two photons simultaneously to reach its excited state.

Considering that the wave function follows the time-dependent Schrödinger's equation, given by

$$i\hbar \frac{d\psi(r,t)}{dt} = \hat{H}\psi(r,t) \tag{2.3}$$

We can describe the interaction of the electromagnetic field $\vec{A}$ with the electron through the simplified Hamiltonian[4]

$$H = H_0 + V(t) = \frac{\vec{p}^2}{2m} + V_0 - \frac{e}{m}\vec{A}(t)\cdot\vec{p} \tag{2.4}$$

where *m* is the electron mass, *e* the electron charge, $\vec{p}$ is the non-perturbative momentum and V_0 is the electric potential without the applied field. $\vec{A}(t)\cdot\vec{p}$ is the term that represents the momentum that can be transferred from the field to the electron. Considering a monochromatic plane wave as the incident field, which is the case for a laser beam,

$$\vec{A} = \frac{A_0}{2} e^{i(-\vec{k}\cdot\vec{r}+\omega t)}\hat{e} + c.c. \tag{2.5}$$

with A_0 being the wave amplitude, $\vec{k}$ is the wave vector, ω is its frequency and $\hat{e}$ is the versor which describes light polarization.

If we consider that $\vec{A}(t)\cdot\vec{p}$ is much smaller than the non-perturbative Hamiltonian, H_0, and that it acts for a very short time (t→0), we can use the time dependent perturbation theory to solve Eq. (2.4).

$$\frac{dC_f^{(N)}(t)}{dt} = \frac{1}{i\hbar}\sum_i C_i^{N-1}(t)\, V_{fi}(t) e^{-i\omega_{if}t} \tag{2.6}$$

in which $\omega_{fi} = (E_f^{(0)} - E_i^{(0)})/\hbar$, and C_i and C_f describe the probability of the particle being in its initial or final state, respectively. The sum is over all electronic states of the material, that is, over the initial state (g), intermediate states (m) and the final

state (f). A scheme showing these states can be seen in Figure 2.1, in which $\vec{\mu}_{fi}$ is the dipole moment of the transition.

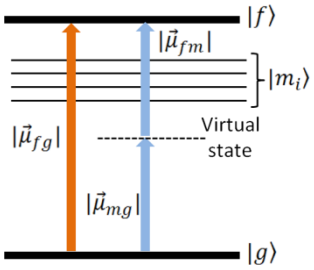

Figure 2.1 - Representative diagram of the one-photon absorption (orange line) and of two-photon absorption (blue lines).
Source: By the author.

Obtaining $C_f(t)$ exactly in Eq. (2.6) is, in general, a difficult task and, therefore, usually a perturbative expansion is used to solve it; in this case, we approximate $C_f(t) = C_f^{(0)} + C_f^{(1)} + C_f^{(2)} + \cdots$. Each term of this expression is related to an absorption process. Assuming there are α states allowed by one-photon absorption (1PA) and β states allowed by two-photon absorption (2PA), and considering that the system is in its ground state $|g\rangle$ in the absence of magnetic fields, we have that

$$C_i^{(0)}(t) = 1, i = g$$
$$C_i^{(0)}(t) = 0, i \neq g \tag{2.7}$$

To simplify our calculations, it is convenient to rewrite the term $V_{fi}(t)$. First, we use a dipole approximation by expanding the plane wave term as

$$e^{-i\vec{k}\cdot\vec{r}} = 1 + \frac{i\omega n}{c}\vec{n}\cdot\vec{r} + \cdots \tag{2.8}$$

Then, by rewriting $\vec{p}$ as $\vec{r}$, $V_{fi}(t)$ can be written as

$$V_{fi}(t) = \frac{A_0\omega_{fi}e^{i\omega t}}{2}\hat{e}\cdot\langle f|e\vec{r}|i\rangle + c.c. \tag{2.9}$$

We can find the term associated to the one-photon absorption, $C_\alpha^{(1)}$, by replacing $C_i^{(0)}$in Eq.**Erro! Fonte de referência não encontrada.** (2.6), **Erro! Fonte de referência não encontrada.Erro! Fonte de referência não encontrada.**

$$C_\alpha^{(1)}(t) = \frac{A_0}{2\hbar}\sum_\alpha \omega_{\alpha g}\hat{e}\cdot\langle\alpha|e\vec{r}|g\rangle\left(\frac{1-e^{-i(\omega_{\alpha g}-\omega)t}}{i(\omega_{\alpha g}-\omega)}\right) + \frac{A_0}{2\hbar}\sum_\alpha \omega_{\alpha g}\hat{e}\cdot\langle\alpha|e\vec{r}|g\rangle\left(\frac{1-e^{+i(\omega_{\alpha g}-\omega)t}}{-i(\omega_{\alpha g}-\omega)}\right) \quad (2.10)$$

The $S_{\alpha g}^{(1)} = \sum_\alpha \omega_{\alpha g}\hat{e}\langle\alpha|e\vec{r}|g\rangle$ term is the tensor which describes the one-photon absorption process. The sum in α indicates the sum over all electronic states allowed by 1PA.

Analogously we can find the $C_f^{(2)}$ term that corresponds to the two-photon absorption process. For this, we consider that there is no linear absorption. In this process, the first photon excites the electron to an intermediate virtual state (m), and the other one promotes the excitation from the virtual state to the final state (f). Therefore, replacing Eq. (2.8) in Eq. (2.6) without the complex conjugated term, we have that

$$C_\beta^{(2)}(t) = \left(\frac{A_0}{2\hbar}\right)^2\sum_{\alpha,\beta}\omega_{\alpha g}\omega_{\beta\alpha}\,\frac{(\hat{e}\cdot\langle\beta|e\vec{r}|\alpha\rangle)(\langle\alpha|e\vec{r}|g\rangle\cdot\hat{e})}{\omega_{\alpha g}-\omega}\left(\frac{1-e^{-i(\omega_{\beta g}-2\omega)t}}{i(\omega_{\beta g}-2\omega)}\right) \quad (2.11)$$

where $S_{\beta g}^{(2)} = \sum_{\alpha,\beta}\omega_{\alpha g}\omega_{\beta\alpha}\,\frac{(\hat{e}\cdot\langle\beta|e\vec{r}|\alpha\rangle)(\langle\alpha|e\vec{r}|g\rangle\cdot\hat{e})}{\omega_{\alpha g}-\omega}$ is the tensor which describes the 2PA. The $\langle f|e\vec{r}|i\rangle$ terms are the transition dipole moments, being written as $\vec{\mu}_{fi}$. In this case, the sum represents the summation over all electronic states allowed by one and two photon absorption.

From these coefficients it is possible to find the two-photon absorption cross-section, which is a purely molecular parameter. For that, it is necessary to calculate the probability (P_{2PA}) of the process occurring, defined as the square of the absolute value of the perturbative expansion coefficient. Therefore,

$$P_{2PA} = \left|C_{\beta}^{(2)}(t)\right|^2 = \left(\frac{A_0}{2\hbar}\right)^4 \left|S_{\beta g}^{(2)}\right|^2 4\frac{sen^2[(\omega_{\beta g} - 2\omega)t/2]}{(\omega_{\beta g} - 2\omega)^2} \quad (2.12)$$

Considering the probability after the interaction, that is, using the limit for $t \to \infty$,

$$P_{2PA} = \left(\frac{A_0}{2\hbar}\right)^4 \left|S_{\beta g}^{(2)}\right|^2 2\pi t\delta(\omega_{\beta g} - 2\omega) \quad (2.13)$$

From this probability, we can write the equations that describe the population promoted to the excited states $N_f(t) = N_i(0)\left|C_f^{(N)}\right|^2$.[49] However, it is necessary to consider the spectral width of the laser pulse ($g_L(\omega)$) and of the populated electronic state due to the molecular vibrations ($g_f(\omega)$), given by functions that satisfy

$$\int g_f(\omega_{fg})d\omega_{fg} = \int g_L(\omega)d\omega = 1 \quad (2.14)$$

The promoted population can be written as

$$N_f(t) = N_i(0)\iint_0^{\infty} \left|C_f^{(N)}\right|^2 g_f(\omega_{fg})g_L(\omega)\ d\omega_{fg}d\omega \quad (2.15)$$

Assuming that $g_L(\omega) << g_f(\omega_{fg})$,

$$\begin{aligned} N_{\beta}(t) = N_g(0)\left(\frac{A_0}{2\hbar}\right)^4 \left|S_{\beta g}^{(2)}\right|^2 2\pi t \int_0^{\infty} \delta(\omega_{\beta g} - 2\omega)\, g_{\beta}(\omega_{\beta g})d\omega_{\beta g} = \\ = N_g(0)\left(\frac{A_0}{2\hbar}\right)^4 \left|S_{\beta g}^{(2)}\right|^2 2\pi t g_{\beta}(2\omega) \end{aligned} \quad (2.16)$$

It is convenient to rewrite this equation as a rate equation, since it has a linear dependence on time, and we know that the cross-section is directly related to it. Therefore,

$$W_{\beta g}^{(2)} = \frac{1}{N_\beta(0)}\frac{dN_\beta(t)}{dt} = 2\pi\left(\frac{A_0}{2\hbar}\right)^4 \omega^4 \left|\sum_{\alpha,\beta}\frac{(\hat{e}\cdot\vec{\mu}_{\beta\alpha})(\vec{\mu}_{\alpha g}\cdot\hat{e})}{\omega_{\alpha g}-\omega}\right|^2 g_\beta(2\omega) \qquad (2.17)$$

We can find the cross-section of the photon absorption by relating the transition rate and the photon flux to the power of the number of photons involved in the desired multi or single photon process. Since we are exclusively interested in the 2PA, we have that

$$\sigma_{\beta g}^{(2)} = \frac{2W_{\beta g}^{(2)}}{\phi^2} \qquad (2.18)$$

In CGS, the flux is given by $\phi = \frac{nc\omega^2 {A_0}^2}{8\pi\hbar\omega}$. Thus,

$$\sigma_{\beta g}^{(2)} = 2\frac{(2\pi)^5}{(nhc)^2}\omega^2 \left|\sum_{\alpha,\beta}\frac{(\hat{e}\cdot\vec{\mu}_{\beta\alpha})(\vec{\mu}_{\alpha g}\cdot\hat{e})}{\omega_{\alpha g}-\omega}\right|^2 g_\beta(2\omega) \qquad (2.19)$$

However, we can see from Eq. (2.19) that its behavior is not physical when $\omega=\omega_{\alpha g}$. This can be avoided if we add a phenomenological dumping factor, $\Gamma_{fi}(\omega)$, associated to the line width of the electronic state. Usually a local field factor is also added, $L = \frac{3n^2}{2n^2+1}$, which is the Onsager local field factor, where *n* is the refractive index of the solvent used. This factor is used to take the interaction of the chromophore with the solvent into account. Therefore, Eq. (2.19) becomes

$$\sigma_{\beta g}^{(2)} = 2\frac{(2\pi)^5}{(nhc)^2}\omega^2 L^4 \left|\sum_{\alpha,\beta}\frac{(\hat{e}\cdot\vec{\mu}_{\beta\alpha})(\vec{\mu}_{\alpha g}\cdot\hat{e})}{(\omega_{\alpha g}-\omega)-i\Gamma_{\alpha g}(\omega)}\right|^2 g_\beta(2\omega) \qquad (2.20)$$

The cross-section is usually represented in Göppert-Mayer (GM) units, which is equivalent to 10^{-50} $cm^4.s.photons^{-1}$.[4]

2.2 Selection rules

From Eq. (2.19), the intensity of the two-photon absorption transition is given by

$$S_{\beta g}^{(2)} = \sum_{\alpha,\beta} \frac{\omega_{\alpha g}\omega_{\beta\alpha}(\hat{e}\cdot\langle\beta|\vec{\mu}|\alpha\rangle)(\langle\alpha|\vec{\mu}|g\rangle\cdot\hat{e})}{(\omega_{\alpha g}-\omega)} \tag{2.21}$$

Centrosymmetric molecules have symmetry characteristics that limit the transitions accessible by multiphotonic processes. This can be understood comparing this kind of molecules to a finite well problem of quantum mechanics. The solution for this kind of problem depends of the parity of the wavefunctions of the involved states. They can have gerade or ungerade symmetries, and obey the following relations[41]:

$$\begin{aligned} \psi_g(r) &= \psi_g(-r) \\ \psi_u(r) &= -\psi_u(-r) \end{aligned} \tag{2.22}$$

There are two possible situations: the ground state has the same parity of the excited state, or they have different parities. From Eq. (2.21), it is clear that if the intermediate state has the same parity than either the ground or excited state, one of the terms will be equal to zero. However, if the intermediate state has its parity different from both ground and excited state, $S_{\beta g}^{(2)} \neq 0$, the transition will be allowed. This shows that two-photon absorption is only allowed if the ground and excited state have the same parity, that is, if the transition happens between *gerade* → *gerade* or *ungerade* → *ungerade*. In the dipole approximation, 2PA transitions between states of different parities are not allowed.

For one-photon absorption, the selection rules are the opposite than the ones from two-photon absorption. That means that only transitions between different parities are allowed, such as *gerade* → *ungerade* or *ungerade* → *gerade*. This shows that 2PA spectroscopy is complimentary to 1PA spectroscopy, allowing the discovery of different characteristics of the studied samples.

However, these selection rules are only valid for centrosymmetric molecules. If the molecule does not present a center of symmetry, all transitions might be allowed for either odd or even multiphoton processes. Also, for centrosymmetric molecules there might be some forbidden states that are still weakly allowed, but their 2PA cross-section will be much lower than the ones for the allowed transitions.[50]

2.3 Sum-over-states model

From Eq. (2.20), we can develop a model to analyze the obtained spectra for the two-photon absorption cross-section, called the **sum-over-states model** (SOS). For that, we first assume that we have a centrosymmetric molecule whose static dipole moment is equal to zero ($\vec{\mu}_{gg} = \vec{\mu}_{ff} = 0$) in a three energy-level system. In this case, we have a ground state (g), a 1PA allowed state ($\alpha = m$) and a 2PA allowed state ($\beta = f$). This system is illustrated in Figure 2.2.

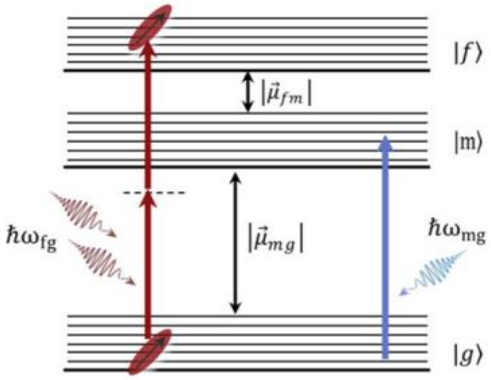

Figure 2.2 - Representative model for the sum-over-states in a centrosymmetric molecule under a two-photon absorption process.
Source: VIVAS et al.[51]

With these considerations, Eq. (2.20) becomes

$$\sigma_{fg}^{(2)} = 2\frac{(2\pi)^5}{(nhc)^2}\omega^2 L^4 \left|\frac{(\hat{e}\cdot\vec{\mu}_{fm})(\vec{\mu}_{mg}\cdot\hat{e})}{(\omega_{mg}-\omega)+i\Gamma_{mg}(\omega)}\right|^2 g_f(2\omega) \qquad (2.23)$$

The cross-section is dependent of the light polarization, as will be seen in section 2.3. To apply our model, however, we will consider an isotropic mean, like a

solution, where the average over all directions of the molecular dipole moment for a linearly polarized beam leads to[52]

$$\langle\left(\hat{e}\cdot\vec{\mu}_{mg}\right)^2\rangle=\frac{1}{3}\left|\vec{\mu}_{mg}\right|^2$$
$$\langle\left(\hat{e}\cdot\vec{\mu}_{fm}\right)^2\left(\vec{\mu}_{mg}\cdot\hat{e}\right)^2\rangle=\frac{2cos^2(\xi)+1}{15}\left|\vec{\mu}_{mg}\right|^2\left|\vec{\mu}_{fm}\right|^2 \quad (2.24)$$

where ξ is the angle between the dipole moments. Here, we adopted the Lorentzian line width, given by

$$g_f(2\omega)=\frac{\Gamma_{fg}(2\omega)}{\pi[\left(\omega_{fg}-2\omega\right)^2+\Gamma_{fg}(2\omega)^2]} \quad (2.25)$$

Replacing equations (**2.24**) and (2.25) in Eq. (2.23), we obtain

$$\sigma_{fg}^{(2)}=\frac{2(2\pi)^5}{15\pi(nhc)^2}L^4[2cos^2(\xi)+1]\left[\frac{\omega^2}{[\left(\omega_{mg}-\omega\right)^2+\Gamma_{mg}(\omega)^2]}\frac{\left|\vec{\mu}_{mg}\right|^2\left|\vec{\mu}_{fm}\right|^2\Gamma_{fg}(2\omega)}{[\left(\omega_{fg}-\omega\right)^2+\Gamma_{fg}(\omega)^2]}\right] \quad (2.26)$$

The term $\frac{\omega^2}{[\left(\omega_{mg}-\omega\right)^2+\Gamma_{mg}(\omega)^2]}$ of Eq. (2.26) shows that when there is a real intermediate state allowed by one-photon absorption, if the transition energy is close to the incident photon energy, there will be a pronounced effect called resonant enhancement. Usually we consider that the dipole moments are parallel, in other words, ξ = 0, giving

$$\sigma_{fg}^{(2)}=\frac{2(2\pi)^5}{5\pi(nhc)^2}L^4\left[\frac{\omega^2}{[\left(\omega_{mg}-\omega\right)^2+\Gamma_{mg}(\omega)^2]}\frac{\left|\vec{\mu}_{mg}\right|^2\left|\vec{\mu}_{fm}\right|^2\Gamma_{fg}(2\omega)}{[\left(\omega_{fg}-\omega\right)^2+\Gamma_{fg}(\omega)^2]}\right] \quad (2.27)$$

Now considering non centrosymmetric molecules, whose energy level model can be seen in Figure 2.3, they will have ground and final states with static dipole moments different from zero, that is, $\vec{\mu}_{gg}\neq 0, \vec{\mu}_{ff}\neq 0$. Therefore, Eq. (2.20) becomes

$$\sigma_{fg}^{(2)} = \frac{2}{5}\frac{(2\pi)^5}{(nhc)^2}\omega^2 L^4 \left| \frac{(\hat{e}\cdot\vec{\mu}_{gg})(\vec{\mu}_{fg}\cdot\hat{e})}{-\omega} + \frac{(\hat{e}\cdot\vec{\mu}_{mg})(\vec{\mu}_{fm}\cdot\hat{e})}{(\omega_{mg}-\omega)+i\Gamma_{mg}(\omega)} + \frac{(\hat{e}\cdot\vec{\mu}_{fg})(\vec{\mu}_{ff}\cdot\hat{e})}{(\omega_{fg}-\omega)+i\Gamma_{fg}(\omega)} \right|^2 g_f(2\omega) \quad (2.28)$$

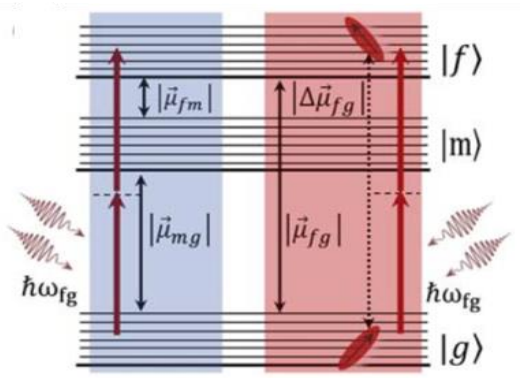

Figure 2.3 - Representative model for the sum-over-states of a non centrosymmetric molecule under a two-photon absorption process.
Source: VIVAS et al.[51]

The permanent dipole moments $\vec{\mu}_{gg}$ and $\vec{\mu}_{ff}$ are different from zero in this case, just as $\vec{\mu}_{fg}$. We can simplify the equation by considering that the final energy level will never be resonant with the excitation photons in a degenerate 2PA process, in other words, $\omega_{fg}-\omega \gg \Gamma_{fg}(\omega)$. In a degenerate process, $\omega_{fg}-\omega = 2\omega-\omega = \omega$, and assuming $\Delta\vec{\mu}_{fg} = \vec{\mu}_{ff} - \vec{\mu}_{gg}$, Eq. (2.28) becomes

$$\sigma_{fg}^{(2)} = \frac{2}{5}\frac{(2\pi)^5}{(nhc)^2}\omega^2 L^4 \left| \frac{(\hat{e}\cdot\vec{\mu}_{mg})(\vec{\mu}_{fm}\cdot\hat{e})}{(\omega_{mg}-\omega)+i\Gamma_{mg}(\omega)} + \frac{(\hat{e}\cdot\Delta\vec{\mu}_{fg})(\vec{\mu}_{fg}\cdot\hat{e})}{\omega} \right|^2 g_f(2\omega) \quad (2.29)$$

Developing the squared absolute value, we have

$$\sigma_{fg}^{(2)} = \frac{2}{5}\frac{(2\pi)^5}{(nhc)^2}\omega^2 L^4 \left[\frac{(\hat{e}\cdot\vec{\mu}_{fg})^2(\Delta\vec{\mu}_{fg}\cdot\hat{e})^2}{\omega^2} + \frac{(\hat{e}\cdot\vec{\mu}_{mg})^2(\vec{\mu}_{fm}\cdot\hat{e})^2}{(\omega_{mg}-\omega)^2+\Gamma_{mg}(\omega)^2} + 2\frac{(\omega_{mg}-\omega)}{\omega}\frac{(\vec{\mu}_{fm}\cdot\hat{e})(\hat{e}\cdot\vec{\mu}_{mg})(\vec{\mu}_{fg}\cdot\hat{e})(\Delta\vec{\mu}_{mg}\cdot\hat{e})}{(\omega_{mg}-\omega)^2+\Gamma_{mg}(\omega)^2} \right] g_f(2\omega) \quad (2.30)$$

Each term from Eq. (2.30) can be associated with a different phenomenon. The first term describes a two-level transition between the ground and final state, with a change in its permanent dipole moment related to the lowest energy multiphotonic transition, called a polar term. The second term represents a three-level transition, between the intermediate state (m) with the ground (g) and final (f) states, in which the intermediate state is allowed by both one and two-photon absorption. This term shows the contribution of the resonant enhancement. The third term describes interference between the two previous contributions, becoming null when the intermediate state is halfway between the final excited state and the ground state.

We can find the dipole moments through the linear absorption of the studied material through the formula[53]

$$\left|\vec{\mu}_{if}\right|^2 = \frac{3 \times 10^3 \ln(10)\, hc}{(2\pi)^3 N_A} \frac{n}{L^2} \frac{\varepsilon^{max}}{\omega_{if}\theta_{if}} \tag{2.31}$$

in which ε^{max} is the maximum molar absorptivity, N_A is the Avogadro number and $\theta_{01} = \sqrt{4\ln(2)/\pi\Gamma_{if}^2}$ is the maximum value of the normalized Gaussian line width.

2.4 Nonlinear Dichroism (Linear-circular and circular)

The study of the two-photon absorption with polarization control allows discovering sample properties that would not be observed using only linearly polarized light, such as the angle between dipole moments,[52] symmetry between excited states[54] and, for chiral samples, it enables obtaining information about the electric dipole and magnetic quadrupole.[47-48,55]

The two-photon absorption circular-linear dichroism (2PACLD) is a third order effect dominated by the electric dipole, and is given by

$$\Delta\sigma_{CLD}^{2PA} = \frac{\Omega_{CLD}^{A2F} - 1}{\Omega_{CLD}^{A2F} + 1} \tag{2.32}$$

in which

$$\Omega_{CLD}^{2PA} = \frac{\sigma_{CP}^{2PA}(\lambda)}{\sigma_{LP}^{2PA}(\lambda)} \tag{2.33}$$

and $\sigma_{CP}^{2PA}(\lambda)$ is the 2PA cross-section of the sample under circularly polarized light and $\sigma_{LP}^{2PA}(\lambda)$ the 2PA cross-section under linearly polarized light.

Differences have been previously observed[56] in samples submitted to circularly polarized light and linearly polarized light. These differences are associated with 2PA tensor elements and can be related to the electronic states symmetry, as well as to the angle between electric dipole moments.

The way that the 2PACLD spectrum behaves brings information about the bands allowed by two-photon absorption. According to Vivas et al.[56] for a sample that has only a single accessible electronic state for 2PA, Ω_{CLD}^{2PA} will be constant along the spectrum (Figure 2-4a), while for two or more electronic states Ω_{CLD}^{2PA} varies between two constant values (Figure 2-4b), having an intermediate region where the value either increase or decrease depending of the symmetry between these states. If the variation is negative, the final state has the same symmetry as the ground state, and if it is positive, they have different symmetries.

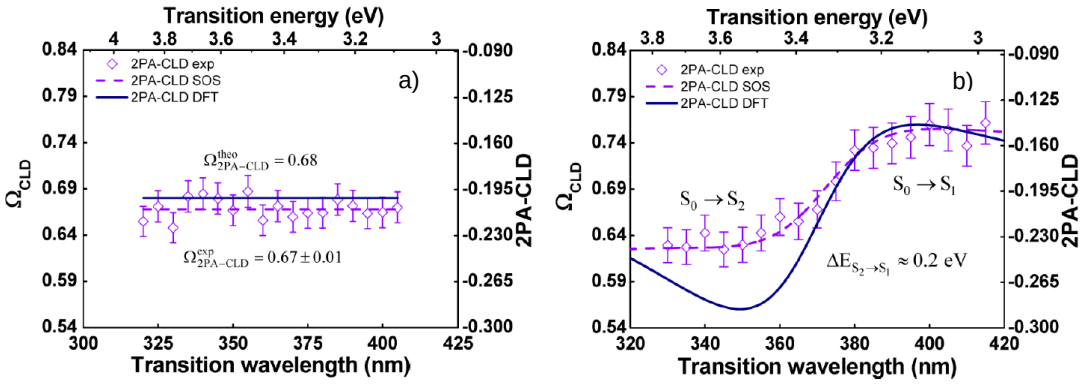

Figure 2-4 - $\boldsymbol{\Omega_{CLD}^{2PA}}$ for samples with (a) a single allowed electronic state and (b) two or more allowed electronic states.

Source: VIVAS et al.[56]

When one considers light polarization in two-photon absorption, this must be a part of the simulation and used models, such as the sum-over-states model.

Following the perturbation theory used in section 2.1, it is necessary to make an orientational average over all the possible directions of the dipole moment. Therefore, using the Euler formula, the factor $S_{\alpha\beta}^{(n)}$ from Eq. (2.16) becomes

$$S_{\alpha\beta}^{(n)} = \frac{1}{8\pi^2}\int_0^{2\pi} d\phi \int_0^{2\pi} d\psi \int_0^{\pi} sin(\theta) \sum_{\alpha,\beta} \left(\hat{e}.\overrightarrow{\mu_{fg}^{\alpha\beta}}\right)\left(\hat{e}.\overrightarrow{\mu_{fg}^{\alpha\beta}}\right)^* \left(\Delta\overrightarrow{\mu_{fg}^{\alpha\beta}}.\hat{e}\right)\left(\Delta\overrightarrow{\mu_{fg}^{\alpha\beta}}.\hat{e}\right)^* d\theta \quad (2.34)$$

where $\overrightarrow{\mu_{fg}^{\alpha\beta}}$ is the magnetic dipole moment between the ground state *g* and the final state *f*, *ê* is the versor that indicates the direction of the polarized light and θ is the angle between the dipole moments. Depending on the number of states, the number of terms in the sum varies, just like the integral over the angle θ. If the sample is centrosymmetric, the integral will become null, and there will not be an allowed two-photon absorption band. For the centrosymmetric case, there are mainly two kinds of systems studied, one of two-energy levels and one of three-energy levels.

For two energy-level systems there are only the final state *f* and the ground state *g*. Therefore, the sum presents two terms and the cross-section can be written as

$$\sigma_{fg}^{2PA}(\omega) = \frac{2(2\pi)^5}{30(nhc)^2} L^4 P\left(\theta_{\vec{\mu}_{fg}\Delta\vec{\mu}_{fg}}\right)\left|\vec{\mu}_{fg}\right|^2\left|\Delta\vec{\mu}_{fg}\right|^2 g_{fg}(2\omega) \quad (2.35)$$

Where

$$\eta = P_{Linear} = 2\left(2cos^2\left(\theta_{\vec{\mu}_{fg}\Delta\vec{\mu}_{fg}}\right)+1\right)$$
$$\tau = P_{Circular} = \left(cos^2\left(\theta_{\vec{\mu}_{fg}\Delta\vec{\mu}_{fg}}\right)+3\right) \quad (2.36)$$

Applying Eqs. (2.35) and (**2.36**) on Eq. (2.33), we obtain

$$\Omega_{CLD}^{2PA} = \frac{cos^2\left(\theta_{\vec{\mu}_{fg}\Delta\vec{\mu}_{fg}}\right)+3}{2\left(2cos^2\left(\theta_{\vec{\mu}_{fg}\Delta\vec{\mu}_{fg}}\right)+1\right)} \quad (2.37)$$

From Eq. (2.37) it is possible to notice that Ω_{CLD}^{2PA} must be within 0.667 and 1.5 for any angle and is independent of the wavelength. Therefore, for a two-level system, the expected Ω_{CLD}^{2PA} will have its behavior as seen in Figure 2-4a.

For a three level system, we will have transitions between the ground state *g* (0) and an intermediate final state *e'* (1), as well as a possible transition between the ground state *g* and the final state *f* (2). Therefore,

$$\sigma_{02}^{2PA}(\omega) = \frac{2(2\pi)^5}{30(nhc)^2} L^4 \omega^2 \left| \sum_{\alpha\beta} \left(\frac{(\hat{e}.\vec{\mu}_{01})(\vec{\mu}_{02}.\hat{e})}{(\omega_{01} - \omega) + i\Gamma_{01}(\omega)} + \frac{(\hat{e}.\vec{\mu}_{02})(\Delta\vec{\mu}_{02}.\hat{e})}{\omega} \right) \right|^2 g_{02}(\omega) \tag{2.38}$$

Using the Euler integral for each term of Eq. (2.38), we have that

$$\begin{aligned} &\sigma_{02}^{2PA}(\omega) \\ &= \frac{2(2\pi)^5}{30(nhc)^2} L^4 \left[P\left(\theta_{\vec{\mu}_{02}\Delta\vec{\mu}_{02}}\right) |\vec{\mu}_{02}|^2 |\Delta\vec{\mu}_{02}|^2 + R(\omega) P\left(\theta_{\vec{\mu}_{01}\vec{\mu}_{12}}\right) |\vec{\mu}_{01}|^2 |\vec{\mu}_{12}|^2 \right. \\ &\left. + 2R(\omega) \frac{\omega_{01} - \omega}{\omega} P(\theta_{\vec{\mu}_{01}\vec{\mu}_{12}\vec{\mu}_{02}\Delta\vec{\mu}_{02}}) |\vec{\mu}_{01}||\vec{\mu}_{12}||\vec{\mu}_{02}||\Delta\vec{\mu}_{02}| \right] g_{02}(\omega) \end{aligned} \tag{2.39}$$

where R(ω) is the resonant enhancement factor given by

$$R(\omega) = \frac{\omega^2}{(\omega_{01} - \omega)^2 + {\Gamma_{01}}^2(\omega)} \tag{2.40}$$

and the angles for linearly polarized light are given by

$$\begin{aligned} \rho = \ P_L\left(\theta_{\vec{\mu}_{02}\Delta\vec{\mu}_{02}}\right) &= 2(2cos^2\left(\theta_{\vec{\mu}_{02}\Delta\vec{\mu}_{02}}\right) + 1) \\ \kappa = \ P_L\left(\theta_{\vec{\mu}_{01}\vec{\mu}_{12}}\right) &= 2(2cos^2\left(\theta_{\vec{\mu}_{01}\vec{\mu}_{12}}\right) + 1) \\ \xi = \ P_L\left(\theta_{\vec{\mu}_{01}\vec{\mu}_{12}\vec{\mu}_{02}\Delta\vec{\mu}_{02}}\right) &= [2(\cos\left(\theta_{\vec{\mu}_{02}\Delta\vec{\mu}_{02}}\right)\cos\left(\theta_{\vec{\mu}_{01}\vec{\mu}_{12}}\right) + \\ \cos\left(\theta_{\vec{\mu}_{12}\Delta\vec{\mu}_{02}}\right)\cos\left(\theta_{\vec{\mu}_{01}\vec{\mu}_{02}}\right) + \cos\left(\theta_{\vec{\mu}_{01}\Delta\vec{\mu}_{02}}\right)\cos\left(\theta_{\vec{\mu}_{02}\vec{\mu}_{12}}\right))] \end{aligned} \tag{2.41}$$

while for circularly polarized light Eqs. (**2.41**) are written as

$$\begin{aligned}\psi = P_C\left(\theta_{\vec{\mu}_{02}\Delta\vec{\mu}_{02}}\right) = cos^2\left(\theta_{\vec{\mu}_{02}\Delta\vec{\mu}_{02}}\right) + 3 \\ \lambda = P_C\left(\theta_{\vec{\mu}_{01}\vec{\mu}_{12}}\right) = cos^2\left(\theta_{\vec{\mu}_{01}\vec{\mu}_{12}}\right) + 3 \\ \upsilon = P_C\left(\theta_{\vec{\mu}_{01}\vec{\mu}_{12}\vec{\mu}_{02}\Delta\vec{\mu}_{02}}\right) = [-2\cos\left(\theta_{\vec{\mu}_{02}\Delta\vec{\mu}_{02}}\right)\cos\left(\theta_{\vec{\mu}_{01}\vec{\mu}_{12}}\right) + \\ 3\cos\left(\theta_{\vec{\mu}_{12}\Delta\vec{\mu}_{02}}\right)\cos\left(\theta_{\vec{\mu}_{01}\vec{\mu}_{02}}\right) + 3\cos\left(\theta_{\vec{\mu}_{01}\Delta\vec{\mu}_{02}}\right)\cos\left(\theta_{\vec{\mu}_{02}\vec{\mu}_{12}}\right)]\end{aligned} \tag{2.42}$$

Through Eq. (2.39) it is possible to notice that there are three different contributions for the 2PA cross-section in a three-energy level system; one transition in a two-level sub-system, with $\Delta\vec{\mu}_{02} \neq 0$, one transition in three levels with a final excited state (S_2) and an intermediary state (S_1), responsible for the resonant enhancement and the interference between the two other excitation possibilities, whose contribution is very small if the photon energy is close to the real intermediary state. These three possibilities are exactly the same as in the sum-over-states model mentioned in section 2.3. In this case, the behavior of Ω_{CLD}^{2PA} is the one shown in Figure 2-4b, and the equation that describes it becomes

$$\Omega_{CLD}^{2PA} = \frac{\alpha\eta g_{01}(\omega) + \left[\beta\kappa + R(\omega)\chi\rho + 2R(\omega)\gamma\frac{\omega_{01}-\omega}{\omega}\xi\right]g_{02}(\omega)}{\alpha\tau g_{01}(\omega) + \left[\beta\psi + R(\omega)\chi\lambda + 2R(\omega)\gamma\frac{\omega_{01}-\omega}{\omega}\upsilon\right]g_{02}(\omega)} \tag{2.43}$$

where

$$\begin{aligned}\alpha = |\vec{\mu}_{01}|^2|\Delta\vec{\mu}_{01}|^2 \\ \beta = |\vec{\mu}_{02}|^2|\Delta\vec{\mu}_{02}|^2 \\ \chi = |\vec{\mu}_{01}|^2|\vec{\mu}_{12}|^2 \\ \gamma = |\vec{\mu}_{01}||\vec{\mu}_{12}||\vec{\mu}_{02}||\Delta\vec{\mu}_{02}|\end{aligned} \tag{2.44}$$

Parameters α, β, χ and γ can be obtained either from solvatochromic curves or from their linear absorption spectra,[53; 57] with

$$\left|\vec{\mu}_{gf}\right|^2 = \frac{3.10^3 \ln(10)\, hc}{(2\pi)^2 N_A} \frac{n}{L^2} \frac{\varepsilon_{gf}^{max}}{g_{gf}^{max} \omega_{gf}^{max}} \tag{2.45}$$

$$\left|\Delta\vec{\mu}_{gf}\right|^2 = \frac{5 N_A hc}{6.10^3 (2\pi)^3 \ln(10)} \frac{n}{L^2} \frac{\omega_{gf}^{max}}{\varepsilon_{gf}^{max}} \sigma_{gf}^{Max2PA}(\omega_{gf}) \tag{2.46}$$

where *h* is the Planck constant, *c* is the speed of light, *n* is the refractive index of the used solvent, *L* is the Onsager factor ($L = 3n^2/(2n^2+1)$), N_A is Avogadro's number, ε_{gf}^{max} is the maximum molar absorptivity of the material, g_{gf}^{max} is the line width of the transition corresponding to the largest molar absorptivity, ω_{gf}^{max} is the frequency where ε_{gf}^{max} occurs and $\sigma_{gf}^{Max2PA}(\omega_{gf})$ is the maximum 2PA cross-section for the frequency of the studied transition.

For optically active molecules, another nonlinear dichroism property might appear, which is the two-photon circular dichroism (2PA-CD). It is defined as[56]

$$\Delta\sigma_{CD}^{2PA}(\omega) = \sigma_L^{2PA}(\omega) - \sigma_R^{2PA}(\omega) \tag{2.47}$$

in which $\sigma_L^{2PA}(\omega)$ is the 2PA cross-section for left circularly polarized light and $\sigma_R^{2PA}(\omega)$ is the 2PA cross-section for right circularly polarized light. This value is very low for most molecules since it depends on the magnetic transition dipole moment and the electric transition quadrupole moment,[48,58] both much smaller than the dominant electric dipole moments in nonlinear transitions.

3 MATERIALS AND METHODS

The two-photon absorption study of organic compounds allows to characterize samples and find their possible nonlinear applications.

During the development of this dissertation, three different kinds of materials had their nonlinear properties studied: Fluorenone and BODIPY-like molecules, both with short conjugation length and few donor or acceptor components, and chiral polymers based on binaphthalene, which have long conjugation length and several donor or acceptor components around its main core.

3.1 Studied Molecules

3.1.1 Fluorenones

Fluorenone-based compounds have been advancing as replacement for fluorene compounds, which are known for large 2PA cross-sections.[59] Even though fluorenones compounds present, in general, lower 2PA cross-sections[60-61] than fluorene-based ones, their low cytotoxicity[62] and usually high fluorescence still make them interesting candidates for biological systems applications, such as fluorescent molecular probes to indicate nucleic acids, nitric oxide and pH, as well as to investigate living organelles in cells.

Since fluorenones also present high 2PA cross-sections in the near infra-red region[63] together with their previously mentioned characteristics, they have promising applications for two-photon fluorescence microscopy.[12] This tool has been valuable in the study of cell organelles since it provides high resolution three-dimensional images, being a non-invasive method that allows high quality images of living cells. These cells are stained by chromophores that present two-photon absorption in the spectral range of 700 – 1000 nm that are then submitted to the 2PA microscopy. Therefore, to increase the precision of the method, it is necessary that the chromophore presents a large 2PA cross-section within this range.

Here, we present five symmetrical fluorenone derivatives, with structures shown in Fig. 3.1. The fluorenone core is composed by the three rings shown in

black in Fig. 3.1, which has ligands attached to it to form the different compounds studied. F-benzothiophene (2,7-bis(benzo[b]thiophen-2-etinil)-9H-fluorenone), which has the fluorenone core connected to benzothiophene ligands on its extremes; F-cyano (4,4'-(9-oxo-9H-fluorenone-2,7-diil)bis(ethine-2,1-diil)dibenzonitrile), with CN connected to a phenyl group; F-phenyl (2,7-bis(feniletinil)-9H-fluorenone) , with only the phenyl groups on its extremes; F-thiophene (2,7-bis(thiophen-2-etinill)-9H-fluorenone), which has a thiophene group instead of a phenyl one; and F-methoxy (2,7-bis((4-methoxyfenil)etinil)-9H-fluorenone), that has a OCH_3 group connected to the phenyl group on each side. The compounds were provided by professor A.M. Simas group from Universidade Federal de Pernambuco.

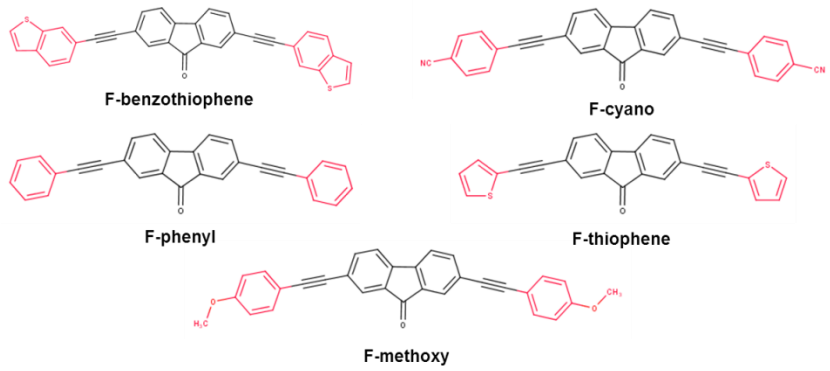

Figure 3.1 - Structures of the fluorenone compounds.
Source: By the author.

3.1.2 BODIPYs

Borondipyrromethene (BODIPY) derivatives have been drawing interest in the last years due to their wide range of potential applications,[64] such as light-harvesting systems,[65] agents in photodynamic therapy,[66] biomolecular labels,[16,67] laser dyes[68] and sensitizer for solar cells,[69] among several others. This large amount of applications comes from the BODIPYs-like inherent features, such as chemical and photochemical stability, easy solubility, high fluorescence yields and molar absorption coefficients, long excited-state lifetimes and sharp fluorescence peaks, which range from the blue to the infrared region.[70]

Molecular systems with 1,8-naphthryridine derivatives have also been used to construct BF_2 compounds in the last years because of their good fluorescence

properties and biocompatibility.[71] These molecules present an attractive tool for identification of novel biological potential with their heterocyclic moiety.[72] The BF_2 organoboron compounds based on 1,8-naphtyridine heterocycles are used as fluorescent dyes due to their high photochemical stabilities[16,73] and fluorescence quantum yields.[74-75] Their large Stoke shifts[76-77] and fluorescence properties[78] have been extensively reported in the literature.

Usually BODIPYs structures do not present high two-photon absorption cross-sections, having an average value in the range of 50 GM[79-82] in visible wavelengths. However, since these compounds present other promising characteristics, especially their high fluorescence quantum yields, methods have been developed to increase their 2PA capabilities. For instance, increasing the conjugation length[79] improved the 2PA cross-section to up to 150 GM, while changing the conjugation length and adding electron-donating and electron-withdrawing groups to the BODIPY-like main structure[83-84] have enable an increase to the order of 400 GM. Such approaches result in large molecules with complex structures, composed of several electron withdrawing and electron donating groups.

We studied seven BF_2-naphthyridine molecules[76] with either one or two electron donating or electron withdrawing groups attached to the core, therefore keeping their structures small and simple as seen in Figure 3.2.

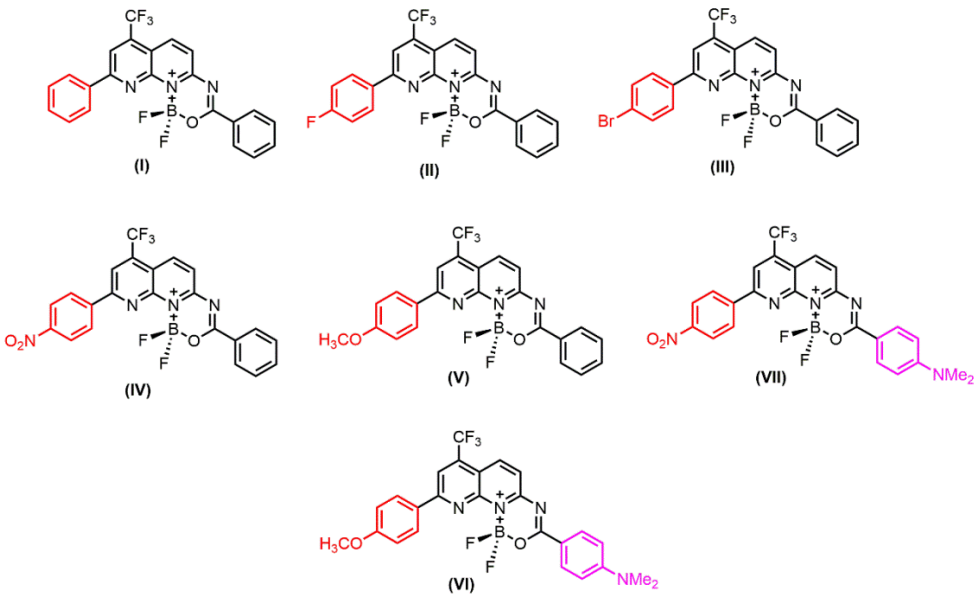

Figure 3.2 - Molecular structures of the BODIPY-like studied compounds.
Source: By the author.

Compound **I** presents the simplest structure, with only the BODIPY-like core and a phenyl added to it. Compounds **II**, **III** and **IV** have an electron withdrawing group in one of the core extremities, while compound **V** has an electron donor group instead. Compounds **VI** and **VII** present a longer structure, having either two electron donor groups (**VI**) or an electron donor and an electron withdrawing group (**VII**). The compounds were provided by Prof. B. A. Iglesias, and were made by Prof. H.G. Bonacorso group at Universidade Federal de Santa Maria.

3.1.3 Chiral Polymers

A molecule is considered chiral if it has a mirror image that is not superimposable with the original one. Therefore, the symmetry of the molecule is what defines if it has chirality or not. If it does not have this property, it is called an achiral molecule, and has the characteristic of getting the exact same molecule after a rotation and reflection on a perpendicular plane to its rotation axis.[85]

There are three different ways of finding chirality in a compound. The first one is if it has a carbon atom bounded to four different groups, which generates a center of chirality (Figure 3.3a). The second one is looking for a chirality plane (Figure 3.3b), which breaks the plane symmetry of the molecule (imaginary plane that divides the molecule in two, with one half being the specular image of the other).[86] This type of molecule is known as chiral-plane. The third element used to find chirality in a molecule is a chirality axis in the molecule, called chiral axis (Figure 3.3c). In these kinds of molecules, the distribution of ligands around the axis will define if there is symmetry or not. Some compounds are chiral due to their geometry, like helicoidal molecules such as DNA, which present rotation to the right or to the left. The case for our studied compounds is the last one, since the polymers have a rigid, rodlike, helical binaphthalene structure.

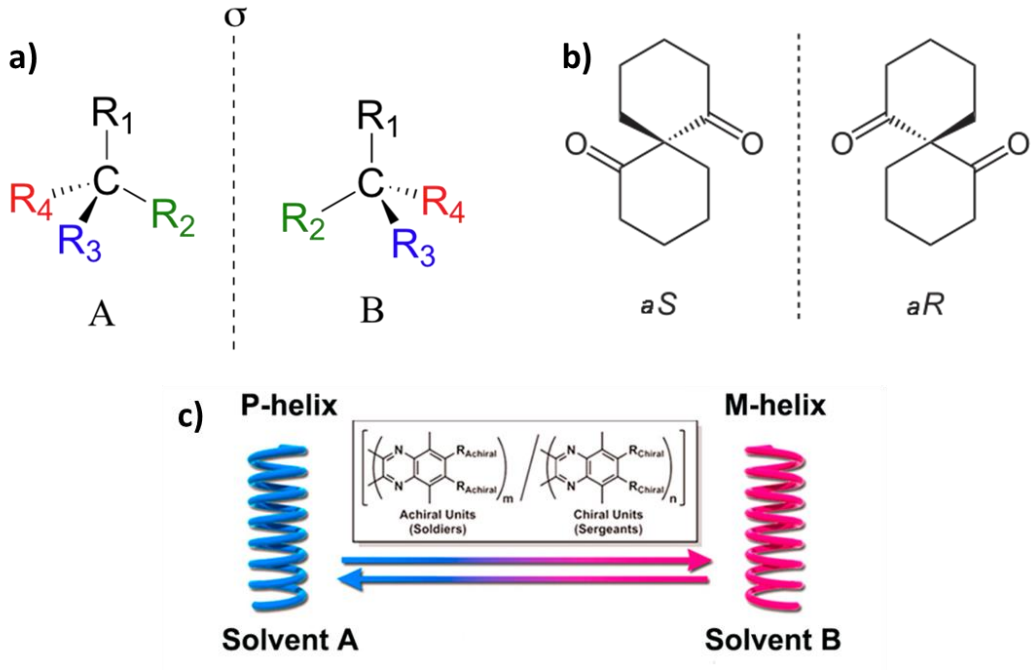

Figure 3.3 – Types of chirality: a) C bounded to four different groups; b) planar chirality and c) axis chirality.
Source: a,b) KENNEPOHL et al.[87]; c) ZIYU et al.[88]

Chirality in nonlinear optics has been thoroughly studied theoretically,[89-90] and revealed some interesting properties, including a natural increase of the nonlinear optical response of the material.[91] Few chiral polymers with helical structures have been made to have their nonlinear properties investigated,[92-95] and even less with a binaphthalene basis.[96-97] In these studies, the main nonlinear optical responses come from the backbone, since they use low hyperpolarizability chromophores that limit their capabilities.

G. Koeckelberghs et al.[98] proposed a new kind of chiral binaphthalene-based polymers for nonlinear optical studies. They are designed from chiral binaphthalene units, connected to rigid triphenylamine groups, which generates a rigid, helical structure. Flexible chromophores with high hyperpolarizabilities are added to this rigid rod-like backbone, creating a tree-like architecture of the molecule. This kind of structure allows a very high chromophore density since it diminishes and almost excludes any dipolar interaction between the chromophores, allowing a higher nonlinear response than random coil polymers have.[99] A previous study[100] has shown that this class of polymers is in fact interesting for nonlinear applications, as

they have both the inherent chirality, as well as no dipole interaction between its chromophores.

The structure of the polymers studied in this dissertation is shown in Figure 3.4. Four different kinds of chromophores were added to the binaphthalene backbone, and will be called as **Polymer 1**, **2**, **3** and **4** along the text. The different polymers are built by connecting different groups to the **R** position of the main structure shown in Figure 3.4 in the left.

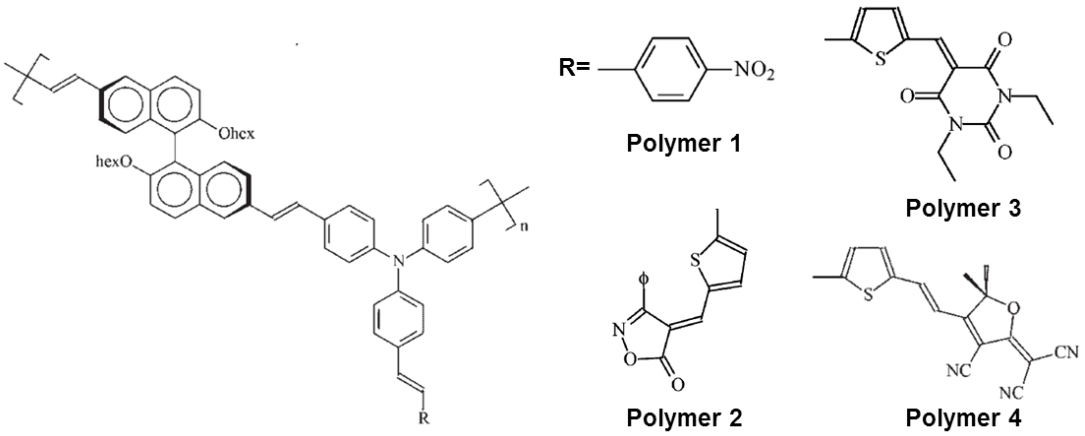

Figure 3.4 - Polymers main backbone structure (left) and the chromophores added to it (right). Source: Adapted from KOECKELBERGHS et al.[98,100]

Polymer **1** has the simplest chromophore added to it, which is a nitrocyclohexatriene ligand. The synthesis of this polymer is described in reference.[98] Polymers **2** and **3** have approximately the same complexity, as well as conjugations lengths, being expected to have similar absorption spectra. Polymer **4** has the most complex structure, as well as the longest conjugation length between the four studied chromophores. The synthesis of polymers **2**, **3** and **4** is described in reference.[100] They were provided by Prof. G. Koeckelberghs group from Katholieke Universiteit Leuven.

3.2 Z-Scan technique

The Z-Scan technique was proposed by Sheik-Bahae[101] in 1990 as a simple method for measuring both nonlinear refractive index and nonlinear absorption coefficient. In this technique, a sample is translated across the waist of a focalized

Gaussian beam while its transmittance is measured in the far-field. To measure the nonlinear refractive index, an iris must be added to the experiment, such that the induces an amplitude change that can be observed in the far field. Nonlinear refraction measurements were not carried out during this study, and will not be further discussed.

To measure the nonlinear absorption coefficient, all light should be collected by the photodetector and, therefore, this method is called *open-aperture Z-Scan*. Its measurement procedure can be visualized in Figure 3.5a-e, as well as in the graphic obtained from it. To avoid linear effects from the sample, what is actually measured is the normalized transmittance (Figure 3.5f) given by $T(z) = P(z)/P(z_\infty)$, which is the transmitted power at the focus divided by the transmitted power far from it, where nonlinear effects are not present.

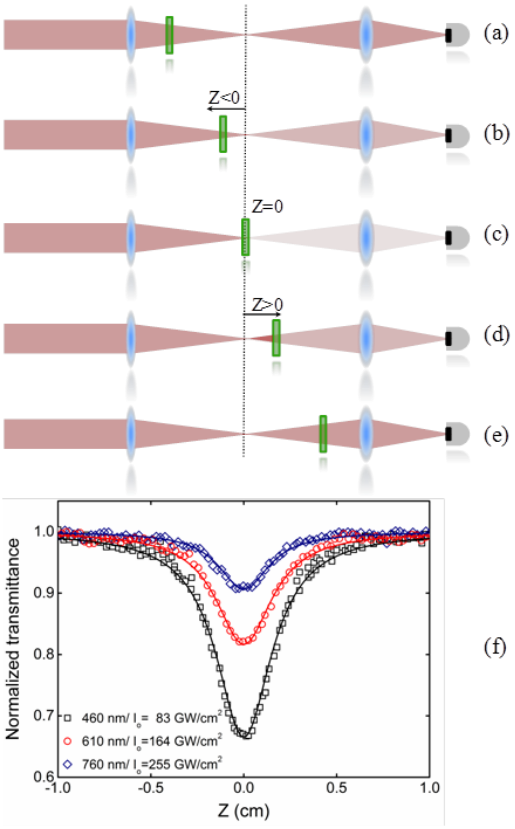

Figure 3.5 - Procedure of the Z-Scan experiment process.
Source: Provided by DE BONI.

3.2.1 Theoretical approach

To be able to do the fitting shown in Figure 3.5f, it is necessary to understand the fundamental aspects of the Z-Scan technique. Since we did not study any one-photon resonant effects or other multiphoton absorption processes, we will focus the theory around the two-photon absorption measurement only.

As we have seen before (Chapter 1), when the laser electric field is of the order of the interatomic electric field, the absorption becomes dependent of the intensity and its coefficient is written as $\alpha = \alpha_0 + \beta I + \alpha_3 I^2 + \cdots + \alpha_n I^{n-1}$. The propagation equation on a two-photon absorption medium is given by

$$\frac{dI(z,r,t)}{dz} = -\beta I^2(z,r,t) \tag{3.1}$$

Equation (3.1) can be solved through

$$\int_{I_I}^{I_o} \frac{dI(z,r,t)}{I^2} = \int_0^L -\beta dz \tag{3.2}$$

where I_I is the intensity of the beam entering the sample, I_o is the intensity of the beam in the exit plane of the sample, and L is the length of the sample, giving

$$I_o(z,r,t) = \frac{I_I(z,r,t)}{1 + \beta L I_I(z,r,t)} \tag{3.3}$$

Considering that the beam used for the measurement has a Gaussian profile

$$I(r,z) = I_0 \left(\frac{w_0}{w(z)}\right)^2 exp\left(\frac{-2r^2}{w(z)^2}\right) \tag{3.4}$$

equation (3.3) can be rewritten as

$$I_o(z,r,t) = \frac{I_0\left(\frac{w_0}{w(z)}\right)^2 exp\left(\frac{-2r^2}{w(z)^2}\right)}{1+\beta L I_0\left(\frac{w_0}{w(z)}\right)^2 exp\left(\frac{-2r^2}{w(z)^2}\right)} \tag{3.5}$$

where *z* is the position of the sample, *r* is the radial coordinate of the beam, $w(z)^2 = w_0^2(1+z^2/z_0^2)$ with w(z) being the width of the beam in a position *z* of the sample and w_0 is the radius of the beam in the focus of the lens, also known as the beam waist.

To obtain the power (P(z,t)) it is necessary to calculate I_o for an area, which will be considered circular (2πrdr). Therefore,

$$P(z,t) = \int_0^\infty \frac{I_0\left(\frac{w_0}{w(z)}\right)^2 exp\left(\frac{-2r^2}{w(z)^2}\right)}{1+\beta L I_0\left(\frac{w_0}{w(z)}\right)^2 exp\left(\frac{-2r^2}{w(z)^2}\right)} 2\pi r dr \tag{3.6}$$

Solving the Eq. (3.6), the beam power in the exit of a sample with two-photon absorption is

$$P(z,t) = \frac{\pi}{2} I_0 w_0^2 e^{-\alpha_0 L} \frac{\ln(q_0+1)}{q_0}, with\ q_0 = \frac{I_0 \beta L w_0^2}{I_0 w_0^2 / w(z)^2} \tag{3.7}$$

We can then obtain the normalized transmittance by integrating Eq. (3.6) over time using the following relation

$$T_n(z) = \frac{\int_{-\infty}^{+\infty} P(z,t)dt}{\int_{-\infty}^{+\infty} P_i(z,t)dt} \tag{3.8}$$

where P(z,t) is the power at the sample exit given by Eq. (3.7), and P_i(z,t) is the input power on the sample, which is measured by a power meter. Equation (3.8) can be written in a simple way as

$$T_n(z) = \frac{1}{\sqrt{\pi} q_0(z,0)} \int_{-\infty}^{\infty} ln\left[1+q_0(z,0)e^{-t^2}\right] dt \tag{3.9}$$

where

$$q_0 = \beta I_0 L \left(1 + \left(\frac{z^2}{z_0^2}\right)\right)^{-1} \quad (3.10)$$

with z_0 being the Rayleigh length, which corresponds to the distance along the propagation direction of a beam from the waist to where the area of the cross-section is doubled. Equation (3.9) is used to do the fitting of the experimental data obtained during the open-aperture Z-Scan measurements. From the experiment, we know I_0, z and L, and from the fitting we obtain β and z_0. However, 2PA absorption is usually quantified by its cross-section, which is an area unit factor that is constant for linear processes. For nonlinear processes this value depends on the intensity, and can be written for two-photon absorption as[102]

$$\sigma = \sigma_{2PA} \frac{I}{h\nu} \quad (3.11)$$

where σ_{2PA} is the two-photon absorption cross-section, which is an absolute value that only depends on the material, and $I/h\nu$ is the photon flux with energy $h\nu$ and intensity I. Knowing that $\sigma = \alpha N_0$ for 2PA, where N_0 is the concentration of molecules (number of molecules/cm^3), and $\alpha = \beta I$ when considering only the 2PA, we can obtain σ_{2PA}

$$\sigma_{2PA} = \frac{\beta h\nu}{N_0} \quad (3.12)$$

Since from the Z-Scan measurement we can obtain β value, the σ_{2PA} can be easily obtained from the method as well.

3.2.2 Experimental setup

The experimental setup is shown in Figure 3.6. The system basis is a Ti:Sapphire Clark-MXR, which emits 150 fs pulses in a repetition rate of 1 kHz with wavelength of 775 nm. It is used as an excitation source for a Topas Optical

Parametric Amplifier (OPA), which generates pulses with 120 fs of duration and wavelengths from 460 nm up to 2200 nm.

The OPA is able to generate such a wide range of wavelengths due to nonlinear effects, as described in Chapter 1. To assure the Gaussian beam profile needed for the Z-Scan, a spatial filter is added in the beam path.

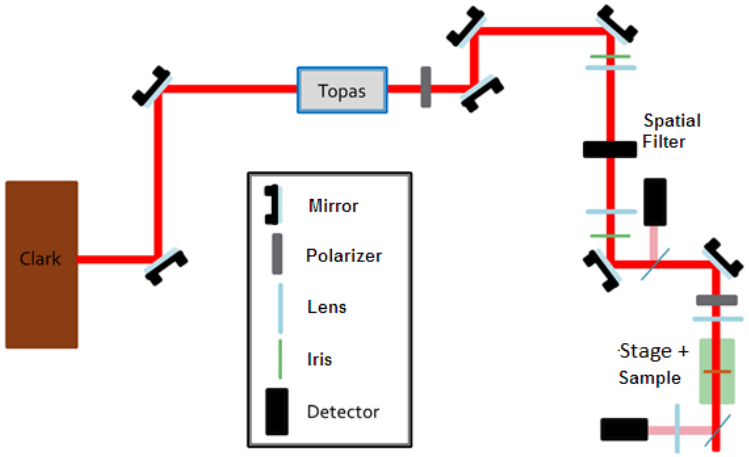

Figure 3.6 - Z-Scan experimental setup.
Source: By the author.

Before the beam reaches the sample, a beam splitter is placed to send around 10% of the light to a photodetector, which is placed to eliminate fluctuations caused by laser instabilities. This also helps in attaining a higher resolution during the experiment. The average power used in the measurements ranges between 0.06 mW to 0.1 mW. The Z-Scan setup itself is constituted by a convergent lens of focal length of approximately 13 cm, and a stage that translates the sample along the beam focus.The stage is controlled by a computer software made in *LabView*. The sample is placed within a 0.2 cm cuvette made from either quartz or glass, which presents very small nonlinearities in comparison to the studied sample. After the sample, another photodetector is placed and its signal is sent to the same software. The program plots the variation of transmittance with the z position of the sample, allowing direct observation of the valley formed by the 2PA in the focus. From these graphics, which are taken every 10 nm, we fit the experimental points with Eq. (3.9) and calculate the 2PA cross-section from it.

3.3 Measurements with polarization control

To evaluate the two-photon linear-circular or circular-circular dichroism of the studied polymers, measurements with polarization control were used to illuminate the sample with either linear or circularly polarized light.

3.3.1 Experimental setup

The experimental setup is essentially the same as the standard Z-Scan. However, for the polarization controlled measurements the sample was not translated along the focus of the lens, but placed exactly at the focus where its two-photon absorption is maximum. This is necessary since the 2PA circular-circular dichroism is a small effect, and can be better studied with large 2PA cross-sections.

To obtain different light polarizations before reaching the sample, a polarizer and a quarter-wave plate are added before the stage, as shown in Figure 3.7 . The first polarizer is used to control the power with which the sample will be shone, while the second one keeps the linear polarization constant for all wavelengths. The quarter-wave plate is connected to a motor, which makes it rotate 360º, stopping every 2º for 300 ms, giving a sequential linear → elliptical → circular polarization four times. The photodetector and the quarter-wave plate motor data are sent to a *LabView* program, which gives a signal to obtain one point each 2º of movement. This measurement is repeated for each studied wavelength.

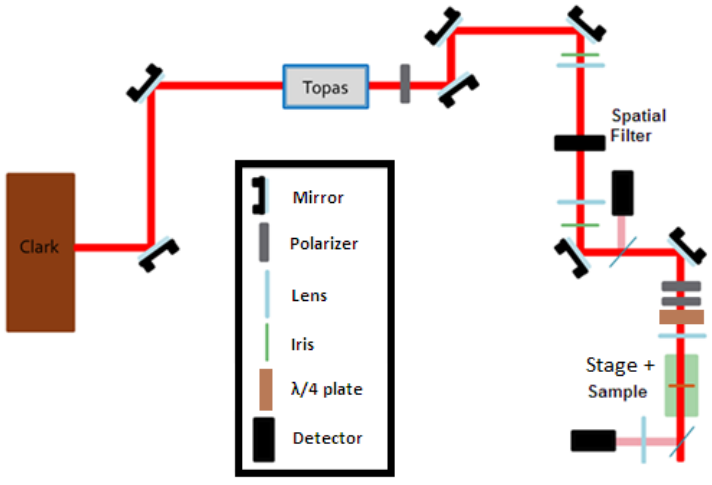

Figure 3.7 - Z-Scan setup with a rotating quarter-wave plate to control light polarization.
Source: By the author.

3.3.2 Data analysis

The 2PA for linear light polarization is stronger, in general, than for circular light polarization, since it aligns with the dipole moment of the compounds. Therefore, with the rotating quarter-wave plate generating linear and circular polarization in sequence, we obtain graphics of maxima and minima like in a sinusoidal curve, which we can normalize for easier evaluation. An example of the obtained curve is shown in Figure 3.8.

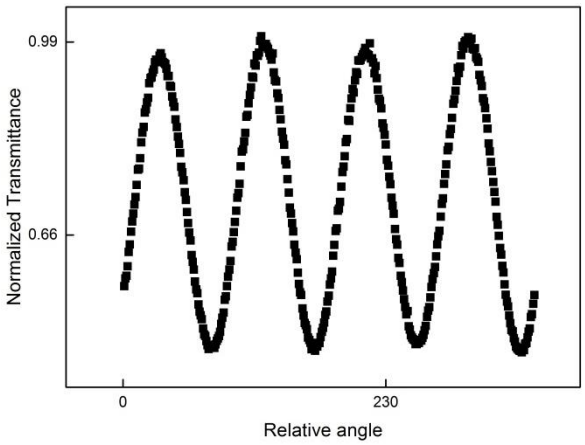

Figure 3.8 - Example of the curves obtained by the polarization control experiment.
Source: By the author.

As it was shown in Eq. (2.32), the 2PA linear-circular dichroism is given by

$$\Delta\sigma_{CLD}^{2PA} = \frac{\Omega_{CLD}^{A2F} - 1}{\Omega_{CLD}^{A2F} + 1}, where\ \Omega_{CLD}^{2PA} = \frac{\sigma_{CP}^{2PA}(\lambda)}{\sigma_{LP}^{2PA}(\lambda)} \tag{3.13}$$

Since Ω_{CLD}^{2PA} is calculated by the relation between the 2PA cross-section with circularly polarized light and the cross-section with linearly polarized light, this value can be directly calculated from the obtained curves. Knowing that the maxima values from the curves after normalization are related to linearly polarized light, the minima values are already the relation between transmittance for circularly and linearly polarized light, and, therefore, it gives Ω_{CLD}^{2PA} without any further manipulation. Since we have four different minima values, the average between them is taken to increase the precision of the measurement.

It is also possible to observe circular-circular dichroism from these measurements directly. Since the quarter-wave plates rotate 360º, it will provide in sequence light circularly polarized to the right→left→right→left. If the 2PA is different for each case, we would see a difference in the minima values between them, and would be able to calculate the two-photon absorption circular dichroism from it.

4 FLUORENONES

As previously mentioned, fluorenones usually present low two-photon absorption cross-sections, but their high fluorescence and low cytotoxicity still make them promising compounds for applications in 2PA microscopy. Here, we characterized the two-photon absorption cross-section of five different fluorenone-based compounds, obtaining their spectra from 560 nm to 800 nm. We found 2PA cross-sections of up to 220 GM for F-benzothiophene, and the smallest value of 130 GM for F-cyano. Through a sum-over-states modeling, we could also obtain the compounds spectroscopic parameters, such as the dipole moments for each transition, their wavelengths and width. Density Functional Theory (DFT) calculations were made in collaboration with prof. Daniel L. Silva from UFSCar, which provided the HOMO-LUMO transitions, as well as the expected two-photon absorption cross-section for each possible transition. Comparing these values with the maxima 2PA cross-section of each studied molecule we could observe a good agreement between theory and experiment. These results have been published in a scientific paper, which can be found in reference.[103]

4.1 Linear absorption

All compounds were diluted in Dimethylformamide (DMF) with concentrations of ~10^{-5} M. The linear absorption was measured by a commercial UV-1800 Shimatzu Spectrometer. The spectra for the compounds are shown in Figure 4.1, along with a zoom around the smaller energy band.

All compounds present similar features, with two strong absorption bands at 300 and 350 nm, and a weaker one around 450 nm. The band centered on 350 nm is related to the fluorenone group, while the one around 450 nm is caused by an intra-molecular charge transfer processes.[104-105]

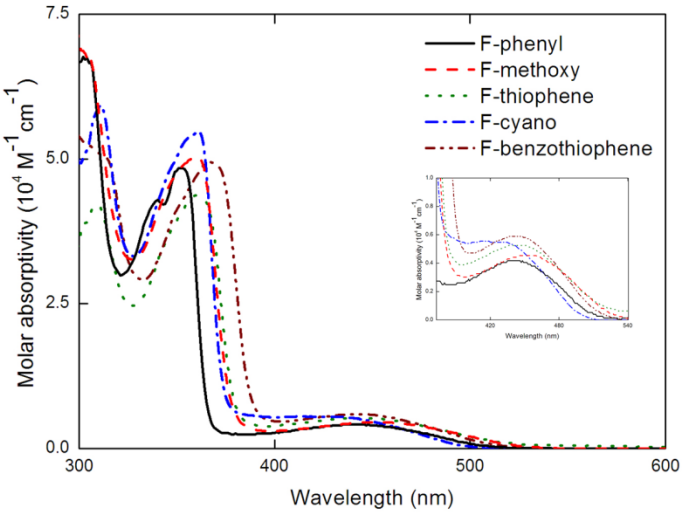

Figure 4.1 - Linear absorption spectra for the fluorenone compounds with an inset showing in detail the band around 450 nm.
Source: By the author.

F-benzothiophene has its first peak (375 nm) shifted 25 nm in relation to F-phenyl due to its longer conjugation length. The other three compounds, F-methoxy, F-thiophene and F-cyano have their first absorption band around 360 nm, shifted 10 nm in relation to F-phenyl for the same reason, though their conjugation lengths are smaller than the one for F-benzothiophene. The molar absorptivity for this transition is approximately the same for the five compounds, approximately 5 x 10^4 $Lmol^{-1}cm^{-1}$, while for the transition at 450 nm this value is about ten times smaller. This indicates that the compounds in the DMF solution have quasi-planar geometry, as expected because of the triple bonds in their structures.

4.2 Quantum Yield measurements

The fluorescence measurements were made with a HITACHI F7000 fluorimeter. To obtain the molecules quantum yields (φ), disodium fluorescein was used as the reference material. Since its quantum yield is known for methanol (0.97),[106] it is possible to find φ for other compounds through

$$\varphi_f = \varphi_{f_{ref}} \frac{\int_{\lambda_0}^{\lambda_f} F(\lambda)d\lambda}{\int_{\lambda_0}^{\lambda_f} F_{ref}(\lambda)d\lambda} \frac{f_{ref}}{f} \frac{n^2}{{n_{ref}}^2} \quad (4.1)$$

in which $\boldsymbol{\varphi_{f_{ref}}}$ is the quantum yield of the reference, **F(λ)** is the fluorescence spectrum, **f** is the absorption factor given by $f = 1 - 10^{-A(\lambda_{exc})}$, in which $\mathbf{A(\lambda_{exc})}$ is the absorbance at the excitation wavelength and **n** is the refractive index of the solvent.

The samples were excited at 450 nm, and their absorbances were kept lower than ~0.1 to avoid fluorescence reabsorption. Their fluorescence spectra can be seen in Figure 4.2, showing that they are all similar and have peaks between 550 and 600 nm. Using Eq. 4.1, the quantum yield for each sample was calculated, and the results are shown in Table 4.1.

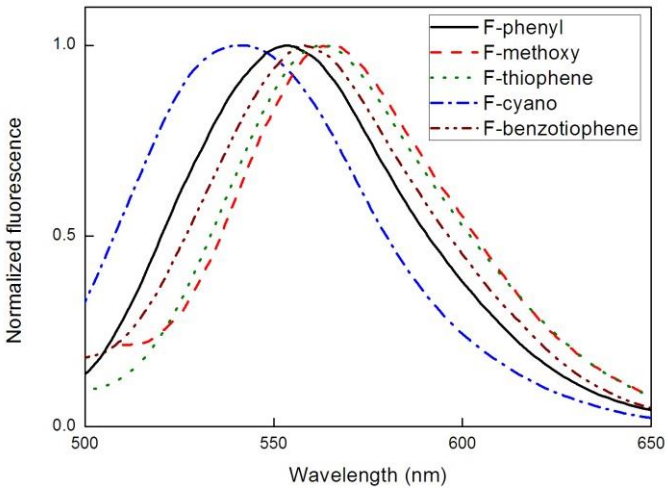

Figure 4.2 - Normalized fluorescence spectra for the studied compounds.
Source: By the author

Table 4.1 - Quantum yield for the fluorenone samples.

Sample	Quantum Yield
F-phenyl	0.17
F-methoxy	0.05
F-thiophene	0.06
F-cyano	0.31
F-benzotiophene	0.19

Source: By the author

4.3 Two-photon absorption results

For the nonlinear measurements, the samples were diluted in DMF with a 10^{-3} M concentration. The Z-scan measurements were performed between 560 and 800 nm to obtain their two-photon absorption cross-section spectra, since no signal was seen above this wavelength. The shortest wavelength chosen was 560 nm since the samples absorb linearly up to 500 nm, avoiding resonant effects that could happen due to one-photon absorption close to the linear band. An example of a Z-scan curve obtained is shown in Figure 4.3 for F-benzothiophene at 710 nm. The dots are the experimental points and the black line is the fitting made from Eq. 3.9, from which we can obtain the 2PA cross-section for each wavelength.

In Figure 4.4, we show the 2PA cross-section spectra for the five studied compounds. For comparison purposes, the linear absorption spectrum is also shown for each sample in the left axis (black dashed line). A similar behavior is observed for all compounds, with a peak near 700 nm and a resonant enhancement when nearing the linear absorption region, with exception of F-phenyl and F-thiophene that present a non-resonant peak near 600 nm.

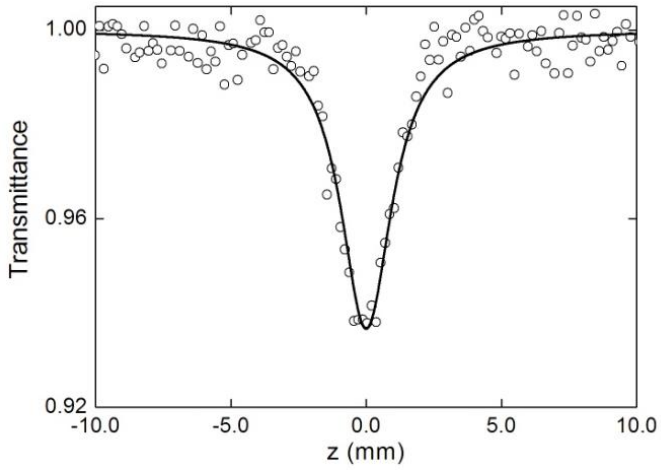

Figure 4.3 - Typical open-aperture Z-scan curve.
Source: By the author.

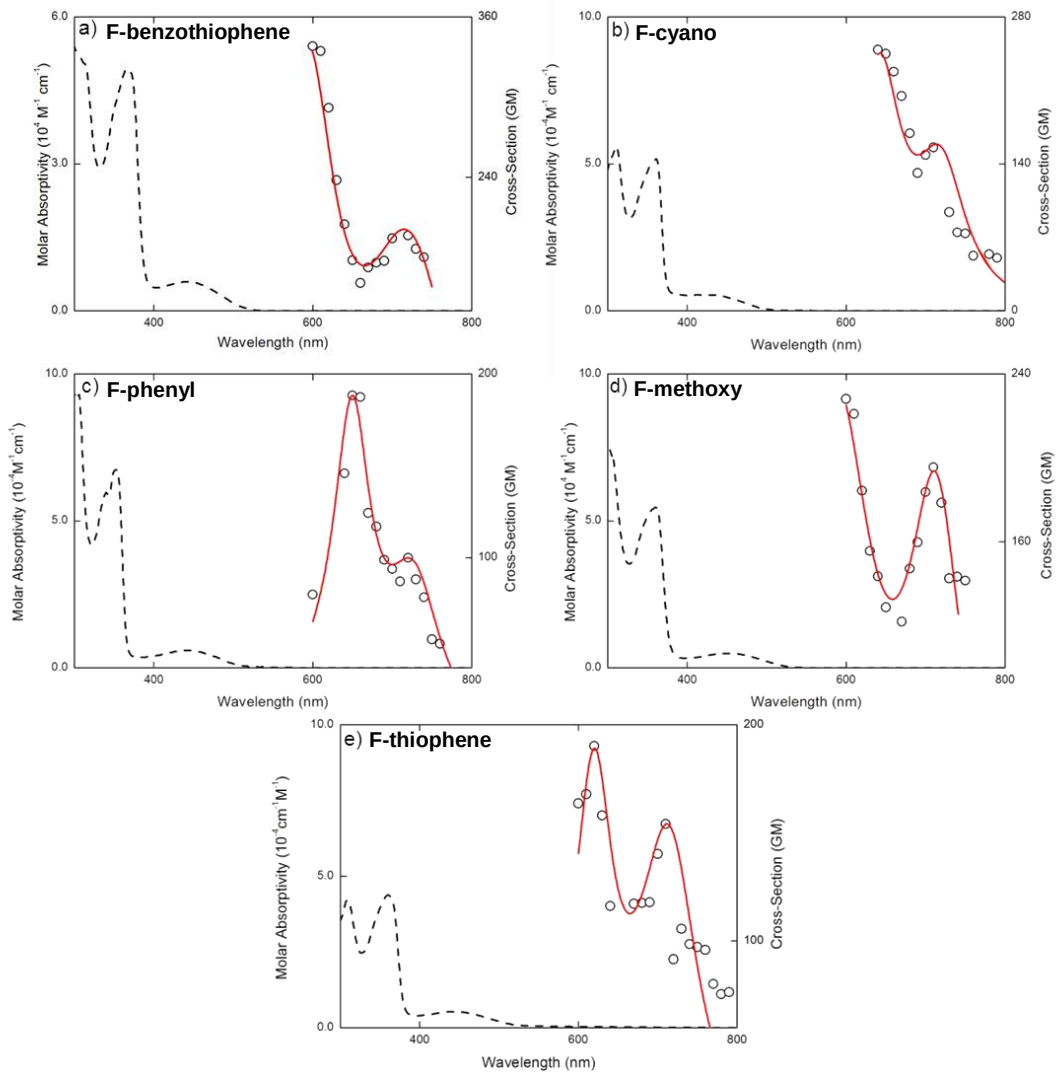

Figure 4.4 - 2PA cross-section (black dots), SOS fitting (red line) and linear absorption (dashed black line) for a) F-benzothiophene, b) F-cyano, c) F-phenyl, d) F-methoxy and e) F-thiophene.

Source: By the author.

For F-benzothiophene, the highest 2PA cross-section is seen at 710 nm, with 220 GM, which is the highest value between the compounds as expected due to its higher intra-charge transfer. F-cyano presents their maxima 2PA cross-section at 720 nm, with 130 GM, which is the smallest cross-section obtained for these compounds. F-phenyl has two peaks, one at 650 nm with 188 GM, and the other at 720 nm with 100 GM. Since we are considering applications for two-photon absorption microscopy and the usual wavelength range for it is from 700 – 1000 nm, we just considered the 2PA cross-section for the 720 nm peak for the rest of this study. F-methoxy has its highest 2PA value at 710 nm, with 200 GM, a value similar to F-benzothiophene since they have similar conjugation length. F-thiophene also presents two peaks, one at 600 nm with 190 GM, and the other one at 710 nm with

154 GM. It is interesting to notice that no bands were observed around 900 nm, which would be correspondent to the 450 nm band seen on the linear absorption spectra. This shows that this transition is basically two-photon forbidden since it wasn't measured on our experiment.

The sum-over-states (SOS) model as presented on Chapter 2 was used to fit the experimental data, whose results are shown by the red line in Figure 4.4. To model these compounds we used a four energy-level diagram based on their one and two-photon absorption spectra, using μ_{01} calculated through Eq. (2.31). Since we considered a single state for the calculation of the dipole moments, the values obtained are likely overestimated, as seen by the high values shown in Table 4.2, which summarizes the parameters determined and used by the fitting. From Figure 4.4 it is clear that the SOS model describes the measured spectra very well, showing that the energy-level diagram chosen is consistent with the experimental results.

Table 4.2 - Spectroscopic parameters for the compounds.

Molecule	**F-phenyl**	**F-benzotiophene**	**F-cyano**	**F-methoxy**	**F-tiophene**
λ_{01} (nm)	430	444	410	441	434
λ_{02} (nm)	366	366	361	359	360
λ_{03} (nm)	326	300	323	300	311
Γ_{01} (10^{14} Hz)	1.2	1.5	1.7	2.1	1.5
Γ_{02} (10^{13} Hz)	9.7	14.5	9	9.5	10.5
Γ_{03} (10^{13} Hz)	8.0	14.0	9.6	18.0	9.0
μ_{01} (D)	3.3	3.3	3.2	3.05	3.09
$\Delta\mu_{01}$ (D)	1.56	1.25	1.42	1.29	1.42
μ_{02} (D)	20.0	35.5	29.0	29.2	29.0
μ_{03} (D)	19.0	27	30.0	26.9	19.6

Source: By the author

To help interpret the experimental results, quantum chemistry calculations were performed by prof. Daniel L. Silva from UFSCAR. Comparing the theoretical maxima two-photon absorption with the experimental ones, as shown in Table 4.3, we can see that the wavelengths obtained theoretically are slightly blue shifted compared to the measured ones, which is within expectations for the used method.

Table 4.3 - Experimental and calculated maxima 2PA cross-sections and their wavelengths for the studied compounds.

	Experimental		Theoretical Quantum Chemistry	
Molecule	λ_{2PA}^{peak}**(nm)**	σ_{2PA}^{peak}**(GM)**	λ_{2PA}^{peak}**(nm)**	σ_{2PA}^{peak}**(GM)**
F-benzothiophene	710	220±50	684	456
F-thiophene	720	210±40	688	340
F-methoxy	710	200±40	696	279
F-phenyl	655	200±40	650	289
F-cyano	720	130±30	642	66

Source: By the author

The 2PA cross-section values ($\boldsymbol{\sigma_{2PA}^{peak}}$), however, present larger values and variation between the theoretical calculations and the experimentally observed ones. Even though the absolute values differ, Figure 4.5 shows that the behavior between the compounds 2PA cross-sections are in good agreement. The increasing tendency of the $\boldsymbol{\sigma_{2PA}^{peak}}$ from F-cyano to F-benzothiophene seems to be related to the conjugation length and the strength of the different electron-acceptor and electron-donor groups of each molecule.

To understand how the charges move within the molecules, we also calculated the main molecular orbitals (with the highest probability to contribute to the transition) involved in the 2PA transition showed in Table 4.3, which are presented in Figure 4.6. The calculated transitions for F-benzothiophene (a), F-phenyl (c), F-cyano (e) present a charge transfer character, while F-thiophene (b) has a backbone character. For F-methoxy (d), charge transfer and $\pi \rightarrow \pi^*$characters are both present in the mainly involved orbitals.

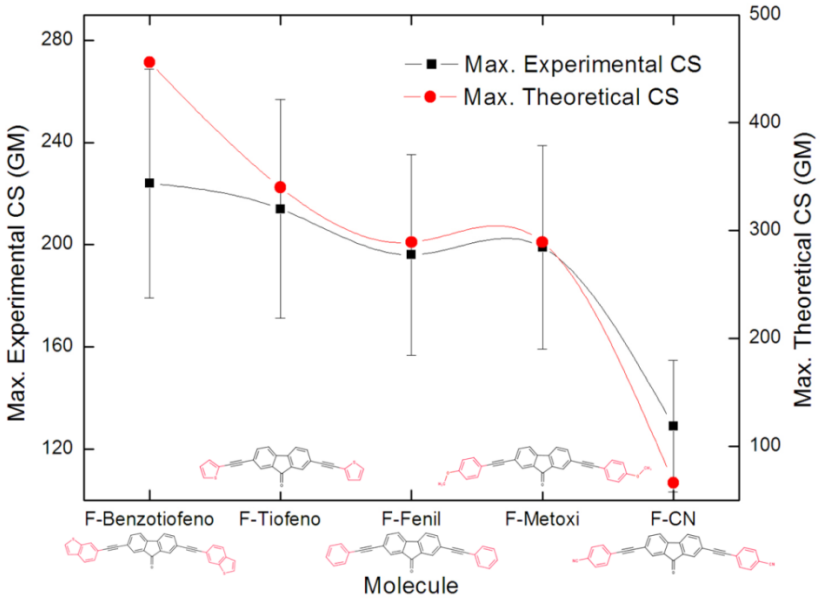

Figure 4.5 - Experimental (left axis – squares) and theoretical (right axis – circles) values of the 2PA cross-section peak values. The error bars for the experimental values is of 10%.
Source: By the author.

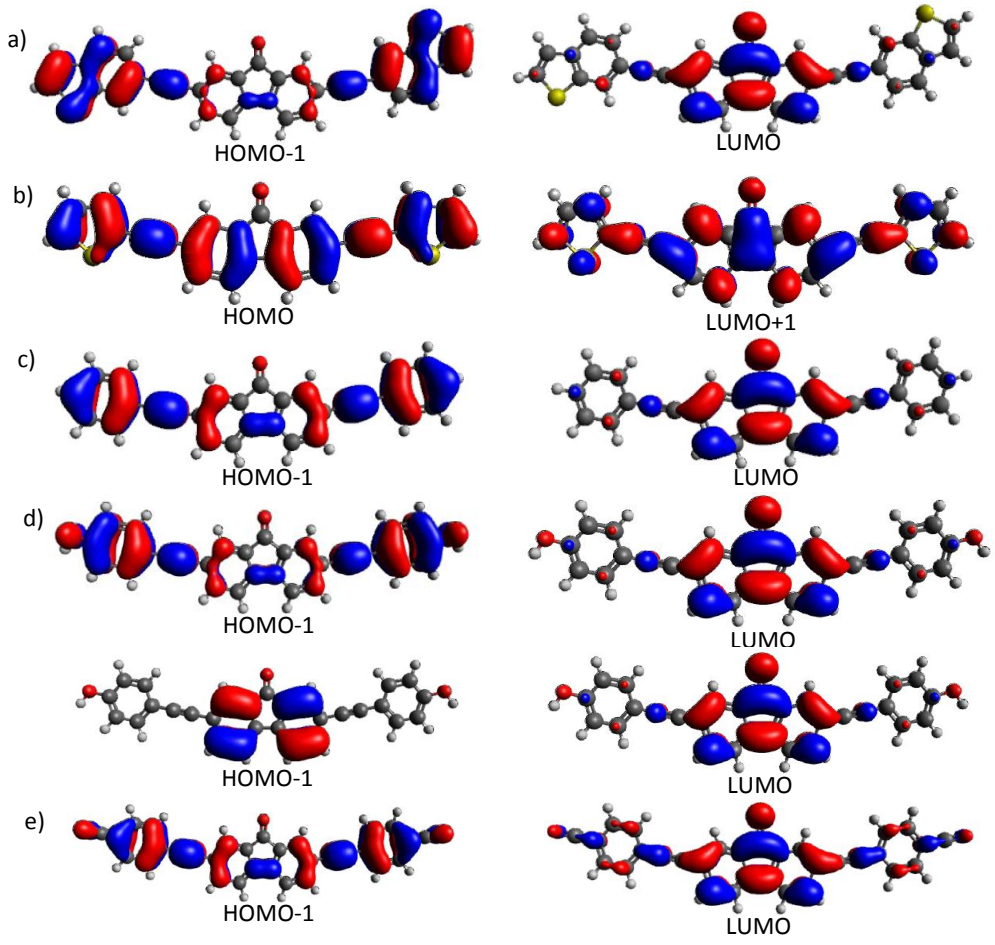

Figure 4.6 - Molecular orbitals involved in the electronic transitions of (a) F-benzothiophene, (b) F-thiophene, (c) F-phenyl, (d) F-methoxy and (e) F-cyano.
Source: SILVA.[103]

Through analysis of the molecular orbitals of the compounds, we observe that F-benzothiophene presents the largest 2PA cross-section due to its larger conjugation length, which allows a large movement of charges from the center to the sides of the molecule (Figure 4.6a). Since F-thiophene differs from F-benzothiophene by two aromatic rings, their 2PA cross-sections are comparable, and there is a clear π→π* charge movement within it (Figure 4.6b). F-methoxy and F-phenyl have shorter conjugation length than the two previously mentioned one, and have similar 2PA cross-sections since they only differ by the OCH_3 groups. F-phenyl presents charge transfer characteristics, moving from the center to the sides of the molecule (Figure 4.6c). For F-methoxy, two different LUMO-HOMO transitions have a high chance of happening: The first one shown in Figure 4.6d, where there is a large charge transfer from the sides to the middle, and the second one, where a π→π* transition happens. Since it presents similar 2PA cross-section to the F-phenyl, it is likely that the transition we observe is the one caused by the charge transfer. F-cyano presents a lower 2PA cross-section than the others due to its very low charge movement within the molecule, clear from Figure 4.6e.

4.4 Final considerations

In this chapter we reported the two-photon absorption study for five different fluorenone-derived compounds. We not only obtained their spectra but also did quantum chemistry calculations to understand their transitions deeper.

The compound that displayed the largest 2PA cross-section was F-benzothiophene, with 224 GM at 710 nm, while the one with the smallest cross-section was F-cyano with 129 GM at 720 nm. A comparison with the theoretical 2PA cross-sections obtained through quantum chemistry calculations was made, reaffirming the ordering of the synthesized molecules in terms of their 2PA cross-sections. From these calculations we also extracted the main molecular orbitals, which showed that F-benzothiophene was expected to have the largest 2PA cross-section due to its largest conjugation length and charge transfer compared to the other studied compounds.

Since all compounds presented large two-photon absorption cross-sections within the 700 nm range, as well as reasonable fluorescence quantum yields, they

can be interesting options, for example, for two-photon microscopy, allowing high resolution imaging of intracellular organelles or living tissues.

5 BODIPYS

Simple BODIPY structures usually present low two-photon absorption cross-sections, of the order of 50 GM as mentioned in Chapter 3. Their high fluorescence quantum yields and other inherent properties, led to searching for manners to increase their 2PA properties to enable more nonlinear applications to this class of compounds. We determined the 2PA spectra of seven BF_2-naphtyridine molecules with simple and short structures, presenting either a single or two electron donating or electron withdrawing groups attached, looking to increase the previously measured average 2PA cross-section without changing the compounds main core drastically. Two-photon absorption cross-section values as high as 270 GM were observed, corresponding to an increase of about five times in comparison to the average cross-section reported for compounds with similar conjugation lengths.

5.1 Linear absorption

The compounds were diluted in dichloromethane (DCM) with a concentration of 10^{-4} M for the linear measurements, which were done in a commercial UV-1800 Shimatzu spectrometer. We divided the compounds (shown in Figure 3.2) in three groups for the analysis: Compound **I**, which is the simpler structure, was studied alone at first; then the single electron acceptor or donor, composed by compounds **II**, **III**, **IV** and **V**, and finally compounds **VI** and **VII** which have two elements each.

In Figure 5.1 the linear absorption spectrum of compound **I** is shown. It presents a peak around 270 nm and two narrow bands around 400 nm. The first peak can be related to the intraligand $\pi \rightarrow \pi^*$ transition, while the ones around 400 nm come from the $n \rightarrow \pi^*$ transition ($S_0 \rightarrow S_1$).[76] The peaks around 400 nm show vibrational progression, which is associated with transitions between non-localized conjugated states (S_1), with a spacing of ~170 meV in agreement with the C=C and C=N vibrational modes of the naphthyridine in the complex.[77]

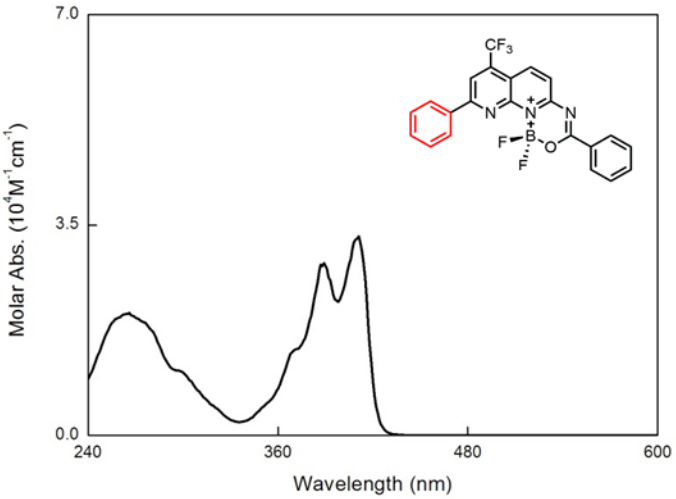

Figure 5.1 - Linear absorption spectrum of compound **I**.
Source: By the author

Since compound **I** structure repeats itself in all other studied compounds, it is expected that the basic shape of the linear absorption remains similar to it for compounds **II**, **III**, **IV** and **V** as they only have one different component. From Figure 5.2, it is possible to see that this assumption is correct except for compound **V**.

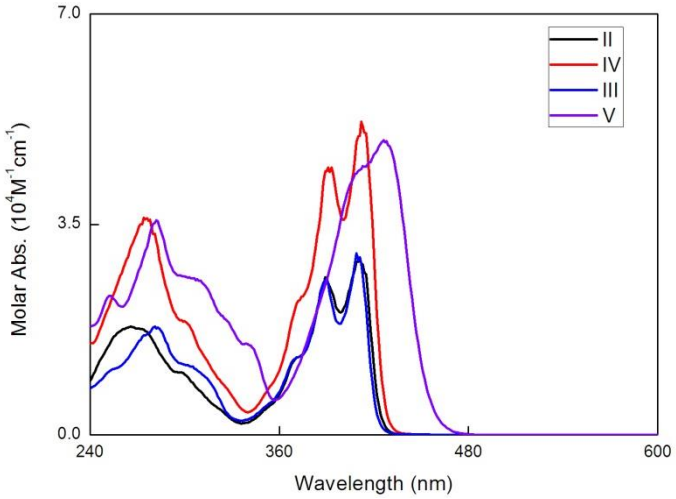

Figure 5.2 - Linear absorption spectra from compounds **II**, **III**, **IV** and **V**.
Source: By the author.

The linear absorption spectrum of compound **V**, which is the only one presenting an electron donor group instead of an electron acceptor one, differs from the compound **I** spectrum at the 400 nm peaks since it does not present a vibrational progression as clear.

Compounds **VI** and **VII** present a different linear absorption from the previous ones, as seen in Figure 5.3. Both have small absorption peaks from 260 to 390 nm,

and a stronger peak around 480 nm. Such molecules also present a red shift in their spectra in comparison to the other ones, possibly due to an intra-molecular charge transfer (ICT) band related to its strong push-pull structure.[77] The absorption band around 480 nm is attributed to a $n \rightarrow \pi^*$ transition, which has a more meaningful contribution for compound **VII**, which contains NO_2 and NMe_2 groups, which also generate a strong ICT that makes its spectrum more red shifted than for compound **VI**.

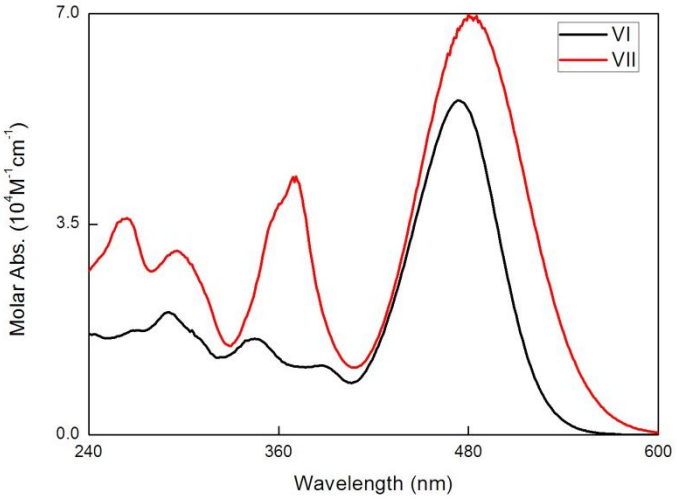

Figure 5.3 - Linear absorption spectra for compounds **VI** and **VII**.
Source: By the author.

5.2 DFT calculations

The quantum chemistry calculations were all performed by me using density functional theory (DFT).[107] First, the molecular structures of the compounds were optimized through the Becke's three parameter exchange, Lee, Yang and Parr correlation (B3LYP) hybrid functional[108-110] and the standard Pople's 6.31G(d,p) basis set[111] employing the Gaussian 09 package.[112] Solvent effects were taken in consideration during the optimization process.

The two-photon absorption transition probabilities calculations were carried out using time dependent density functional theory (TD-DFT) in DALTON 13.[113] Solvent effects were considered using the polarizable continuum model (PCM).[114-115] The hybrid B3LYP functional was employed in combination with the Pople's 6-311G(d,p) basis set. The lowest twenty states were calculated for each compound. The actual

excited states used for the analysis were obtained after removing weaker oscillator strength states, as well as states that were out of the wavelength range used during our measurements. Since the laser beam used for the experiments had a ~10 nm bandwidth, we convoluted states in this range into a single excited state. With this approach, we used the oscillator strength and predicted wavelength to build Gaussian curves around each excitation band with a width of 0.2 eV, originating a predicted spectrum for the 2PA cross-section of each sample.

This part of the work was done in collaboration with prof. F. Eloy Hernandez from the University of Central Florida, with the help of Dr. Julie Donnelly and Eduardo Romero who provided the codes used for these calculations.

5.3 Two-photon absorption

The solutions for the nonlinear measurements were prepared in DCM with a concentration from 10^{-2} to 10^{-3} M. Open-aperture Z-Scan measurements were made in different wavelength ranges for each compound in order to obtain their two-photon absorption cross-section spectra. We fitted the obtained data through a sum-over-states model as mentioned in Chapter 2, and compared it and the experimental data with the theoretically predicted 2PA cross-section spectra.

For these compounds, we used three different energy diagrams depending on their linear absorption spectrum, from which we can obtain the $\Delta\mu_{01}$. Since for some of the samples the first band of the linear absorption spectrum did not present a 2PA transition, the dipolar term of Eq. (2.30) was not considered as in this case $\Delta\mu_{01}$ can be neglected. Otherwise, $\Delta\mu_{01}\neq 0$ and the dipolar term was considered for the SOS fitting.

In Figure 5.4 the two-photon absorption spectrum for compound **I** is shown. The open circles correspond to the measured 2PA cross-section for each wavelength, presenting two peaks as well as the resonant enhancement region starting around 500 nm. The first peak is around 530 nm, with a 2PA cross-section of 47 GM and the second one is located at 580 nm with a 2PA cross-section of 58 GM, which are both of the same order as previously measured BODIPY-like compounds of similar conjugation length. To describe the 2PA spectrum of this molecule a four energy level diagram was employed for the SOS model, shown as the red line in

Figure 5.4, not considering the dipolar term since the first peak is not related to the first linear absorption band, which can also be seen in Figure 5.4 as the black dashed line. In Table 5.1 the fitting parameters obtained for compound **I** can be seen in the first line.

The 2PA spectrum is directly related to the high energy band of the compound's linear absorption. Therefore, we can assume they come from the intraligand $\pi \rightarrow \pi^*$ transition band. The dot-dashed blue line in Figure 5.4 corresponds to the theoretically calculated spectrum determined through DFT calculations. The written values near each peak are the magnitude of the 2PA cross-section calculated for that band. As it can be seen, there is a good agreement between the shape and the spectral position of the 2PA bands. In Figure 5.5a, the low energy electronic transition (HOMO→LUMO) is shown for compound **I**. It shows a small charge transfer character between the extremity rings towards the center, almost negligible, explaining the low observed 2PA cross-sections for it.

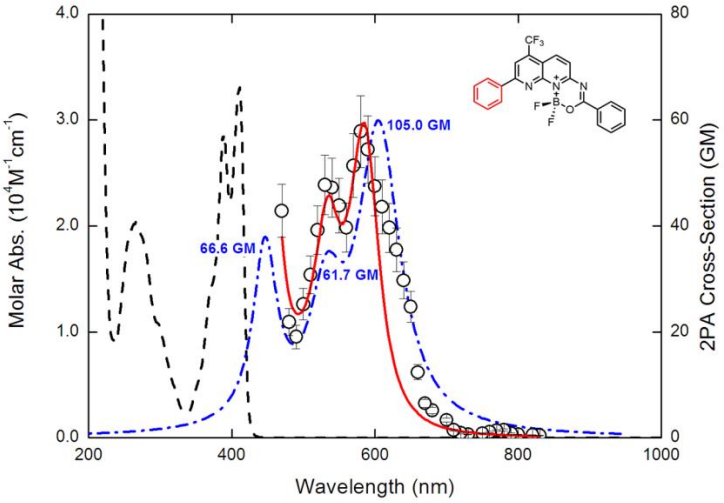

Figure 5.4 - Measured 2PA cross-section (opened black circles) spectrum for compound **I**, along with its SOS fitting (red line) and theoretical prediction (blue dot-dashed line), as well as its linear absorption spectrum (black dashed line).
Source: By the author.

Table 5.1 - Spectroscopic parameters obtained from the SOS fitting for the BODIPY compounds.

Compound	μ_{01} (D)	$\Delta\mu_{01}$ (D)	λ_{01} (nm)	Γ_{01} (10^{14} Hz)	μ_{12} (D)	λ_{02} (nm)	Γ_{02} (10^{14} Hz)	μ_{13} (D)	λ_{03} (nm)	Γ_{03} (10^{14} Hz)	μ_{14} (D)	λ_{04} (nm)	Γ_{04} (10^{14} Hz)
I	5.9	-	394	0.9	6.0	294	0.9	3.3	268	0.9	2.5	227	1.0
II	5.7	-	395	0.9	5.2	294	0.8	3.4	267	0.8	2.2	234	1.0
III	5.7	-	397	0.9	5.0	318	0.8	5.0	280	0.9	3.6	231	1.0
IV	6.9	-	393	0.9	7.2	294	0.6	4.0	268	0.8	3.8	231	0.8
V	7.9	4.8	426	0.8	7.3	337	0.8	3.1	270	0.9	2.3	240	0.8
VI	8.6	8.7	482	0.7	7.8	385	0.9	6.5	300	0.8	-	-	-
VII	10.5	13.0	492	0.8	6.1	368	0.8	3.8	303	0.8	-	-	-

Source: By the author.

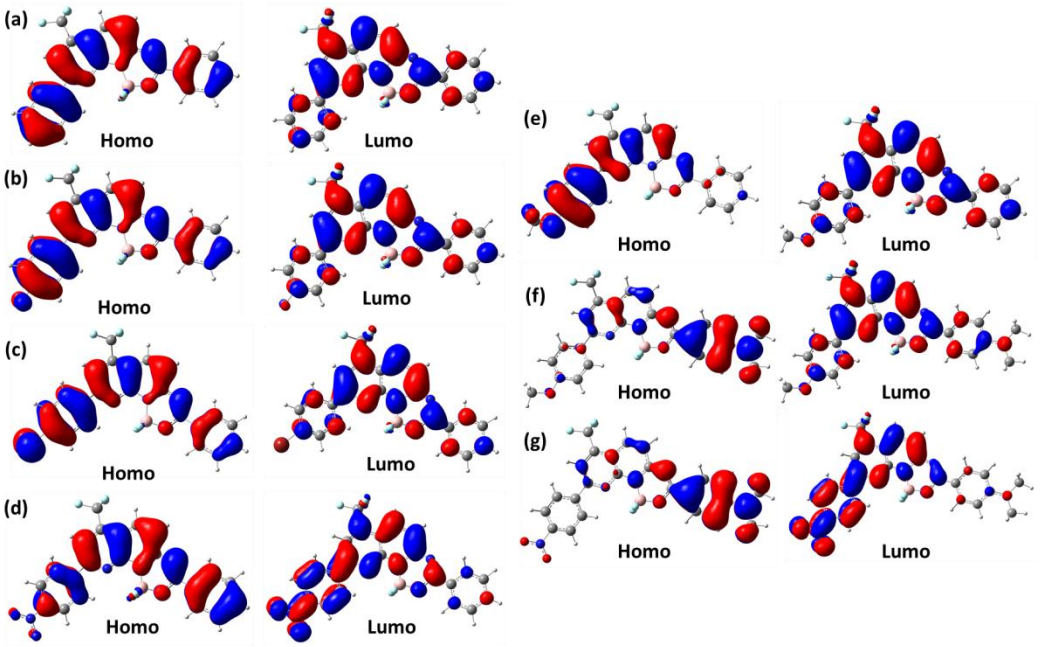

Figure 5.5 - Orbital HOMO→LUMO transitions for compounds (a) I, (b) II, (c) III, (d) IV, (e) V, (f) VI and (g) VII calculated for the highest 2PA transitions through TD-DFT.
Source: By the author.

Figure 5.6 shows the spectra for compounds **II**, **III**, **IV** and **V**. Since the linear absorption spectra of compounds **II**, **III** and **IV** are similar, it was expected that their 2PA cross-section spectra would also present similar shapes. These spectra are also similar to the one seen for compound **I** (Figure 5.4). Compound **II** (Figure 5.6a) has two peaks of about the same magnitude, one at 530 nm and the other at 580 nm, both with a 2PA cross-section of 46 GM. Compound **III** (Figure 5.6b), which presents Br, exhibits a larger 2PA cross-section, with a peak of approximately 53 GM at 560 nm and a smaller one of 32 GM at 630 nm. The opposite behavior happens for compound **IV** (nitro group, Figure 5.6c), with a larger peak at 590 nm with 156 GM and a smaller one at 540 nm with 83 GM. For compound **V** (Figure 5.6d), which has

a donor group (HCO_3) in its phenyl ring, a third peak is observed at 850 nm with 24 GM, which corresponds to the electronic state at 400 nm observed in its linear absorption spectrum. This feature arises possibly due to the dipolar characteristic of this compound, and it also occurs for compounds **VI** and **VII** as will be shown later. Compound **V** has a larger peak at 670 nm with 120 GM and a smaller one of 88 GM at 540 nm. Compounds **IV** and **V** present 2PA cross-sections of the same order of previously measured molecules with larger conjugation lengths.[82]

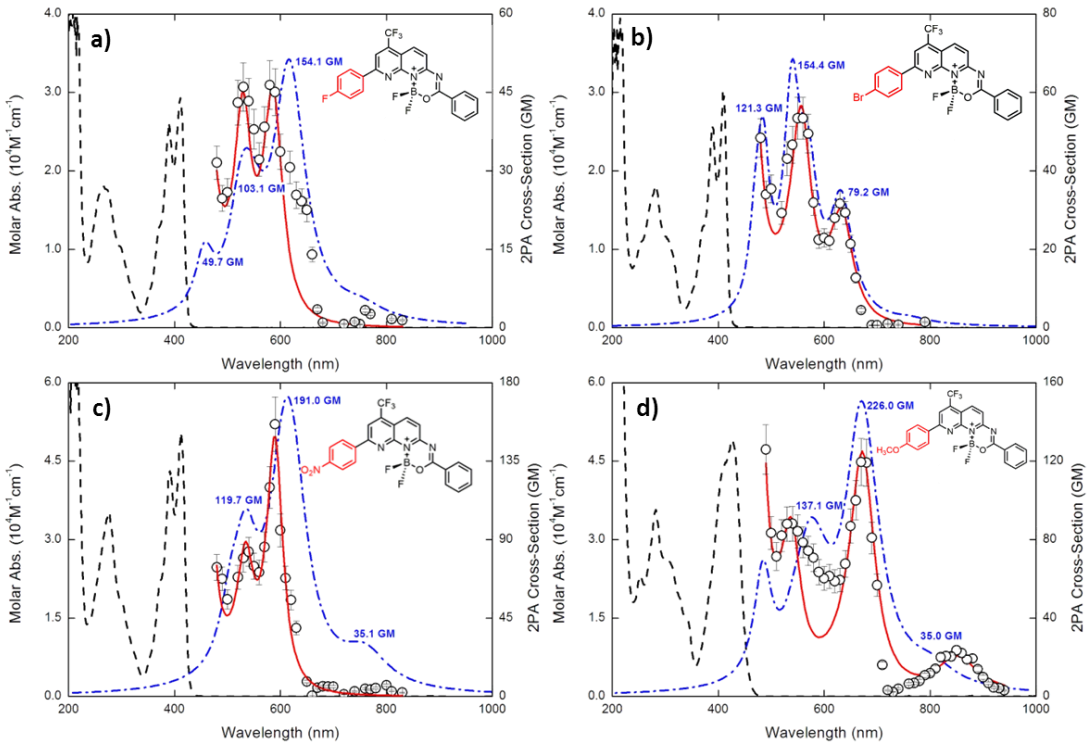

Figure 5.6 - Measured 2PA cross-section spectra (black circles) for compounds a) **II**, b) **III**, c) **IV** and d) **V**, along with its SOS fitting (red line) and theoretical spectra (blue dot-dashed line), as well as their linear absorption spectra (black dashed line).
Source: By the author.

Since compounds **II**, **III** and **IV** (Figure 5.6a-c) display three 2PA peaks that are not related to their first linear absorption band, a four energy-level diagram without the polar term was used for the SOS fitting, shown as a continuous red line in all graphics in Figure 5.6. For compound **V**, the dipolar term had to be considered so a five energy-level diagram was used for the SOS. The parameters of the SOS found through fitting for these four compounds can also be seen in Table 5.1 - Spectroscopic parameters obtained from the SOS fitting for the BODIPY compounds..

In this context, compound **I** presents a similar maximum 2PA cross-section to compound **II**, followed by compounds **III** and **IV**. From Figure 5.5, the charge transfer that happens in the HOMO→LUMO transition for compounds **II** (Figure 5.5) and **III** (Figure 5.5c) are similarly negligible, both happening from the rings towards the center of the compound. Compound **IV** (Figure 5.5d) presents a small charge transfer into the nitro group from the right to the left side of the molecule, which explains the largest 2PA cross-section observed in it. Compound **V** (Figure 5.5e) presents a comparable maximum 2PA cross-section to compound **IV** due to its push-pull like transition, which happens between the two extremities of the molecule. Since the electron density is pulled more efficiently by the nitro group in compound **IV** than given by the methoxy in compound **V,** we observe a larger 2PA cross-section in compound **IV**.

The 2PA spectra for compounds **VI** and **VII** are shown in Figure 5.7. They present similar shapes, with two 2PA peaks. Compound **VI** has a peak at 770 nm, with 148 GM, and the second peak at 960 nm with 80 GM, while for compound **VII** the peaks are at 730 and 990 nm, with magnitudes of 210 and 268 GM. This result shows an increase of about five times in the value of the 2PA cross-section in comparison to previously studied BODIPY compounds with similar length, and are of the same order of recently studied BODIPYs[83] with larger conjugation lengths and more than two electron acceptor or donor groups.

For these compounds a four energy-level diagram was used for the SOS fitting, presented in Figure 5.7 as a red continuous line, with their parameters shown in Table 5.1.

For both compounds the lowest energy 2PA peak corresponds to the 480 nm band of the linear absorption spectrum. Such transition is attributed to a $n \rightarrow \pi$ transition, having a more meaningful contribution for compound **VII**, which contains NO_2 and NMe_2 groups. The high energy peak is red-shifted for compound **VII**, which is related to its strong ICT, once strong donor (NMe_2) and acceptor (NO_2) groups are bonded to the *para*-position of phenylene aromatic rings (like push-pull systems) of this compound.

From compound **VI** and **VII** HOMO-LUMO transition, presented on Figure 5.5f and Figure 5.5g, it is possible to see a difference between the moving charges pattern for both compounds. On compound **VI** there is an evident charge transfer from the dimethyl amine into the first half of the molecule during the transition, while

for compound **VII** there is a large charge transfer from the NMe_2 group to the NO_2 group, creating a push-pull structure since the two ligands are located in opposite sides of the molecule. Since the charge transfer is much larger for compound **VII**, it presents a larger 2PA cross-section value than compound **VI**.

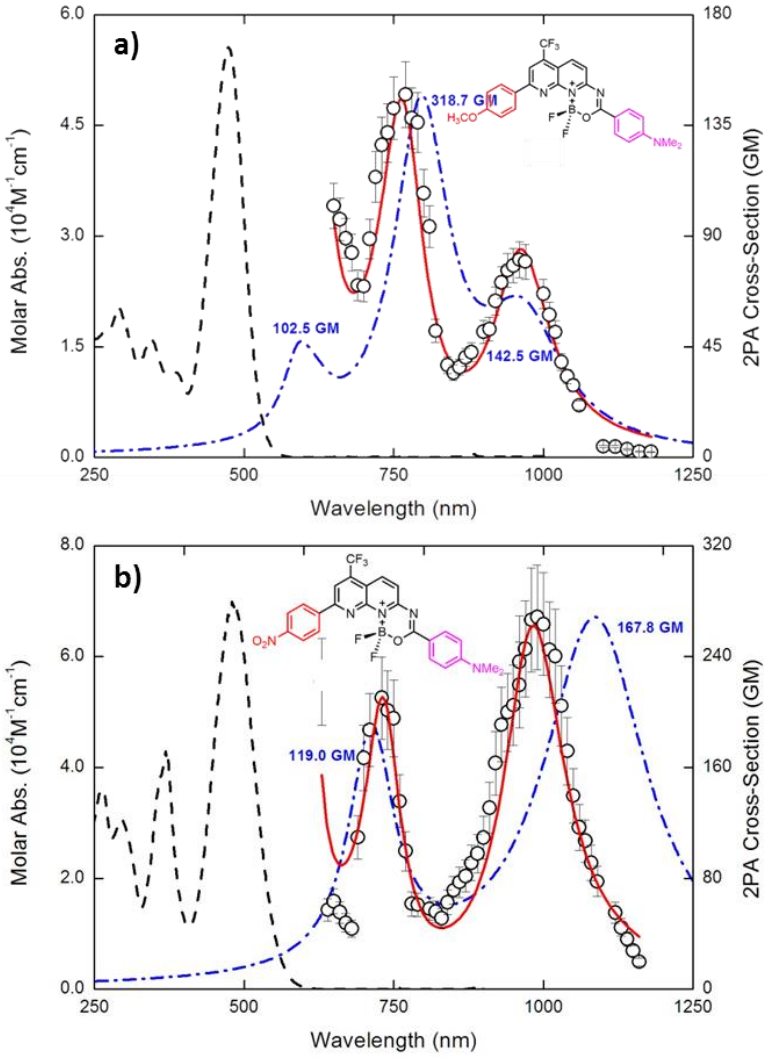

Figure 5.7 - Measured 2PA cross-section spectra (black circles) along with its SOS fitting (red line) and calculated spectra (blue dot-dashed line), as well as their linear absorption (black dashed line) for compounds (a) **VI** and (b) **VII**.
Source: By the author

We also compared the maxima 2PA cross-section measured with the ones calculated with quantum chemistry, which are summarized in Table 5.2. The wavelengths of the measured spectra for the compounds are blue-shifted from 50 to 60 nm, which is within the usual deviation from theory. For compounds **I** to **VI** the difference between measured and calculated wavelengths was no larger than 35 nm, while for compound **VII** this difference goes up to 75 nm. This bigger difference between the values, both for the wavelength and the 2PA cross-section, happens

due to the zwitterionic character and the charge transfer characteristics for this compound. Examining the obtained data, we can conclude that the inclusion of donating or accepting groups into the molecule increases its 2PA cross-sections considerably, and this increment depends on the capacity of such groups to withdraw or donate electron density towards the π system of the molecule.

Table 5.2 - Comparison between the maxima 2PA cross-section calculated through DFT and measured for the BODIPY compounds.

Compound	λ_{2PA} theo. (nm)	σ_{2PA} theo. (GM)	λ_{2PA} exp. (nm)	σ_{2PA} exp. (GM)
II	615	154	580	46
III	540	154	550	53
IV	612	191	590	156
V	670	226	670	120
VI	796	344	770	133
VII	1065	182	990	268

Source: By the author

To verify our measured data further, the dipole moments for each compound were also calculated through DFT, and their values are compared to the ones measured experimentally in Table 5.3.

Table 5.3 – Comparison between calculated and measure dipole moments for all compounds.

Compound	Measured μ_{01} (D)	Theoretical μ_{01} (D)	Measured μ_{12} (D)	Theoretical μ_{12} (D)	Measured μ_{13} (D)	Theoretical μ_{13} (D)	Measured μ_{14} (D)	Theoretical μ_{14} (D)
I	5.9	6.7	6.0	4.0	3.3	1.9	2.5	1.7
II	5.7	3.2	5.2	2.9	3.4	1.1	2.2	1.8
III	5.7	4.0	5.0	4.0	5.0	2.3	3.6	1.0
IV	6.9	8.6	7.2	10.15	4.0	1.9	3.8	2.4
V	7.9	6.8	7.3	12.2	3.1	3.6	2.3	2.3
VI	8.6	17	7.8	12.6	6.5	2.0	-	-
VII	10.5	30.9	6.1	5.9	3.8	1.3	-	-

Source: By the author.

Compounds **I** to **V** show good agreement between the experimental and theoretical dipole moments, all of them being of the same order of magnitude and with differences under 5 D. However, for compounds **VI** and **VII** the differences are much larger, particularly for the first dipole moment ($\boldsymbol{\mu_{01}}$). This is due to the previously mentioned issues with the amount of charge transfer present in these compounds,

which led to an overestimation of their 2PA cross-sections as well as of their dipole moments.

5.4 Final considerations

Seven new BF_2-naphthyridine compounds developed to have a larger 2PA cross-section than previous ones of the same conjugation length were studied. The compounds that presented the larger 2PA cross-section were compound **VII**, with 268 GM at 990 nm, and compound **IV**, with 156 GM at 590 nm, both having NO_2 as a substituent. The smallest observed 2PA cross-section was 46 GM for compound **II** at 580 nm. Considering previously studied BODIPY compounds, most of them present intricate structures and several substituents to increase their conjugation length and internal charge transfer to enlarge the 2PA cross-sections to up to 350 GM in the visible region. The compounds studied during this dissertation revealed cross-sections of the same order of magnitude with a simpler structure, demonstrating that these compounds have a good potential for nonlinear applications in the visible and near infrared spectral regions.

6 CHIRAL POLYMERS

Chiral structures have their nonlinear properties inherent to their basic characteristics. Adding chirality to a polymeric structure is supposed to generate even higher nonlinear properties, since it also increases the compound conjugation length and amount of added chromophores. The chiral polymers studied present a main binaphthalene backbone rod, with a high concentration of chromophores added as branches. Four different polymers were studied, with differences only on the chromophores, as seen in Figure 3.4.

Two different kinds of studies were carried out in these polymers. The first one was a study of their two-photon absorption spectra with linearly polarized light through open-aperture Z-Scan measurements. The highest 2PA cross-section obtained in this case was for polymer **2**, with 680 GM at 1100 nm, while the smallest one was polymer **1**, with 349 GM at 890 nm.

The second study was a polarization controlled 2PA measurement, where we looked for the linear-circular dichroism, as well as the circular dichroism for the four polymers. Three of the polymers presented a single allowed transition level for their first absorption peaks, while for the second peak two or more allowed states have been observed. Polymer 3 had the opposite behavior. Small circular dichroism for particular wavelengths were observed in two of the polymers.

6.1 Linear absorption

The four studied polymers were diluted in tetrahydrofuran (THF) in concentrations of 10^{-5} M for the linear absorption measurements. The spectra were obtained with a commercial UV-1800 Shimatzu spectrometer and are shown in Figure 6.1.

All polymers present two linear absorption peaks: the first one around 350 nm for all studied samples, related to the binaphthalene backbone,[98] while the second peak is related to the different chromophores of the polymers composition. For polymer **1**, which has the smallest chromophore, the second peak is located around 440 nm. Polymers **2** and **3** have chromophores of similar conjugation length, and their second absorption peaks are close, being at 550 nm for polymer **2** and 560 nm

for polymer **3**. Polymer **4** has the longest conjugation length on its attached chromophore and, therefore, has a larger wavelength for its second peak, around 600 nm.

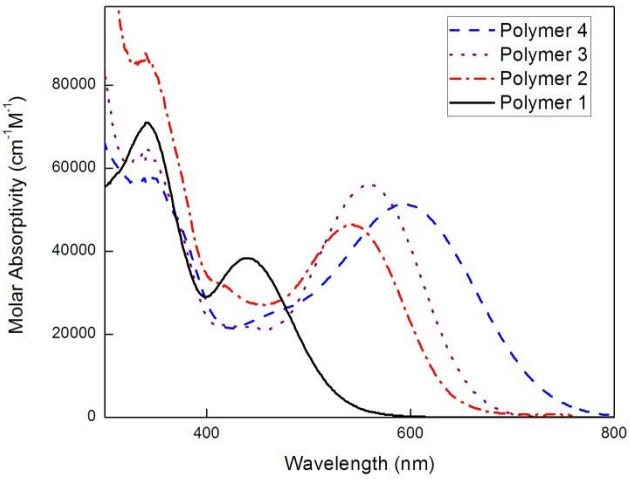

Figure 6.1 - Linear absorption for the studies polymers.
Source: By the author

6.2 Two-photon absorption with linear polarization

For the two-photon absorption measurements, the polymers were diluted in concentrations of 10^{-4} to 10^{-3} M in THF. The measurements were made through the absorptive Z-Scan technique, and the wavelength range was different for each polymer, considering their distinct linear absorption spectra ranges. A sum-over-states model was then applied with four energy levels for all compounds, following Eq. (2.30) seen in Chapter 2.

In Figure 6.2, the 2PA spectrum for polymer **1** is shown. There are two 2PA cross-section maxima, one at 890 nm with 349 GM, and the second one at 650 nm with 340 GM. The shortest wavelength peak is mixed with the resonant enhancement since it is close to the last band of the linear absorption, and is related to the binaphthalene backbone of the polymer. The SOS model applied for this compound has four-energy levels, and can be seen as a red line in Figure 6.2, and the fitting parameters obtained from it are shown in Table 6.1.

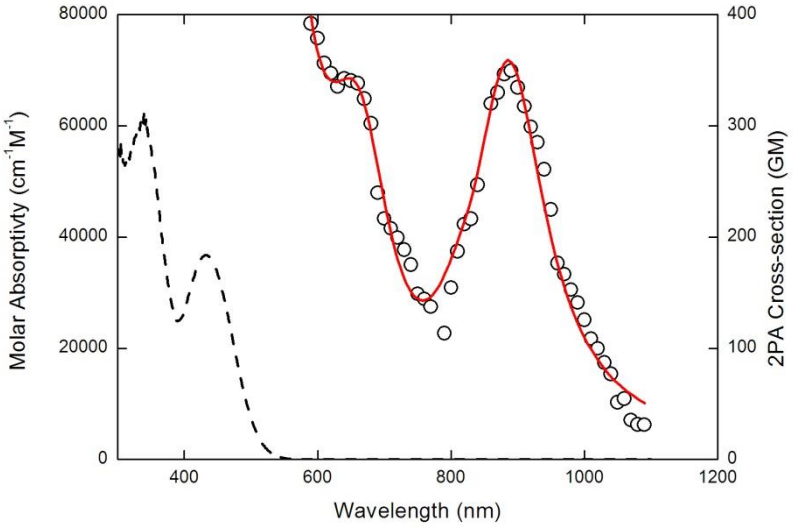

Figure 6.2 - Linear absorption spectrum (black dashed line) along with two-photon absorption measurements (circles) and its SOS fitting (red line) for polymer **1**.
Source: By the author.

Table 6.1 - Spectroscopic parameters obtained from the SOS for all polymers.

Polymer	μ_{01} (D)	$\Delta\mu_{01}$ (D)	λ_{01} (nm)	Γ_{01} (10^{14} Hz)	μ_{12} (D)	λ_{02} (nm)	Γ_{02} (10^{14} Hz)	μ_{13} (D)	λ_{03} (nm)	Γ_{03} (10^{14} Hz)
1	8.5	22.1	442	1.1	13.1	336	1.6	30.0	231	1.8
2	13.2	16.7	545	0.8	7.0	430	0.8	20.0	333	0.7
3	11.7	15.6	559	1.3	10.7	432	1.8	20.0	303	1.6
4	14.2	11.2	612	1.6	8.6	517	1.4	11.5	416	1.6

Source: By the author

The two-photon absorption spectrum shape for polymer **2** is similar to polymer **1**, with two 2PA cross-section peaks as seen in Figure 6.3. The smaller peak around 850 nm shows a cross-section of 422 GM, while the largest peak at 1100 nm has a maximum 2PA cross-section of 680 GM. Both peaks are red shifted in respect to polymer **1**, which was expected since the conjugation length of its chromophore is larger, and its linear absorption is red shifted in respect to polymer **1** as well. The SOS model for four-energy states was applied to the 2PA spectrum, and is shown as a red line in Figure 6.3. The spectroscopic parameters obtained from the fitting are reported in Table 6.1.

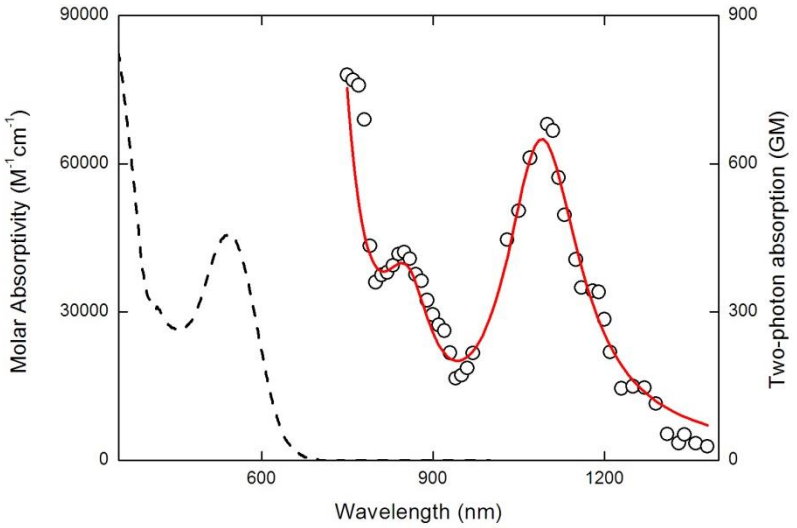

Figure 6.3 - Linear absorption (black dashed line) and two-photon absorption (black circles) spectra for polymer **2**, along with its SOS fitting (red line).
Source: By the author.

Polymer 3 has a small red-shift in respect to polymer **2**, as seen in Figure 6.4. Since the wavelength we started measuring for this polymer was farther from its linear absorption, the resonant enhancement is not apparent in the 2PA spectrum. A four-energy level system was used for the SOS fitting, which is shown as a red line in Figure 6.4, while the fitting parameters are listed in Table 6.1. There are two maxima 2PA cross-sections for polymer **3** as well, one at 860 nm with 618 GM, and the other at 1140 nm with 563 GM.

Polymer **4** also presents two maxima 2PA absorption peaks, one at 1020 nm with 537 GM, and the second one at 1230 nm with 362 GM, as seen in Figure 6.5. The resonant enhancement for this polymer was the strongest one between them, and the peaks are the farthest to the red. This was expected since the chromophore added to the binaphthalene backbone of this polymer has the longest conjugation length. A four energy-level system was used for the SOS fitting, and the parameters obtained from it can be seen in Table 6.1.

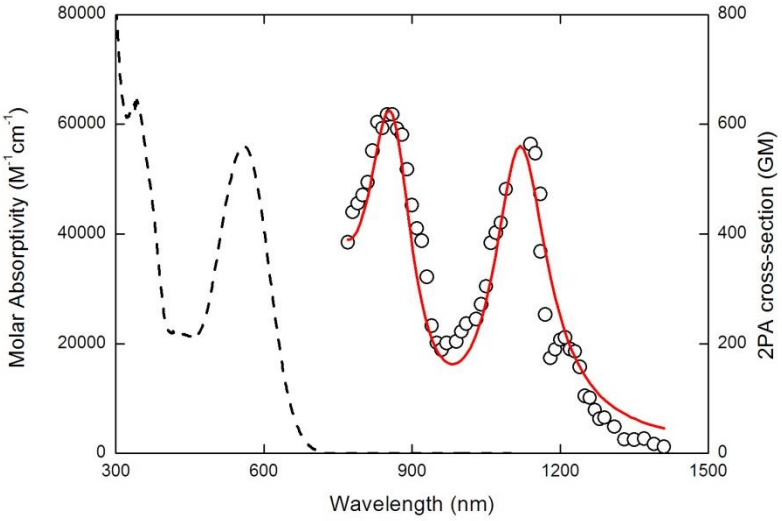

Figure 6.4 - Two-photon (black circles) and linear (black line) spectrum for polymer **3**, along with the SOS fitting (red line).
Source: By the author.

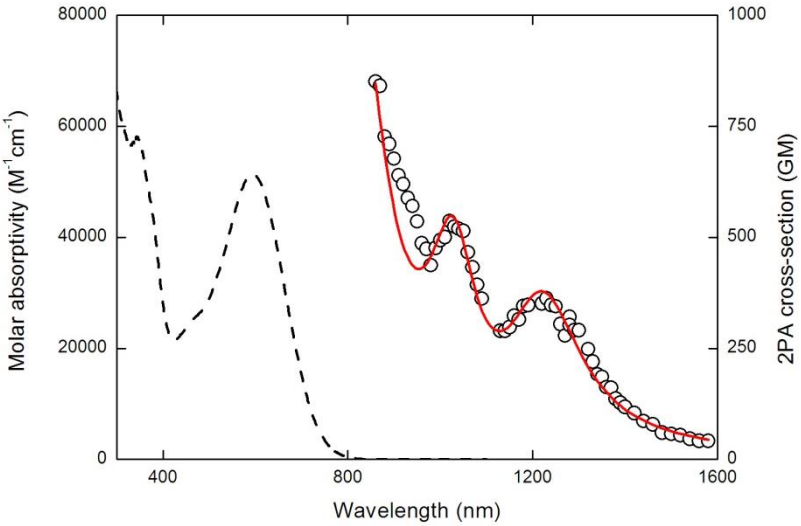

Figure 6.5 - Linear (black dashed line) and two-photon (black circles) absorption spectrum for polymer **4**, as well as its SOS fitting (red line).
Source: By the author.

Although the spectra for the four polymers are similar in shape, their values and the wavelength position of their maxima are different. Also, for polymers **1** and **2**, the second peak has the largest 2PA cross-section, while for polymers **3** and **4** the highest 2PA cross-section occurs at the shortest wavelength. This means that for the first two polymers, the chromophores have a bigger influence on the two-photon transitions, while for polymers **3** and **4** the largest influence is given by the naphthalene backbone. The maximum 2PA cross-section and its wavelength for each polymer are summarized in Table 6.2.

Table 6.2 - Summary of the 2PA maxima cross-sections for all polymers.

Polymer	λ_{2PA}(nm)	σ_{2PA} (GM)
1	890	349
2	1100	680
3	860	618
4	1020	537

Source: By the author.

Polymer **2** shows the largest 2PA cross-section among the studied polymers, with 680 GM at 1100 nm, while the smallest cross-section is given by polymer **1** at 890 nm. This shows that the chromophore used in the polymer **2** synthesis probably allows a larger charge mobility along the polymer structure than the others, which can be endorsed by its dipole moment value (13.2 D), smaller only than the one of polymer **4** (14.2 D).

6.3 Two-photon absorption with polarization variation

Because these are chiral polymers, it is interesting to study their 2PA as a function of light polarization. For that, we used the procedure described in Chapter 3.3, adding a rotating quarter-wave plate before the Z-Scan setup to obtain the transmittance variation between linear, elliptical and circular polarizations. Examples of the obtained curves for Polymer **2** can be seen in Figure 6.6. In this figure, the peaks correspond to the linear polarization transmittance, while the valleys correspond to the circular polarization. We measured 360º to obtain four different transmittances for both linearly and circularly polarized light, which also allowed us to see two circularly polarizations, i.e, light circularly polarized to the right and to the left.

It is possible to obtain the factor Ω_{CLD}^{2PA} directly from these plots using Eq. (2.33) ($\Omega_{CLD}^{2PA} = \sigma_{CP}^{2PA}(\lambda)/\sigma_{LP}^{2PA}(\lambda)$). Since the 2PA cross-section is directly related to the sample transmittance and we need the relation between the 2PA cross-sections for circularly and linearly polarized light, Ω_{CLD}^{2PA} is calculated by dividing the valley transmittance by the peak transmittance for each wavelength. Since there is a series of four peak-valleys, we then take the average to obtain a final value for Ω_{CLD}^{2PA} and plot its spectra.

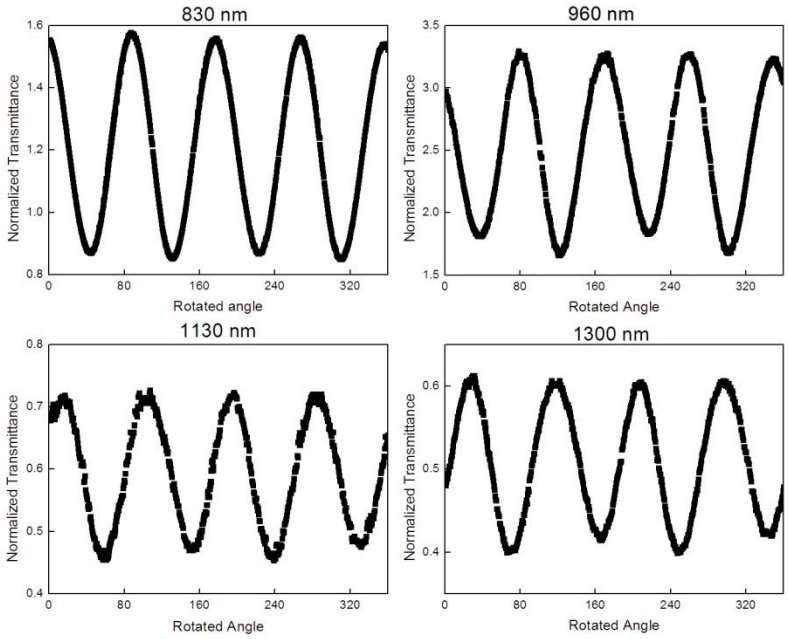

Figure 6.6 - Examples of polarization variation measurements in four different wavelengths for Polymer **2**.

Source: By the author

Before starting the measurements with polarization control, we reevaluated the wavelength to start the spectra by removing the resonant enhancement, by subtracting such effect according to the SOS model. This allows us to obtain the first two-photon absorption peak more clearly. Since Polymer **3** did not present resonant enhancement in the measured spectral range, this process was not performed for it. For Polymers **1**, **2** and **4**, the spectra without the resonant enhancement are shown as blue circles in Figure 6.7.

For Polymer **1**, the Ω_{CLD}^{2PA} spectrum is shown in Figure 6.8a-b, with two separated spectral regions since there are two two-photon absorption peaks in two different wavelengths. It is also possible to observe that the Ω_{CLD}^{2PA} spectrum presents two different behaviors: an approximately constant value, considering the experimental error, from 630 nm up to 700 nm (Figure 6.8a), and two different values separated by a slope for higher wavelengths (Figure 6.8b).

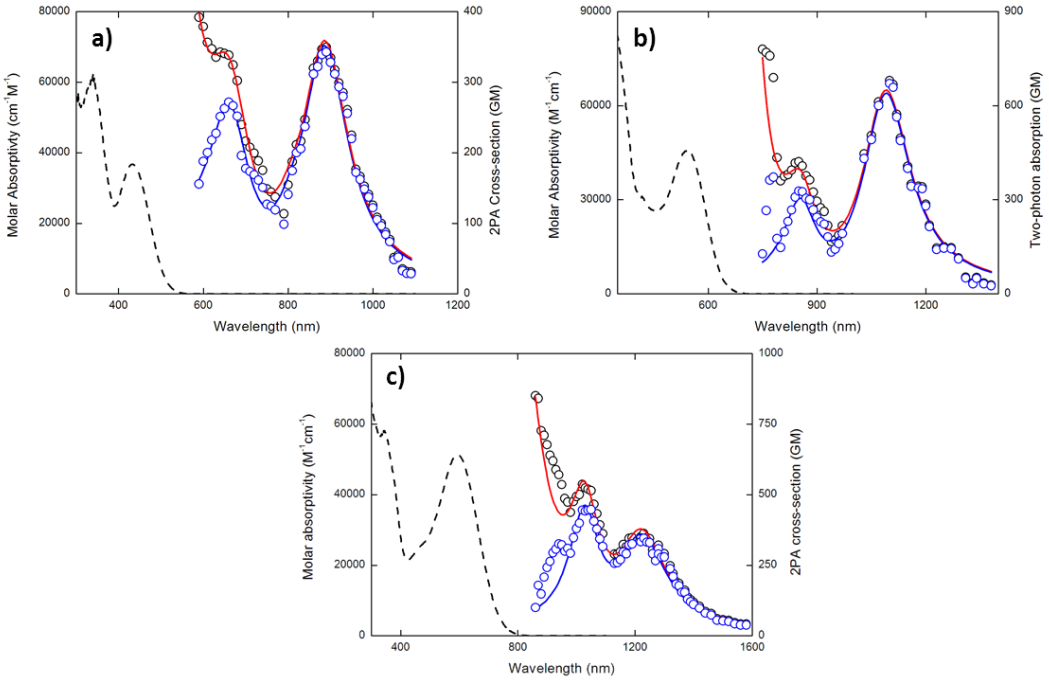

Figure 6.7 - TPA cross-section spectra with (black circles) and without (blue circles) the resonant enhancement, as well as their linear absorption (dashed black line) and SOS fittings (red and blue line) for Polymer (a) **1**, (b) **2** and (c) **4**.
Source: By the author.

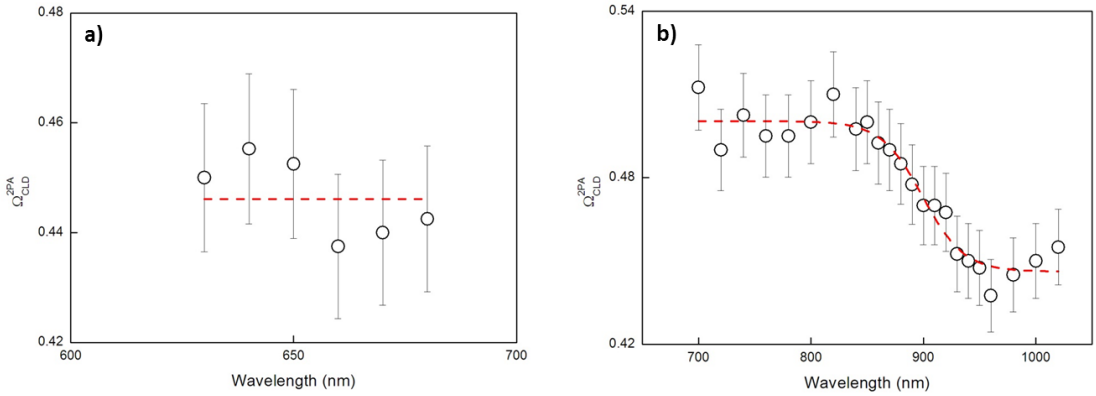

Figure 6.8 - Ω^{2PA}_{CLD} spectrum in (a) the first 2PA peak region and in (b) the second 2PA peak region of polymer **1**. The red dashed lines are for shape comparison purposes.
Source: By the author.

In Figure 6.8a, the behavior is approximately constant, within the experimental error, with Ω^{2PA}_{CLD} = 0.45. The red dashed line shown in the picture is plotted only to guide the eye, not being a theoretical fitting for the spectrum. Considering the shape of this part of the spectrum, one would argue that there is a single level allowed for the 2PA transition, as it would occur for molecular non polymeric systems in a two-

level approximation. However, in such case it would be expected that $0.67 \leq \Omega_{CLD}^{2PA} \leq 1.5$, which is not the case for the observed results. A possibility to explain such result may be related to the complexity of polymeric systems, in which the symmetry of involved states is not precisely defined, such that the theory presented on Chapter 3 is not absolutely applicable here, since it considers molecules completely non-centrosymmetric with defined parity. Even so, since the same type of behavior has been observed, in general, we believe it can be used to give some indications about details of the nonlinear spectrum.

Figure 6.8b shows the Ω_{CLD}^{2PA} spectrum in the region of the second peak of the 2PA cross-section spectrum. There are two regions where Ω_{CLD}^{2PA} has a constant value, one between 700 and 850 nm with Ω_{CLD}^{2PA} ~ 0.5, and the other between 960 and 1020 nm with Ω_{CLD}^{2PA} ~ 0.44. This suggests that there are, at least, two different states allowed for the 2PA transition in this wavelength range. By verifying the energy difference between the constant values, the energy difference between these two energy-levels is of approximately 0.17 eV. From Eq. (2.32), the circular-linear dichroism can be calculated, being $\Delta\sigma_{CLD}^{2PA}$ = -0.33 for the first constant wavelength range, and $\Delta\sigma_{CLD}^{2PA}$ = -0.39 for the second value. The fact that $\Delta\sigma_{CLD}^{2PA} < 0$ within this spectral range points out that the excited states responsible for the 2PA band have the same symmetry as the ground state.[116] This is only an absolute true if we had a centrosymmetric sample, since its states parities would be well defined, while for non-centrosymmetric the electric dipole selection rules are relaxed and do not allow the affirmation of the states parities.[41] Since the polymer has a very long chain and there is no way of knowing its exact symmetry, we cannot affirm the validity of the symmetry assumptions from the negative circular-linear dichroism but, again, the similarity of such results with the ones observed for non-polymeric molecular systems can give an indication of such spectral features, as in an effective type of model.

The red dashed line shown in Figure 6.8b is also not a theoretical fitting for the plot. Equation (2.43) would give a theoretical fitting for the spectrum. However, since the sample is a polymer, applying the equation becomes difficult since it would be difficult to obtain the angles between the dipole moments from quantum chemistry calculations.

From the value obtained for Ω_{CLD}^{2PA} and the spectra obtained for linear polarization shown in Figure 6.7 - TPA cross-section spectra with (black circles) and without

(blue circles) the resonant enhancement, as well as their linear absorption (dashed black line) and SOS fittings (red and blue line) for Polymer (a) 1, (b) 2 and (c) 4.Figure 6.7, it is possible to calculate the TPA cross-section spectrum for circularly polarized light and verify their magnitude difference. From Figure 6.9, we can see that the linearly polarized light cross-section is more than twice the value of the circularly polarized light, showing that for Polymer **1** the incident polarization is an important parameter to be considered for its application.

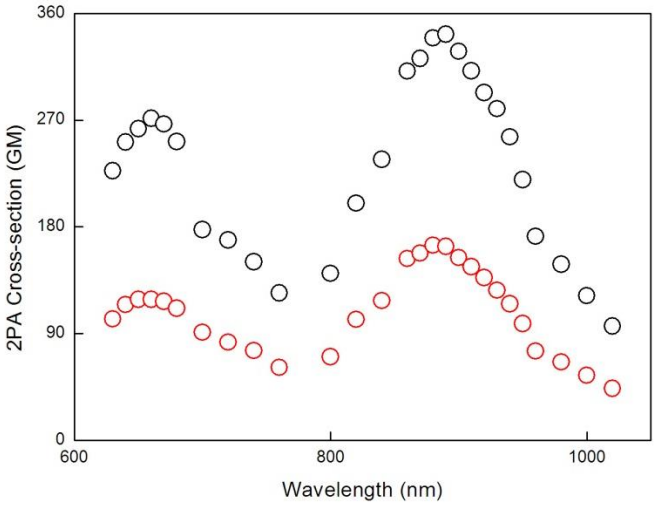

Figure 6.9 - 2PA cross-section spectrum for Polymer **1** with incident linearly polarized light (black circles) and circularly polarized light (red circles).
Source: By the author.

Polymer **2** Ω_{CLD}^{2PA} spectrum has again two different behaviors, both shown in Figure 6.10ab. It was measured between 830 and 1340 nm, which is the wavelength correspondent to its 2PA cross-section spectrum without the resonant enhancement as shown in Figure 6.7b.

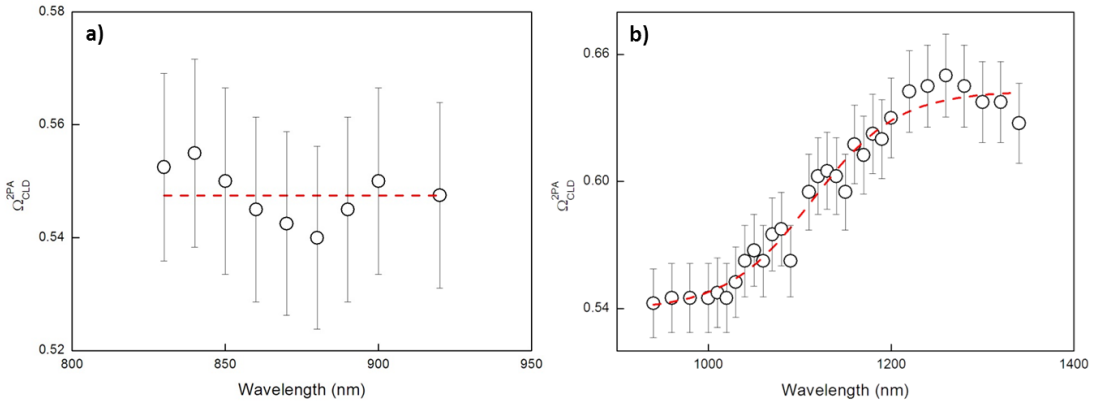

Figure 6.10 - Ω_{CLD}^{2PA} for the (a) first and (b) second peaks of the 2PA absorption of Polymer **2**. The red dashed lines are for eye guides.
Source: By the author.

In Figure 6.10a, an apparent constant behavior can be observed, with Ω_{CLD}^{2PA} = 0.55. However, just like for Polymer **1**, the Ω_{CLD}^{2PA} value is lower than what was predicted theoretically, which, as mentioned before may be related to the lack of well-defined symmetry of the molecular states for polymeric systems. Figure 6.10b shows the behavior of the second 2PA absorption peak. By looking at the red dashed line, which is a sigmoidal-shaped curve meant to guide the eye only, we can see that there are two constant values of Ω_{CLD}^{2PA} separated by a slope towards a higher value. This shows that this 2PA transition is accessible for two or more states, with Ω_{CLD}^{2PA} = 0.64 for wavelengths between 1220 and 1340 nm and Ω_{CLD}^{2PA} = 0.54 for wavelengths between 940 and 1020 nm. The energy separation between these two levels is ~ 0.2 eV, which is larger than the energy separation for the accessible states of Polymer **1**. Calculating $\Delta\sigma_{CLD}^{2PA}$, we obtain $\Delta\sigma_{CLD}^{2PA}$ = -0.30 for 940 – 1020 nm, and $\Delta\sigma_{CLD}^{2PA}$ = -0.22 for 1220 – 1340 nm, both values smaller than zero. If Polymer **2** had defined parities, this would mean that the accessible 2PA states have the same symmetry as the ground state. However, since it is not possible to define the Polymer symmetry properly, this cannot be taken as certain, but only as an indicative.

With the Ω_{CLD}^{2PA} spectrum and the 2PA for linearly polarized light, it is possible to calculate the two-photon absorption cross-section spectrum for incident circularly polarized light, shown in Figure 6.11. For Polymer **2** the difference between the cross-sections in the linear and circular cases is less than 50% for all wavelengths, with the largest differences near the 2PA absorption peaks.

The spectrum for Polymer **3** is shown in Figure 6.12, presenting its two different behaviors separately from 760 to 1410 nm. Differently from Polymers **1** and

2, Polymer **3** does not show a constant behavior on its Ω_{CLD}^{2PA} spectrum related to the first 2PA peak, as shown in Figure 6.12a. It shows instead two constant values, one between 770 and 830 nm with Ω_{CLD}^{2PA} = 0.6, and another one between 900 and 960 nm, with Ω_{CLD}^{2PA} = 0.57, which can be better noticed by the sigmoidal curve exhibited as a red dashed line of Figure 6.12a. That means that this energy transition has two or more accessible states, with an energy difference of ~0.12 eV. For 700 – 830 nm, $\Delta\sigma_{CLD}^{2PA}$ = -0.25, while for 900 – 960 nm, $\Delta\sigma_{CLD}^{2PA}$ = -0.27. Since both calculated $\Delta\sigma_{CLD}^{2PA}$ are smaller than zero, this may indicate that the parity between ground and the accessible excited states are the same. However, since the symmetry of the polymer is not well-defined, this is just an assumption.

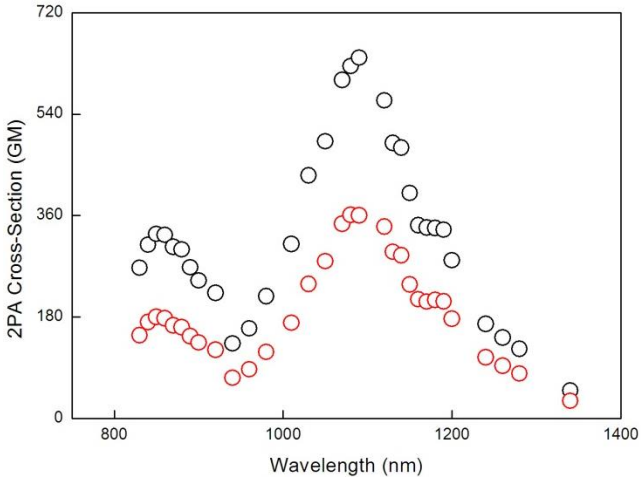

Figure 6.11 - 2PA cross-section spectrum for incident linear (black circles) and circular (red circles) polarized light for Polymer **2**.
Source: By the author.

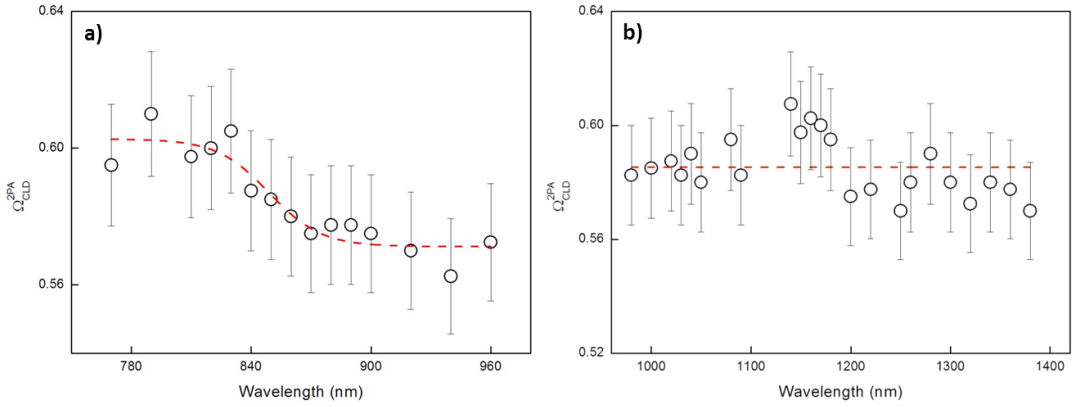

Figure 6.12 - Ω_{CLD}^{2PA} related to the (a) first and (b) second peak of the 2PA cross-section spectrum for Polymer **3**. The red dashed lines are for eye guiding only.
Source: By the author.

Figure 6.12b shows the Ω_{CLD}^{2PA} spectrum related to the second peak of the 2PA. Differently from the previous studied polymers, Polymer **3** exhibits a constant behavior for its second peak, with Ω_{CLD}^{2PA} = 0.59 between 970 and 1410 nm. This would lead us to consider a single state accessible by two-photon absorption in this case. However, since Ω_{CLD}^{2PA} is smaller than the theoretically calculated values expected for this case, there must be more than one accessible state for the transition, causing interference between them and making the Ω_{CLD}^{2PA} spectrum look constant but with a smaller value.

From the Ω_{CLD}^{2PA} spectrum and the linearly polarized light 2PA spectrum, it is possible to calculate the 2PA cross-section for circularly polarized light, shown in Figure 6.13. The first 2PA peak has a difference close to 50% in cross-section values, while for the second peak the difference is smaller. This was expected since the Ω_{CLD}^{2PA} value for the second peak is smaller than for the first one, which shows that the difference between linearly and circularly polarized light 2PA cross-sections is also smaller.

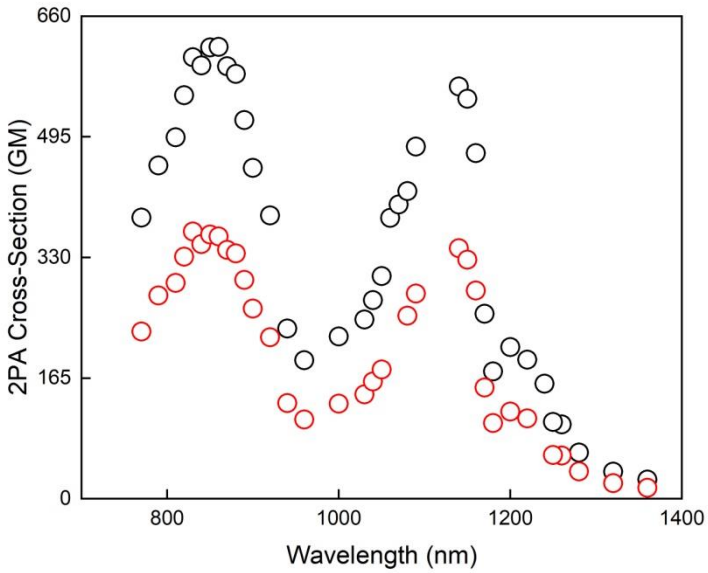

Figure 6.13 – 2PA spectrum for linearly (black circles) and circularly (red circles) polarized light for Polymer **3**.

Source: By the author.

Polymer **4** has its Ω_{CLD}^{2PA} spectrum shown in Figure 6.14. By removing the resonant enhancement (Figure 6.7c), the measurements were taken from 960 to 1460 nm, and present two different behaviors as the previous polymers.

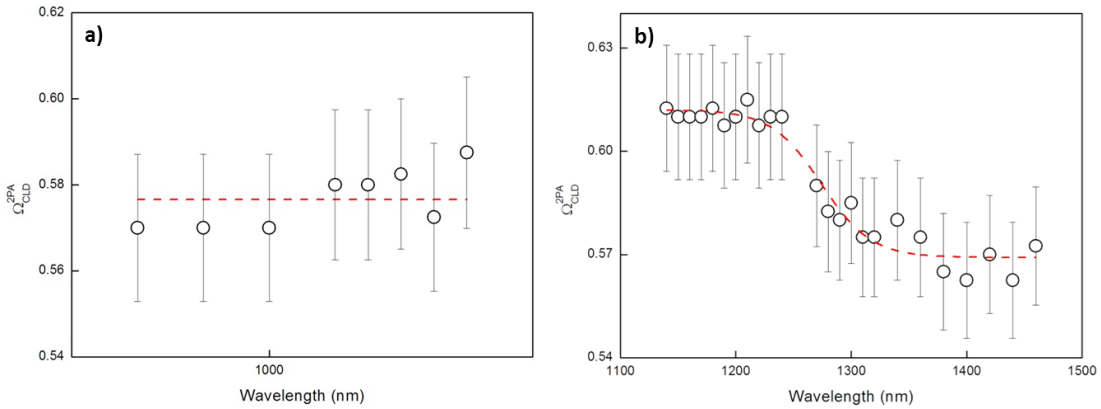

Figure 6.14 - Ω_{CLD}^{2PA} related to the (a) first and (b) second peaks of the 2PA spectrum of polymer **4**. The red dashed lines are for reference only.
Source: By the author.

In Figure 6.14a the Ω_{CLD}^{2PA} spectrum related to the first 2PA peak (950 – 1060 nm) is shown. From it, we can see that it shows an approximately constant behavior, with Ω_{CLD}^{2PA} = 0.58. Similarly to Polymers **1** and **2**, this would show a single accessible state by 2PA transition, but the value is smaller than the theoretically predicted for this case. For the second 2PA peak related curve (Figure 6.14b), there are two constant Ω_{CLD}^{2PA} values separated by a slope. The first level has Ω_{CLD}^{2PA} = 0.61 between 1140 and 1230 nm, while the second one has Ω_{CLD}^{2PA} = 0.57 between 1360 and 1460 nm. This gives an energy difference of ~0.1 eV between the two or more accessible states, which is the smallest among the four studied polymers. Calculating $\Delta\sigma_{CLD}^{2PA}$, we have $\Delta\sigma_{CLD}^{2PA}$ = -0.24 for the first region, and $\Delta\sigma_{CLD}^{2PA}$ = -0.27 for the second one, both values smaller than zero. If the polymer had a defined symmetry, this would allow us to say that the parity between the ground state and the 2PA accessible states is the same. However, since this affirmative is not certain, this remains just a hypothesis.

With the Ω_{CLD}^{2PA} and 2PA for linearly polarized light spectra, we calculated the 2PA cross-section for circularly polarized light, comparing it with the linearly polarized light spectrum without the resonant enhancement (Figure 6.15). The difference between both is smaller than 50% for the whole spectrum, with the largest differences on the first peak where Ω_{CLD}^{2PA} is smaller.

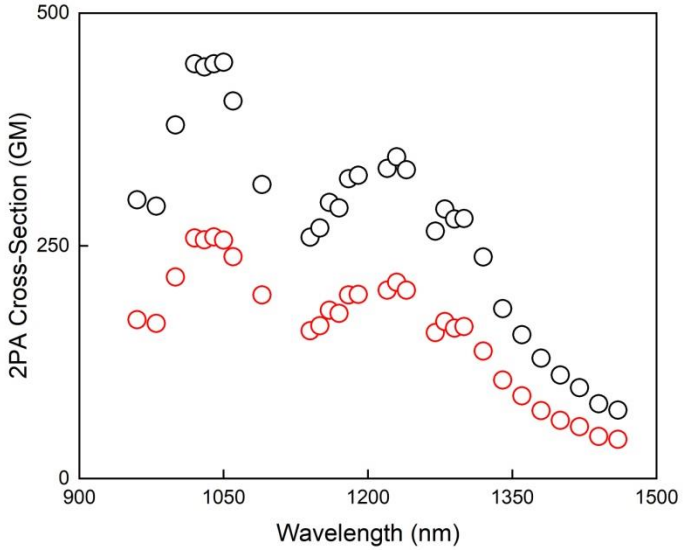

Figure 6.15 – 2PA spectrum for linearly (black circles) and circularly (red circles) polarized light for Polymer **4**.
Source: By the author.

One interesting aspect regarding polarization control studies on the 2PA of chiral materials is to study the difference between the 2PA cross-sections for light circularly polarized to the right and to the left. However, since these differences are usually very small (differences of the order of 1 GM),[117-119] it would be necessary to have a more sensitive experimental system.

For Polymer **2** and **3**, there were wavelengths with two-photon absorption circular dichroism (TPCD), as shown in Figure 6.16. The difference between circularly polarized light to the right and to the left can be seen by the difference in height of the valleys from both graphics, where we have two lower values and two higher values intercalated.

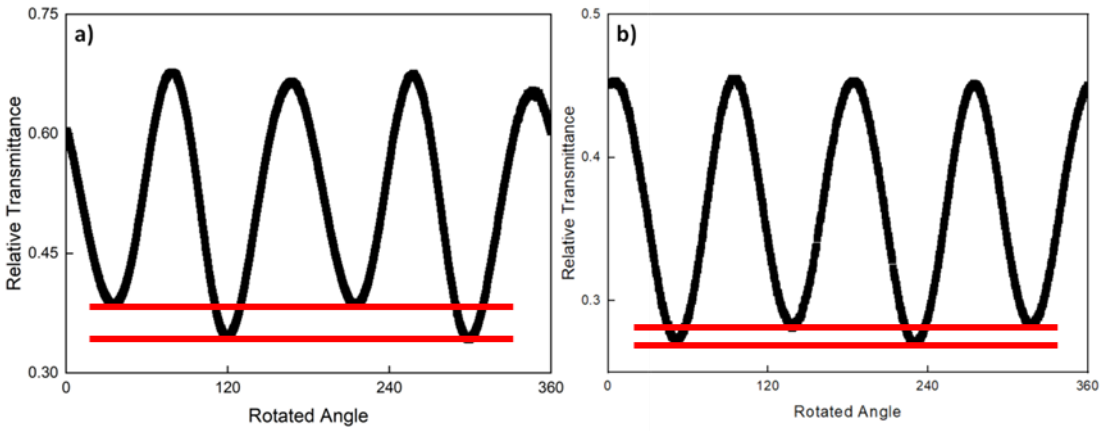

Figure 6.16 - Ω_{CLD}^{2PA} measurements for (a) Polymer **2** at 1000 nm and (b) Polymer **3** at 790 nm.
Source: By the author.

For Polymer **2** (Figure 6.16a), Ω_{CLD}^{2PA} = 0.59 for the first circularly polarized light, while for the second Ω_{CLD}^{2PA} = 0.51. This is a 15% difference considering the average value of the Ω_{CLD}^{2PA} for 1000 nm, which can be considered enough to indicate the existence of TPCD for this wavelength. Calculating the 2PA-CD from Eq. (**2**.**47**), we have $\Delta\sigma_{CD}^{2PA}(\omega)$ = 21 GM, which is a high value compared to previously measured 2PA-CD ones.

For Polymer **3** (Figure 6.16b), Ω_{CLD}^{2PA} = 0.6 for the first circularly polarized light, while for the second Ω_{CLD}^{2PA} = 0.62, which is a 3% difference between both values. This difference is about the same as the experimental error, not allowing a conclusion about the actual existence of TPCD for this wavelength. Calculating the 2PA-CD, $\Delta\sigma_{CD}^{2PA}(\omega)$ = 9 GM, of the same order of magnitude as previously measured 2PA-CD. This effect was not seen in Polymer **1** or **4**, possibly for lack of sensitivity for the detection, or for low concentration of the studied samples during the measurement.

6.4 Final considerations

Four new binaphthalene-based polymers were studied. They had large conjugation lengths and different cromophores added to their main backbone to present different nonlinear properties. The largest 2PA cross-section was given by Polymer **2**, with 680 GM at 1100 nm, while the smallest is of Polymer **1** with 349 GM at 890 nm. Still, all four studied samples have a high 2PA cross-section, enough for nonlinear applications.

Polarization controlled measurements were also taken in order to search for two-photon absorption circular dichroism. This effect was seen for Polymers **2** and **3** for 1000 and 790 nm respectivelly, with intensities of 15% and 3%. However, the most interesting information taken from this measurement was the circular-linear 2PA dichroism, which gave us information about the number of accessible states for the two-photon transitions, which were two or more for the four polymers, and it would also provide information on the states parity if the symmetries of the polymers were known. Since their structure is too long and it might not be completely non-centrosymmetric, it was not possible to make statements about the parities between states.

7 CONCLUSIONS

Two-photon absorption studies on three different kinds of organic molecules were carried out along this dissertation.

The first study was made on five novel fluorenone-based compounds on Chapter 4. Both absorptive Z-Scan measurements and DFT analysis were made for these compounds, allowing a direct comparison between them. Quantum yield measurements were also made for these molecules, in order to verify their possible applications in two-photon absorption microscopy. F-benzothiophene presented the largest 2PA cross-section, with 224 GM at 710 nm, with a quantum yield of 0.19, showing promising nonlinear properties for applications. Comparing the ordering of the 2PA cross-sections obtained through experimental measurements with the theoretically calculated ones revealed good agreement, and also allowed a better understanding of the charge movement within the compounds through its HOMO-LUMO transitions. Overall, the five samples presented reasonable 2PA cross-section and quantum yields, showing promising value for two-photon microscopy in living tissues.

Seven new BF_2-naphthyridine compounds were studied, as shown in Chapter 6. These compounds present small conjugation length and simple structures, and were designed to have competitive 2PA cross-sections compared to larger and more complex compounds of the same kind. Absorptive Z-Scan measurements were made, as well as DFT calculations to obtain the theoretical 2PA cross-section spectra for these compounds. Both compounds that presented higher 2PA cross-section had a strong donor as a substituent (NO_2), which were compound **VII** with 268 GM at 990 nm, and compound **IV**, with 156 GM at 590 nm. These values are of the same order of magnitude from previously measured BODIPY molecules with much longer conjugation length and more substituents, showing that it is possible to have simpler molecules with high nonlinearities as well. With the theoretical calculations, it was possible to observe the HOMO-LUMO transitions to understand the charge movement within the molecules and verify that they corroborate with the observed results. It was also possible to calculate the dipole moments for each sample and compare them with the experimentally obtained ones, as well as use the calculated cross-sections and oscillator strengths to make theoretical 2PA cross-section

spectra. Comparing these data with our measured ones, it was possible to verify their good agreement, corroborating our experimental results even more.

In Chapter 7, four new binaphthalene-based polymers were studied. Since these compounds presented inherent chirality, two different kinds of two-photon absorption studies were done: one with linearly polarized light to obtain the 2PA cross-section spectra, and one with polarization control to verify differences between circular-linear and circular-circular polarized light. The largest 2PA cross-section was given by Polymer **2**, with 680 GM at 1100 nm, measured through absorptive Z-Scan with linearly polarized light. All four polymers presented high 2PA cross-sections, above 300 GM, showing that they have promising nonlinear properties for applications. For the polarization controlled measurements the Ω_{CLD}^{2PA} spectrum was obtained for each polymer, which is capable of showing properties that the regular 2PA measurement is not able to, such as the number of accessible states and the parity between the ground state and the excited state. All four polymers presented more than one accessible state for each 2PA transition, with the ground state having the same parity of the excited states. However, this last affirmation is not completely certain as the symmetry of the polymers are not well-known. Differences between circularly polarized to the right and to the left were also seen for polymers **2** and **3**, with a 15% difference for the first one and 3% for the latter one. Since the sensitivity of the measurement is not high enough, we could not verify the same effect for polymers **1** and **4** or other wavelengths for polymers **2** and **3**, showing the difficulty of measuring the two-photon absorption circular dichroism through this method.

During this dissertation we presented three groups of molecules with large nonlinear properties, showing their two-photon absorption spectra. From this information, it is possible to decide which kind of application fits each sample better, and from the comparisons between each different compound within the groups, it was also possible to show which characteristics matter most for increasing their nonlinearities.

8 BIBLIOGRAPHIC PRODUCTION

Papers published on journals

DIPOLD, J.; BATISTA, R. J. M. B.; FONSECA, R. D.; SILVA, D. L.; MOURA, G. L. C.; DOS ANJOS, J. V.; SIMAS, A. M.; DE BONI, L.; MENDONCA, C. R. Synthesis and two-photon absorption spectrum of fluorenone based molecules. **Chemical Physics Letters**, v. 661, p. 143-150, 2016.

DIPOLD, J.; ROMERO, E.; DONNELLY, J.; CALHEIRO, T. P.; BONACORSO, H. G.; IGLESIAS, B. A.; SIQUEIRA, J.; DE BONI, L.; HERNANDEZ, F. E.; MENDONÇA, C. R. Two-photon Absorption Properties of BODIPYs-like compounds based on BF_2-naphthyridine Complexes. **Physical Chemistry Chemical Physics**, 2019, Accepted Manuscript.

Event participation

DIPOLD, J.; BATISTA, R. J. M. B.; FONSECA, R. D.; SILVA, D. L.; SIMAS, A. M.; DE BONI, L.; MENDONCA, C. R. Two-photon absorption spectrum of fluorenone-based molecules. **Encontro de Física 2016** – Natal, RN, Brasil.

DIPOLD, J.; MARTINS, R. J.; FUENDLING, S.; VOSS, T.; WAAG, A.; MENDONÇA, C. R. Two-photon coefficient measurements of GaN film. **Encontro de Física 2016** – Natal, RN, Brasil.

DIPOLD, J.; BATISTA, R. J. M. B.; FONSECA, R. D.; SILVA, D. L.; SIMAS, A. M.; DE BONI, L.; MENDONÇA, C. R. Two-photon absorption spectrum of fluorenone-based molecules. **Frontiers in Optics 2016** – Rochester, NY, USA. doi: 10.1364/LS.2016.LF2D.3

DIPOLD, J.; KOECKELBERGHS, G.; VIVAS, M. G.; DE BONI, L.; MENDONCA, C. R. Two-photon circular-linear dichroism on a Binaphthalene-based polymer. **Frontiers in Optics 2017** – Washington, DC, USA.

DIPOLD, J.; KOECKELBERGHS, G.; VIVAS, M. G.; DE BONI, L.; MENDONCA, C. R. Two-photon circular-linear dichroism study of a Binaphthalene-based polymer. **XVI SWIECA School** – São Paulo, SP, Brazil.

DIPOLD, J.; CALHEIRO, T. P.; BONACORSO, H. G.; IGLESIAS, B. A.; DONELLY, J.; ROMERO, E.; SIQUEIRA, J. P., HERNANDEZ, F. E.; DE BONI, L.; MENDONCA, C. R. Nonlinear spectroscopy of novel borondipyrromethenes complexes. **JSAP-OSA Joint Symposia at the JSAP Autumun Meeting**, 2018, Nagoya, Japan.

REFERENCES

1 HE, G. S. et al. Multiphoton absorbing materials: molecular designs, characterizations, and applications. **Chemical Reviews,** v. 108, n. 4, p. 1245-1330, 2008.

2 BOYD, R. W. **Nonlinear optics**. 3rd ed. London, UK: Academic Press, 2008.

3 REITZ, J. R.; MILFORD, F. J. **Foundations of electromagnetic theory**. Reading, Massachussets: Addison-Wesley Publishing Company, Inc., 1960.

4 GÖPPERT-MAYER, M. On elementary acts with two quantum jumps. **Annalen der Physik,** v. 8, n. 1, p. 273-294, 1931.

5 KAISER, W.; GARRETT, C. G. B. 2-photon excitation in CAF2 - EU2+. **Physical Review Letters,** v. 7, n. 6, p. 229-&, 1961.

6 CORREA, D. S. et al. Two-photon polymerization for fabricating structures containing the biopolymer chitosan. **Journal of Nanoscience and Nanotechnology,** v. 9, n. 10, p. 5845-5849, 2009.

7 CUMPSTON, B. H. et al. Two-photon polymerization initiators for three-dimensional optical data storage and microfabrication. **Nature,** v. 398, n. 6722, p. 51-54, 1999.

8 SUGIOKA, K.; CHENG, Y. Ultrafast lasers-reliable tools for advanced materials processing. **Light-Science & Applications,** v. 3, p. e149, 2014. doi: 10.1038/lsa.2014.30.

9 KAWATA, S. et al. Finer features for functional microdevices - micromachines can be created with higher resolution using two-photon absorption. **Nature,** v. 412, n. 6848, p. 697-698, 2001.

10 AVILA, O. I. et al. Femtosecond laser writing of PPV-doped three-dimensional polymeric microstructures. **Journal of Polymer Science Part B** - polymer physics, v. 56, n. 6, p. 479-483, 2018.

11 KONIG, K. Multiphoton microscopy in life sciences. **Journal of Microscopy,** v. 200, p. 83-104, 2000.

12 DENK, W.; STRICKLER, J. H.; WEBB, W. W. 2-Photon laser scanning fluorescence microscopy. **Science,** v. 248, n. 4951, p. 73-76, Apr. 1990.

13 HE, R. Y. et al. Surface plasmon-enhanced two-photon fluorescence microscopy for live cell membrane imaging. **Optics Express,** v. 17, n. 8, p. 5987-5997, Apr. 2009.

14 MCCONNELL, G.; RIIS, E. Two-photon laser scanning fluorescence microscopy using photonic crystal fiber. **Journal of Biomedical Optics,** v. 9, n. 5, p. 922-927, Sep-Oct. 2004.

15 KIM, H. M.; CHO, B. R. Two-photon probes for intracellular free metal ions, acidic vesicles, and lipid rafts in live tissues. **Accounts of Chemical Research,** v. 42, n. 7, p. 863-872, July 2009.

16 ALAMUDI, S. H. et al. Development of background-free tame fluorescent probes for intracellular live cell imaging. **Nature Communications,** v. 7, June 2016. doi: 10.1038/ncomms11964.

17 CAHALAN, M. D. et al. Two-photon tissue imaging: seeing the immune system in a fresh light. **Nature Reviews Immunology,** v. 2, n. 11, p. 872-880, Nov. 2002.

18 CELLI, J. P. et al. Imaging and photodynamic therapy: mechanisms, monitoring, and optimization. **Chemical Reviews,** v. 110, n. 5, p. 2795-2838, May 2010.

19 HUANG, Z. A review of progress in clinical photodynamic therapy. **Technology in Cancer Research & Treatment,** v. 4, n. 3, p. 283-293, June 2005.

20 GOYAN, R. L.; CRAMB, D. T. Near-infrared two-photon excitation of protoporphyrin IX: Photodynamics and photoproduct generation. **Photochemistry and Photobiology,** v. 72, n. 6, p. 821-827, Dec. 2000.

21 BONNETT, R. Photosensitizers of the porphyrin and phthalocyanine series for photodynamic therapy. **Chemical Society Reviews,** v. 24, n. 1, p. 19-33, Feb. 1995.

22 ETHIRAJAN, M. et al. The role of porphyrin chemistry in tumor imaging and photodynamic therapy. **Chemical Society Reviews,** v. 40, n. 1, p. 340-362, 2011.

23 KAMKAEW, A. et al. BODIPY dyes in photodynamic therapy. **Chemical Society Reviews,** v. 42, n. 1, p. 77-88, 2013.

24 KOMAR, A. A. et al. **Optical limiters for laser radiation based on reverse saturable polymethine dyes**. In: INTERNATIONAL CONFERENCE ON COHERENT AND NONLINEAR OPTICS, 2007, Minsk. **Proceedings**... Minsk: SPIE, 2007.

25 LI, F. et al. Optical limiting properties of two phthalocyanines using 1064-nm laser in solution. **Materials Letters,** v. 62, n. 17-18, p. 3059-3062, June 2008.

26 TUTT, L. W.; BOGGESS, T. F. A review of optical limiting mechanisms and devices using organics, fullerenes, semiconductors and other materials. **Progress in Quantum Electronics,** v. 17, n. 4, p. 299-338, 1993.

27 WANG, X. S. et al. Upconversion luminescence and optical power limiting effect based on two- and three-photon absorption processes of ZnO crystal. **Optics Communications,** v. 280, n. 1, p. 197-201, Dec. 2007.

28 CHEN, Y. et al. Axially modified gallium phthalocyanines and naphthalocyanines for optical limiting. **Chemical Society Reviews,** v. 34, n. 6, p. 517-529, 2005.

29 SPANGLER, C. W. Recent development in the design of organic materials for optical power limiting. **Journal of Materials Chemistry,** v. 9, n. 9, p. 2013-2020, Sept. 1999.

30 ZHOU, Y. et al. Hydrothermal dehydration for the "Green" reduction of exfoliated graphene oxide to graphene and demonstration of tunable optical limiting properties. **Chemistry of Materials,** v. 21, n. 13, p. 2950-2956, July 2009.

31 MULLER, O. et al. Nonlinear optical behavior of porphyrin functionalized nanodiamonds: an efficient material for optical power limiting. **Applied Optics,** v. 55, n. 14, p. 3801-3808, May 2016.

32 KAWATA, S.; KAWATA, Y. Three-dimensional optical data storage using photochromic materials. **Chemical Reviews,** v. 100, n. 5, p. 1777-1788, May 2000.

33 MOREL, Y. et al. Two-photon absorption and optical power limiting of bifluorene molecule. **Journal of Chemical Physics,** v. 114, n. 12, p. 5391-5396, Mar. 2001.

34 TORIUMI, A.; KAWATA, S.; GU, M. Reflection confocal microscope readout system for three-dimensional photochromic optical data storage. **Optics Letters,** v. 23, n. 24, p. 1924-1926, Dec. 1998.

35 GU, M. et al. Effect of saturable response to two-photon absorption on the readout signal level of three-dimensional bit optical data storage in a photochromic polymer. **Applied Physics Letters,** v. 79, n. 2, p. 148-150, July 2001.

36 POLYZOS, I. et al. Two-photon absorption properties of novel organic materials for three-dimensional optical memories. **Chemical Physics Letters,** v. 369, n. 3-4, p. 264-268, Feb. 2003.

37 WANG, M. M.; ESENER, S. C. Three-dimensional optical data storage in a fluorescent dye-doped photopolymer. **Applied Optics,** v. 39, n. 11, p. 1826-1834, Apr. 2000.

38 DAY, D.; GU, M. Use of two-photon excitation for erasable-rewritable three-dimensional bit optical data storage in a photorefractive polymer. **Optics Letters,** v. 24, n. 14, p. 948-950, July 1999.

39 MCPHAIL, D.; GU, M. Use of polarization sensitivity for three-dimensional optical data storage in polymer dispersed liquid crystals under two-photon illumination. **Applied Physics Letters,** v. 81, n. 7, p. 1160-1162, Aug. 2002.

40 DAGANI, R. Two photons shine in 3-D data storage. **Chemical & Engineering News,** v. 74, n. 39, p. 68-70, Sept. 1996.

41 BONIN, K. D.; MCILRATH, T. J. 2-Photon electric-dipole selection-rules. **Journal of the Optical Society of America B** - optical physics, v. 1, n. 1, p. 52-55, 1984.

42 PRASAD, P. N.; WILLIANS, D. J. **Introduction to nonlinear optical effects in molecules and polymers**. New York: Wiley-Interscience, 1991.

43 VIVAS, M. G. **Relação entre a estrutura molecular e as propriedades de absorção de multi-fótons em compostos orgânicos pi-conjugados**. 2011. 177 p. Tese (Doutorado em Ciências) - Instituto de Física de São Carlos, Universidade de São Paulo, São Carlos, 2011.

44 QIAN, Y. et al. Multiphoton upconversion fluorescence properties of heteroaromatic push-pull polymer. **Acta Physico-Chimica Sinica,** v. 25, n. 6, p. 1149-1155, June 2009.

45 AKEMANN, W. et al. Photoinduced intramolecular charge transfer in push-pull polyenes: effects of solvation, electron-donor group, and polyenic chain length. **Journal of Physical Chemistry B,** v. 112, n. 2, p. 358-368, Jan. 2008.

46 LEE, S. et al. Dependence of the two-photon absorption cross section on the conjugation of the phenylacetylene linker in dipolar donor-bridge-acceptor chromophores. **Journal of Physical Chemistry A,** v. 109, n. 43, p. 9767-9774, Nov. 2005.

47 POWER, E. A. 2-Photon circular-dichroism. **Journal of Chemical Physics,** v. 63, n. 4, p. 1348-1350, 1975.

48 TINOCO, I. 2-Photon circular-dichroism. **Journal of Chemical Physics,** v. 62, n. 3, p. 1006-1009, 1975.

49 LIM, E. C. **Excited states**. New York: Academic Press, 1977.

50 FRIEDRICH, D. M. Tensor patterns and polarization ratios for 3-Photon transitions in fluid media. **Journal of Chemical Physics,** v. 75, n. 7, p. 3258-3268, 1981.

51 VIVAS, M. G.; DE BONI, L.; MENDONÇA, C. R. Two-photon spectroscoý of organic materials. In: GUPTA, V. P. (Ed.). **Molecular and laser spectroscopy:** advances and applications. Amsterdam: Elsevier, 2018. cap. 8.

52 MEATH, W. J.; POWER, E. A. ON THE IMPORTANCE OF PERMANENT MOMENTS IN MULTIPHOTON ABSORPTION USING PERTURBATION-THEORY. **Journal of Physics B:** atomic molecular and optical physics, v. 17, n. 5, p. 763-781, 1984.

53 VIVAS, M. G. et al. Experimental and theoretical study on the one- and two-photon absorption properties of novel organic molecules based on phenylacetylene and azoaromatic moieties. **Journal of Physical Chemistry B,** v. 116, n. 50, p. 14677-14688, Dec. 2012.

54 _____. Two-photon circular-linear dichroism of perylene in solution: a theoretical-experimental study. **Journal of Physical Chemistry B,** v. 117, n. 9, p. 2742-2747, Mar. 2013.

55 MEATH, W. J.; POWER, E. A. Differential multiphoton absorption by chiral molecules and the effect of permanent moments. **Journal of Physics B:** atomic molecular and optical physics, v. 20, n. 9, p. 1945-1964, May 1987.

56 VIVAS, M. G. et al. Revealing the electronic and molecular structure of randomly oriented molecules by polarized two-photon spectroscopy. **Journal of Physical Chemistry Letters,** v. 4, n. 10, p. 1753-1759, May 2013.

57 _____. Understanding the two-photon absorption spectrum of PE2 platinum acetylide complex. **Journal of Physical Chemistry A,** v. 118, n. 30, p. 5608-5613, July 2014.

58 POWER, E. A.; THIRUNAMACHANDRAN, T. Circular-dichroism - general theory based on quantum electrodynamics. **Journal of Chemical Physics,** v. 60, n. 9, p. 3695-3701, 1974.

59 BELFIELD, K. D. et al. Spectral properties of several fluorene derivatives with potential as two-photon fluorescent dyes. **Journal of Luminescence,** v. 97, n. 2, p. 141-146, May 2002.

60 HUANG, T.-H. et al. Investigation on the linear and nonlinear optical properties of fluorenone-based linear conjugated oligomers: the influence of pi-spacer. **Journal of Photochemistry and Photobiology A**: chemistry, v. 261, p. 41-45, June 2013.

61 _____. Effects of pi-spacers on the linear and nonlinear optical properties of novel fluorenone-based D-pi-A-pi-D type conjugated oligomers with different donors. **Optical Materials,** v. 35, n. 7, p. 1373-1377, May 2013.

62 CAPODILUPO, A.-L. et al. A series of diphenylamine-fluorenone derivatives as potential fluorescent probes for neuroblastoma cell staining. **Tetrahedron,** v. 72, n. 22, p. 2920-2928, June 2016.

63 CAPODILUPO, A. L. et al. Design and synthesis of fluorenone-based dyes: two-photon excited fluorescent probes for imaging of lysosomes and mitochondria in living cells. **Journal of Materials Chemistry B,** v. 3, n. 16, p. 3315-3323, 2015.

64 ZIESSEL, R.; ULRICH, G.; HARRIMAN, A. The chemistry of Bodipy: a new El Dorado for fluorescence tools. **New Journal of Chemistry,** v. 31, n. 4, p. 496-501, 2007.

65 ZHANG, X. L.; XIAO, Y.; QIAN, X. H. Highly efficient energy transfer in the light harvesting system composed of three kinds of boron-dipyrromethene derivatives. **Organic Letters,** v. 10, n. 1, p. 29-32, Jan. 2008.

66 LOVELL, J. F. et al. Activatable photosensitizers for imaging and therapy. **Chemical Reviews,** v. 110, n. 5, p. 2839-2857, May 2010.

67 URANO, Y. et al. Selective molecular imaging of viable cancer cells with pH-activatable fluorescence probes. **Nature Medicine,** v. 15, n. 1, p. 104-109, Jan. 2009.

68 GOMEZ-DURAN, C. F. A. et al. 8-PropargylaminoBODIPY: unprecedented blue-emitting pyrromethene dye. synthesis, photophysics and laser properties. **Chemical Communications,** v. 46, n. 28, p. 5103-5105, 2010.

69 HATTORI, S. et al. Charge separation in a nonfluorescent donor-acceptor dyad derived from boron dipyrromethene dye, leading to photocurrent generation. **Journal of Physical Chemistry B,** v. 109, n. 32, p. 15368-15375, Aug. 2005.

70 BENNISTON, A. C.; COPLEY, G. Lighting the way ahead with boron dipyrromethene (Bodipy) dyes. **Physical Chemistry Chemical Physics,** v. 11, n. 21, p. 4124-4131, 2009.

71 KATZ, J. L.; GELLER, B. J.; FOSTER, P. D. Oxacalixarenes and oxacyclophanes containing 1,8-naphthyridines: a new class of molecular tweezers with concave-surface functionality. **Chemical Communications**, n. 10, p. 1026-1028, 2007.

72 FU, L. et al. Efficient synthesis and evaluation of antitumor activities of novel functionalized 1,8-naphthyridine derivatives. **Acs Combinatorial Science,** v. 17, n. 1, p. 24-31, Jan. 2015.

73 BONACORSO, H. G. et al. 1,1-Difluoro-3-aryl(heteroaryl)-1H-pyrido 1,2-c 1,3,5,2 oxadiazaborinin-9-ium-1-uides: synthesis; structure; and photophysical, electrochemical, and BSA-binding studies. **New Journal of Chemistry,** v. 42, n. 3, p. 1913-1920, Feb. 2018.

74 ZHENG, J. et al. The aggregation-induced emission enhancement properties of BF2 complex isatin-phenylhydrazone: synthesis and fluorescence characteristics. **Dyes and Pigments,** v. 113, p. 502-509, Feb. 2015.

75 BONACORSO, H. G. et al. Multinuclear NMR spectroscopy, photophysical, electrochemical and DNA-binding properties of fluorinated 1,8-naphthyridine-based boron heterocycles. **Journal of Fluorine Chemistry,** v. 205, p. 8-14, Jan. 2018.

76 _____. Synthesis, B-11- and F-19 NMR spectroscopy, and optical and electrochemical properties of novel 9-aryl-3-(aryl/heteroaryl)-1, 1-difluoro-7-(trifluoromethyl)-1H- 1,3,5,2 oxadiazaborinino 3,4-a 1,8 naphthyridin-11-ium-1-uide complexes. **Tetrahedron Letters,** v. 57, n. 46, p. 5017-5021, Nov. 2016.

77 WU, Y. Y. et al. Large stokes shift induced by intramolcular charge transfer in N,O-Chelated naphthyridine-BF2 complexes. **Organic Letters,** v. 14, n. 20, p. 5226-5229, Oct. 2012.

78 HIKISHIMA, S. et al. Synthesis of 1,8-naphthyridine C-nucleosides and their base-pairing properties in oligodeoxynucleotides: thermally stable Naphthyridine : imidazopyridopyrimidine base-pairing motifs. **Angewandte Chemie International Edition,** v. 44, n. 4, p. 596-598, 2005.

79 BARROS, L. W. et al. Enhancement of two-photon absorption in highly emissive BODIPY dyes. CONFERENCE ON LASERS AND ELECTRO-OPTICS (CLEO), 2016, San Jose. **Proceedings**… São José: IEEE, 2016.

80 WANG, Y. C. et al. Nonlinear optical properties and ultrafast dynamics of three novel boradiazaindacene derivatives. **Journal of Applied Physics,** v. 108, n. 3, Aug. 2010.
81 PORRES, L.; MONGIN, O.; BLANCHARD-DESCE, M. Synthesis, fluorescence and two-photon absorption properties of multichromophoric boron-dipyrromethene fluorophores for two-photon-excited fluorescence applications. **Tetrahedron Letters,** v. 47, n. 12, p. 1913-1917, Mar. 2006.

82 ZHENG, Q. D.; XU, G. X.; PRASAD, P. N. Conformationally restricted dipyrromethene boron difluoride (BODIPY) dyes: highly fluorescent, multicolored probes for cellular imaging. **Chemistry:** a european journal, v. 14, n. 19, p. 5812-5819, 2008.

83 BARROS, L. W. T. et al. Two-photon absorption in a series of 2,6-disubstituted BODIPY dyes. **Physical Chemistry Chemical Physics,** v. 19, n. 32, p. 21683-21690, Aug. 2017.

84 KUCUKOZ, B. et al. Enhancement of two photon absorption properties and intersystem crossing by charge transfer in pentaaryl boron-dipyrromethene (BODIPY) derivatives. **Physical Chemistry Chemical Physics,** v. 18, n. 19, p. 13546-13553, May 2016.

85 ATKINS, P.; DE PAULA, J. **Physical chemistry for the life science**. New York: W. H. Freeman Company, 2006.

86 FLACK, H. D. Louis Pasteur's discovery of molecular chirality and spontaneous resolution in 1848, together with a complete review of his crystallographic and chemical work. **Acta Crystallographica A**: foundation and advances, v. 65, p. 371-389, Sept. 2009.

87 KENNEPOHL, D. et al. Chiral molecules. libre text, 2015. Available from: <https://chem.libretexts.org/Bookshelves/Organic_Chemistry/Map%3A_Organic_Chemistry_(Vollhardt_and_Schore)/05._Stereoisomers/5.1%3A_Chiral__Molecules >. Accessible at: 23 Jan. 2018.

88 LV, Z. Y. et al. Stimuli-directed helical chirality inversion and bio-applications. **Polymers,** v. 8, n. 8, Aug 2016. doi: 10.3390/polym8080310.

89 VERBIEST, T.; KAURANEN, M.; PERSOONS, A. Second-order nonlinear optical properties of chiral thin films. **Journal of Materials Chemistry,** v. 9, n. 9, p. 2005-2012, Sept. 1999.

90 KAURANEN, M.; VERBIEST, T.; PERSOONS, A. Chiral materials in second-order nonlinear optics. **Journal of Nonlinear Optical Physics & Materials,** v. 8, n. 2, p. 171-189, June 1999.

91 VERBIEST, T. et al. Strong enhancement of nonlinear optical properties through supramolecular chirality. **Science,** v. 282, n. 5390, p. 913-915, Oct. 1998.

92 _____. Second-order nonlinear optical properties of a chromophore-functionalized polypeptide. **Advanced Materials,** v. 8, n. 9, p. 756-&, Sept. 1996.

93 BOUMAN, M. M. et al. Chiroptical properties of regioregular chiral polythiophenes. **Molecular Crystals and Liquid Crystals Science and Technology Section A:** molecular crystals and liquid crystals, v. 256, p. 439-448, 1994. doi: 10.1080/10587259408039274

94 KOECKELBERGHS, G.; VAN BEYLEN, M.; SAMYN, C. Synthesis of new polyisocyanates. **Materials Science & Engineering C:** biomimetic and supramolecular systems, v. 18, n. 1-2, p. 15-20, Dec. 2001.

95 _____. Synthesis of new polyisocyanates. **European Polymer Journal,** v. 37, n. 10, p. 1991-1996, Oct. 2001.

96 MA, L. et al. A new class of chiral conjugated polymers with a propeller-like structure. **Macromolecules,** v. 30, n. 2, p. 204-218, Jan. 1997.

97 _____. Conjugated polymers with main chain chirality .3. Synthesis of optically active poly(aryleneethynylene)s. **Macromolecules,** v. 29, n. 15, p. 5083-5090, July 1996.

98 KOECKELBERGHS, G. et al. Synthesis and properties of chiral donor-embedded polybinaphthalenes for nonlinear optical applications. **Chemistry of Materials,** v. 15, n. 15, p. 2870-2872, July 2003.

99 _____. Donor-embedded polybinaphthalenes for nonlinear optical applications: Influence of the incorporation of a double bond. **Macromolecular Rapid Communications,** v. 26, n. 11, p. 905-910, June 2005.

100 _____. Synthesis and properties of new chiral donor-embedded polybinaphthalenes for nonlinear optical applications. **Macromolecules,** v. 37, n. 23, p. 8530-8537, Nov. 2004.

101 SHEIKBAHAE, M. et al. Sensitive measurement of optical nonlinearities using a single beam. **IEEE Journal of Quantum Electronics,** v. 26, n. 4, p. 760-769, Apr. 1990.

102 CORREA, D. S. et al. Z-scan theoretical analysis for three-, four- and five-photon absorption. **Optics Communications,** v. 277, n. 2, p. 440-445, Sept. 2007.

103 DIPOLD, J. et al. Synthesis and two-photon absorption spectrum of fluorenone-based molecules. **Chemical Physics Letters,** v. 661, p. 143-150, Sept. 2016.

104 LINCKER, F. et al. Fluorenone-based molecules for bulk-heterojunction solar cells: synthesis, characterization, and photovoltaic properties. **Advanced Functional Materials,** v. 18, n. 21, p. 3444-3453, Nov. 2008.

105 KULKARNI, A. P.; KONG, X. X.; JENEKHE, S. A. Fluorenone-containing polyfluorenes and oligofluorenes: photophysics, origin of the green emission and efficient green electroluminescence. **Journal of Physical Chemistry B,** v. 108, n. 25, p. 8689-8701, June 24 2004.

106 SLYUSAREVA, E. et al. Spectral and photophysical properties of fluorone dyes in bio-related films and methanol. **Journal of Photochemistry and Photobiology A**: chemistry, v. 208, n. 2-3, p. 131-140, Dec. 2009.

107 RUNGE, E.; GROSS, E. K. U. Density-functional theory for time-dependent systems. **Physical Review Letters,** v. 52, n. 12, p. 997-1000, 1984.

108 BECKE, A. D. Density-functional thermochemistry .3. the role of exact exchange. **Journal of Chemical Physics,** v. 98, n. 7, p. 5648-5652, Apr. 1993.

109 _____. Density-functional exchange-energy approximation with correct asymptotic-behavior. **Physical Review A,** v. 38, n. 6, p. 3098-3100, Sept. 1988.

110 LEE, C. T.; YANG, W. T.; PARR, R. G. Development of the colle-salvetti correlation-energy formula into a functional of the electron-density. **Physical Review B,** v. 37, n. 2, p. 785-789, Jan. 1988.

111 FRISCH, M. J.; POPLE, J. A.; BINKLEY, J. S. Self-consistent molecular-orbital methods .25. supplementary functions for Gaussian-basis sets. **Journal of Chemical Physics,** v. 80, n. 7, p. 3265-3269, 1984.

112 FRISCH, M. J. et al. **Gaussian 09**. Wallingford CT 2013.

113 AIDAS, K. et al. The Dalton quantum chemistry program system. **Wiley Interdisciplinary Reviews:** computational molecular science, v. 4, n. 3, p. 269-284, May 2014.

114 TOMASI, J.; MENNUCCI, B.; CANCES, E. The IEF version of the PCM solvation method: an overview of a new method addressed to study molecular solutes at the QM ab initio level. **Journal of Molecular Structure:** theochem, v. 464, n. 1-3, p. 211-226, May 1999.

115 TOMASI, J.; MENNUCCI, B.; CAMMI, R. Quantum mechanical continuum solvation models. **Chemical Reviews,** v. 105, n. 8, p. 2999-3093, Aug. 2005.

116 NASCIMENTO, M. A. C. The polarization dependence of 2-photon absorption rates for randomly oriented molecules. **Chemical Physics,** v. 74, n. 1, p. 51-66, 1983.

117 DIAZ, C. et al. Two-photon absorption and two-photon circular dichroism of hexahelicene derivatives: a study of the effect of the nature of intramolecular charge transfer. **RSC Advances,** v. 5, n. 23, p. 17429-17437, 2015.

118VESGA, Y. et al. Two-photon absorption and two-photon circular dichroism of a hexahelicene derivative with a terminal donor-phenyl-acceptor motif. **Journal of Physical Chemistry A,** v. 122, n. 13, p. 3365-3373, Apr. 2018.

119 VESGA, Y.; HERNANDEZ, F. E. Two-photon absorption and two-photon circular dichroism of (L)-tryptophan in the near to far UV region. **Chemical Physics Letters,** v. 684, p. 67-71, Sept. 2017.